The Protonic Brain: Engineering a Simple Brain Emulator and Investigating Physical Mechanisms in Non-Local Communication

by

Nicolas Rouleau

A thesis submitted in partial fulfillment

of the requirements for the degree of

Master of Arts (M.A.) in Experimental Psychology

The Faculty of Graduate Studies

Laurentian University

Sudbury, Ontario, Canada

THESIS DEFENCE COMMITTEE/COMITÉ DE SOUTENANCE DE THÈSE
Laurentian Université/Université Laurentienne
Faculty of Graduate Studies/Faculté des études supérieures

Title of Thesis Titre de la thèse	THE PROTONIC BRAIN: ENGINEERING A SIMPLE BRAIN EMULATOR AND INVESTIGATING PHYSICAL MECHANISMS IN NON-LOCAL COMMUNICATION	
Name of Candidate Nom du candidat	Rouleau, Nicolas	
Degree Diplôme	Master of Arts	
Department/Program Département/Programme	Psychology	Date of Defence Date de la soutenance May 12, 2015

APPROVED/APPROUVÉ

Thesis Examiners/Examinateurs de thèse:

Dr. Michael Persinger
(Supervisor/Directeur de thèse)

Dr. Cynthia Whissell
(Committee member/Membre du comité)

Dr. Matias Mariani
(Committee member/Membre du comité)

Dr. Michael Levin
(External Examiner/Examinateur externe)

Approved for the Faculty of Graduate Studies
Approuvé pour la Faculté des études supérieures
Dr. David Lesbarrères
M. David Lesbarrères
Acting Dean, Faculty of Graduate Studies
Doyen intérimaire, Faculté des etudes supérieures

ACCESSIBILITY CLAUSE AND PERMISSION TO USE

I, **Nicolas Rouleau**, hereby grant to Laurentian University and/or its agents the non-exclusive license to archive and make accessible my thesis, dissertation, or project report in whole or in part in all forms of media, now or for the duration of my copyright ownership. I retain all other ownership rights to the copyright of the thesis, dissertation or project report. I also reserve the right to use in future works (such as articles or books) all or part of this thesis, dissertation, or project report. I further agree that permission for copying of this thesis in any manner, in whole or in part, for scholarly purposes may be granted by the professor or professors who supervised my thesis work or, in their absence, by the Head of the Department in which my thesis work was done. It is understood that any copying or publication or use of this thesis or parts thereof for financial gain shall not be allowed without my written permission. It is also understood that this copy is being made available in this form by the authority of the copyright owner solely for the purpose of private study and research and may not be copied or reproduced except as permitted by the copyright laws without written authority from the copyright owner.

Abstract

The brain is not entirely as it has been described in the classic neuroscientific literature. Physical and chemical properties of brain function can be separated from classical brain structure, allowing for multiple realizations of memory processing and the expression of correlates of consciousness. Further, the brain can be described as energy or information separate from although related to the organic structure which is perhaps subject to technologies which facilitate non-local transfer of data. Chapter 1 introduces the subject and provides sufficient information to explore the major concepts outlined in later sections. Chapter 2 outlines an experimental demonstration of electrophysiological activity in an abiological material which strongly correlates with human quantitative electroencephalographic (QEEG) frequency spectra under specified geometrical and chemical constraints. In Chapter 3, results indicate that this same amorphous material can effectively store and release information when classically conditioned, indicating learning and network formation can be separated from cells proper. Chapter 4 presents a technology which can effectively link two simple chemical systems such that equal and opposite reactions are induced at locus A upon elicitation of a given event within locus B. Chapter 5 provides a systematic analysis of the electromagnetic field dynamics associated with the aforementioned technology, providing both experimental and theoretical grounding. Chapter 6 is a general discussion which links these concepts and provides a summary of the works as they relate to the protonic brain.

Acknowledgements

I must first thank my supervisor and mentor, Dr. Michael Persinger. His fostering of curiosity and understanding of the importance of tinkering allowed me to explore avenues I had never considered. Without his insights and syntheses, the works presented here would not have met their full potential.

I would like to thank my committee members Dr. Matias Mariani and Dr. Cynthia Whissell for their guidance in shaping this dissertation. In challenging me, you promoted necessary re-examinations which lead to new and exciting approaches. To my colleagues in the Neuroscience Research Group, I offer my sincerest thanks. In consultation and confrontation, you continue to inspire me to create and discover. Of course, I'd like to thank my family for their continuing support – I am forever appreciative of this.

Table of Contents

List of Figures

Chapter 1: Introduction

Memory & Consciousness

Though the construct of consciousness has been difficult to define, it is generally considered to represent a mental state in which it is possible to be aware of external events or objects: imbuing matter with the qualities of an observer (Dennett & Kinsbourne, 1992). It must, however, be emphasized that consciousness is in fact a construct – a composite variable requiring operationalization; an ideal object whose presence is correlated with objective variables such as electrical activity that can be quantified, and subjective variables such as phenomenal experience or qualities of mind, which although loosely quantifiable, are always subject to problematic interpretation (Nagel, 1974). Consciousness refers to a brain state or property which, unlike information storage, appears to require a functional human brain to be expressed.

It is in contrast that we find a phenomenon such as memory, involving the encoding, storage, and retrieval of information which has been acquired by experience (Dolan & Fletcher, 1997) which seems to represent a fundamentally different aspect of brain function. Memories as information are thought to be represented as engrams within the cerebral manifold (Bruce, 2001).Tangible memory units such as dendritic spines (Engert & Bonhoeffer, 1999) associated with highly characterized neural (Malenka & Bear, 2004) and molecular pathways (Bortolotto, Bashir, Davies & Collingbridge, 1994) can be observed and quantified quite readily. A detailed understanding of memory is not problematic in the same way as is the case for consciousness. Consciousness is holistic or at least not generated by a single, sufficient brain structure (Dennett, 1993; 2001).Despite extensive, non-overlapping

characteristics, memory and consciousness appear to be functionally related. Conscious states provide windows through which information flows to be represented within brain-space as memory. Recognition, a central process in memory, is the re-elicitation of previously activated pathways which are represented as conscious experiences. Therefore, a thorough study of one must necessarily incorporate an analysis of both.

Information can be stored in spaces other than the human brain such as silicon chips as well as atomic vapour (Phillips, Fleischbauer, Mair, Walsworth & Lukin, 2001), and solids (van Heerden, 1963). It remains unclear, however, whether consciousness or some analogous state can be represented within inanimate matter. Even the identification of consciousness as a phenomenon outside the human brain is beyond most forms of investigation at present. Currently, the pragmatic approach involves a standard of relying upon correlates of consciousness. Among these, quantitative electroencephalography (QEEG) has been indispensable as a tool which allows the neuroscientist to monitor electrical activity over the scalp. It cannot be said that superficial electrical activity alone constitutes consciousness; however, it is clear that these potentials over the scalp and their origins are important factors in the composite. Synchronous states of high-frequency electrical activity (30-100Hz) are observed to increase in conjunction with subjective states characteristic of waking consciousness (Meador, Ray, Echauz, Loring & Vachtsevanos, 2002). These states are punctuated by discrete activations of neuronal populations with slow-wave oscillatory activity. Similar patterns are found within the electromagnetic field in which all humans are immersed (Persinger & Koren, 2007). Just suppose that similarities in oscillatory electrical activity represented at the level of the cerebrum and the Earth share an origin. If a substrate-independent correlate of consciousness can be identified in the extracerebral

environment via experimental methods, the fundamental processes underlying neural activity will require a serious re-examination.

Mainstream theories of consciousness presuppose that a structure of inordinate complexity is required to generate consciousness; an approach which places the brain in an exclusive position with respect to other configurations of matter: emergentism. One alternative, which contrasts emergentism, is panpsychism: the concept of a pervasive force of consciousness throughout the cosmos (Popper, 1977). Panpsychism rejects the idea that consciousness is emergent of a complex system wherein the sum of the parts is not sufficient to account for the whole (Strawson, 2006). In its place, a panpsychic might claim that consciousness is a ubiquitous, field-like, fundamental property of the cosmos, and expresses itself in multiple forms (Nagel, 1979). Persinger (2013) lends quantitative support to similar forces such as the collective unconscious (Jung, 1981), which is thought to consist of shared fields of influence between members of a group. Even personal consciousness has been described as a field (John, 2001) and linked to fundamental forces such as electromagnetism (McFadden, 2002; 2007).

Under the current paradigm of emergentism, neuronal synchronization – a key feature expected in a conscious system – is thought to occur within the brain by means of multiple sources of high frequency neuronal firing (Wittington, Cunningham, LeBeau, Racca, & Traub, 2011). Penrose & Hameroff (2011) claim that gamma synchrony (i.e. 30-90Hz synchronized electroencephalographic oscillations), one of the best measurable correlates of consciousness and potential indicators of binding (John, 2001), does not derive from neuronal origin in the sense of classical neurophysiological mechanisms. Instead, the suggestion is that neurons express a macroscopic firing pattern induced by quantum computations within macromolecules known as tubulin which form

microtubules: a major component of the cytoskeleton. This orchestrated reduction (Orch OR) model describes how quantum events such as wave-function collapse might have downstream implications for neuronal and cerebral processes (Hameroff & Penrose, 1996); however, this popular model is no more than a modern reiteration of what is essentially an emergent theory which attempts to place a consciousness-generator within brain-space. It is, however, sometimes problematic to point to an origin of a signal within the system which is being studied. Without the conceptualization of the photon, the stimulation of a rod within the retina or even the conformational change of a photoreceptive rhodopsin molecule might appear to be the source of visual information within the brain. The quantum of energy carrying information into the brain from the external world is of great consequence when discussing the origin of neural activity reflective of the visual system. The same can be said of any form of neural activity.

The difficulty in validating panpsychic claims is that of the experimental design. Whereas the assumption of a consciousness-generating organ can be immediately assessed by narrowing in on the brain with direct measurement, the assumption of ubiquity greatly widens the scope of exploration. If consciousness and the brain activity associated with conscious states measured at the level of the brain does not wholly emerge from the brain, where might it originate? One solution to this problem is to hypothesize that a pervasive force or proto-consciousness permeates the cosmos which interacts with all matter and imbues some subset of matter with consciousness (Penrose & Hameroff, 2011). Although possible, there are alternative panpsychic views which can be supported more readily. As the brain is a magnetoreceptive organ, and humans are immersed within the Earth's electromagnetic field at all times, it is reasonable to

hypothesize that perhaps this field of force is a type of consciousness generator – ordering neural populations into coherent masses. Personal and collective consciousness would share a common *zeitgeber*; the spectrum of the electromagnetic environment. It has recently been calculated that the Earth's natural EM environment could link all brains at a fundamental level (Persinger, 2013). The planet itself must therefore be considered as a potential regulator of mental states.

It has recently been proposed that the physical characteristics of an object can be separated from objects themselves: quantum Cheshire cats (Aharonov, Popescu & Skryzpczyk, 2013).As the brain is classically considered to be the generator of consciousness by hitherto unidentified means, this discovery in physics provides, in principle, a basis for the separation of consciousness from the brain proper. It therefore follows that this physical property – disembodied from the brain – should be empirically accessible, in practice, as a measurable phenomenon outside the brain. Persinger (2012) suggests a scale-invariant, quantitatively convergent relationship between brain EM activity and lightning. Brain EM activity and lightning share many physical properties including energy densities, current densities, methods of signal propagation, mass-charge velocity ratios, interface times, patterned harmonics, and time constants (Persinger, 2012).Because the EM signatures of the neural correlates of mental processes are identifiable in nature, experimental projects must now attempt to express and measure these signatures as indicators of scale-invariant consciousness in the laboratory.

This type of experimental investigation into origins for the neural correlates of consciousness must not incite attempts to answer certain questions. For example, a phenomenological approach to out-of-brain consciousness by means of reported out-of-

body experiences (Laws & Perry, 2010) is problematic in that the measure, although potentially accurate, can never report itself as a proof. Gödel (1931) proposed that, given a series of statements in a logically consistent system, there will always be one true but unprovable statement; a necessary incompleteness. This is why experimental endeavours which attempt to identify out-of-brain EM signatures of consciousness must not attempt to address the hard problem: the problem of how qualia or phenomenological experiences relate to matter (Chalmers, 1995). Acknowledging that organisms do have subjective experiences, it must be the aim of the scientist in pursuit of extracerebral sources of consciousness to examine only objective referents which can be pointed to, enumerated, and be subject to inter-observer agreement. It could be, after all, that the qualia associated with consciousness are exceptional by-products of a fundamental consciousness interacting with a biological organism.

Theoretical works have been proposed which describe signal-based theories of consciousness. Eccles (1992) proposed that psychons, hypothetical particles, interact with dendrons within the microstructural cytoarchitecture of the cerebral cortex – a theory which has been reiterated with the involvement of zero-energy tachyons (Hari, 2008). If psychons do exist, emergent consciousness is illusory and is a product of cerebral interactions with external sources of energy. Perhaps the psychon operates as a wave instead of a particle with patterned oscillation as a function of the carried information. A search for these oscillations outside the brain is a valid line of inquiry when assuming consciousness is somehow regulated by an external force. Suppose that brains interacting with these waves or particles are incidental phenomena on the cosmic scale whereby the signal is intercepted by some structure within the brain itself such as microtubules (Hameroff & Penrose, 2003). Burke & Persinger (2013) have provided

quantitative support for the idea that the gross structure of the hippocampus could access this type of cosmic signal. The assumption that consciousness resides only in the brain is based upon an absence of evidence which can never be treated as evidence of absence.

The brain can be thought of as an aggregate of cells expressing electrochemical signals and consisting largely of water with ions. It is precisely this structure-function that will indicate where one would look if one were in search of out-of-brain consciousness. As Rouleau & Dotta (2014) have posited: "Suppose consciousness was to the brain as radio waves are to radio receivers. Identifying the structural and functional qualities of the radio receiver can be very informative when in search of the invisible radio waves; the hardware defines at least some subset of the receptive parameters and exclusionary criteria. In pursuit of the origin of the sounds which seem to originate from within the machine, the scientist employs two main methods of investigation. First, he or she attempts to measure the electrical conduction between parts within the machine, carefully examining every piece of hardware in search of the origin of the signal. Second, he or she attempts to remove components manually or study the function of machines which have incurred damage. Without an understanding of the radio wave, sounds and voices emanating from a radio receiver might appear to be emergent of the complexity of the machine. However, once the radio wave is identified, the system can be studied as a passive piece of hardware – its manifest structure-function. The claim here is that the brain is, at least in part, a passive organ which can receive exogenous electromagnetic information and does so naturally."

In search of consciousness, theorists have attempted to identify a *center of consciousness* within the brain or have invoked convoluted explanations based upon the

assumption that the brain is physical, but somehow something more. The claim here is that the brain's structure is such that its function as an electro-chemical organ will reflect commonplace processes in the cosmos including memory storage and the expression of oscillatory patterns that are fundamental indicators of the construct that has been referred to as consciousness.

Water Memory

Water exposed to weak EM fields in dark conditions displayed shifts in peak wavelength of photon emissions within the average width of a cell membrane or ~10nm (Persinger, 2014).This is thought to result as a function of proton organization within the media – an impressed image upon the molecular organization of water itself with dimensions convergent upon the cell. Following from the claim that space-memory is possible in water-based systems, we're faced with the possibility that the brain is not unique with respect to its capacity to store information. Within the brain, neural networks are formed which are thought to be the scaffolding within which the representations of memory reside. However, it is often forgotten that neural networks are accompanied by negative-images of themselves as extracellular spaces occupied by interstitial fluid. This aqueous environment might be a fundamental milieu within which information can be stored. As hydrogen and oxygen, the constituents of the H_2O molecule, are widely available throughout the cosmos (Kotwicki, 1991), it is possible that information storage within the universe is commonplace.

Electromagnetic Fields as Zeitgebers

Rouleau & Dotta (2014) have presented the argument that electromagnetic fields (EMFs) order morphogenesis and consciousness by supplying biological systems with information. The essential argument put forward is that the Earth's electromagnetic field is a *zeitgeber* for processes which order cellular function (Rouleau & Dotta, 2014). Both light as a discrete packet of energy and with an associated wavelength between 200 nm and 1500 nm, as well as temporally complex fields have been shown to induce changes in both structure and the function of biological organisms (Cifra et al., 2011; Gabrielli et al., 2006; Popp, 1979). Mechanisms for EMF or photoreception on the part of the organism have been proposed; however, a systematic, experimental investigation is problematic. If water is hypothesized to drive cellular reception of EMF-mediated information, it is sensible to decrease or increase the water content of the cell in such a way so as to determine the relative contribution of this variable. However, in altering the aqueous solution, many aspects of the cell are expected to be functionally altered due to disequilibrium of the system. This is why attempts must be made to evaluate the relative contribution of cell contents outside the cell or biological paradigm in order to isolate key variables – separating the parts of the cell from the whole of the cell. In this sense, necessary conditions can be deduced which might explain the larger phenomenon.

Excess Correlation

States of "excess correlation" describe phenomena analogous to the historical observation that entangled or non-isolated particles whose state is described by a single

wave function will spin or otherwise operate with equal and opposite magnitude and direction terms. The original work essentially demonstrates that knowledge can be gleaned about the position or momentum of a particle (B) without observing that particle (B) if it is first interacts with a particle (A) that is observed (Einstein, Podolsky, & Rosen, 1935). Theoretically, this class of phenomenon is thought to be restricted to quantum scales of discourse; however, macroscopic demonstrations of states of excess correlation have been reported in the literature. Notably, experiments have suggested that brains separated in space will respond to non-local stimuli applied to a counterpart brain if the two loci are subject to counter-clockwise rotating, weak intensity, electromagnetic field applications (Persinger & Lavallee, 2010). Alternative versions of the equipment employed have been prototyped (Burke et al., 2013), suggesting some degree of generalizability. The mechanism underlying these applications of brain-to-brain communication remains to be elucidated.

The Present Study

The works presented here represent multiple approaches which aim to underline the physical basis of brain function, its grounding outside typical brain structure, and potential technological applications which can be used to link brains functionally. Chapters 2 and 3 investigate electrophysiological correlates of memory and consciousness within an amorphous, abiological material containing many of the constituents of cells. Chapters 4 and 5 provide evidence for an emerging technology which can perhaps link physical-chemical systems non-locally, allowing a transfer of information across what could be vast expanses of space-time. In addition to

experimental data, quantification by dimensional analysis is provided throughout these works in order to predict non-observable features of the respective phenomena. Chapter 6 provides a general summary of the collected works with final thoughts.

References

Aharonov, Y., Popescu, S., Rohrlich, D., & Skrzypczyk, P. (2013).Quantum Cheshire Cats. *New Journal of Physics*, 15(11), 113015.

Bortolotto, Z. A., Bashir, Z. I., Davies, C. H., & Collingridge, G. L. (1994). A molecular switch activated by metabotropic glutamate receptors regulates induction of long-term potentiation.*Nature*, 368, 740-743.

Bruce, D. (2001). Fifty years since Lashley's In search of the Engram: refutations and conjectures. *Journal of the History of the Neurosciences*, *10*(3), 308-318.

Burke, R. C., & Persinger, M. A. (2013). Convergent Quantitative Solutions Indicating the Human Hippocampus as a Singularity and Access to Cosmological Consciousness. *NeuroQuantology*, 11(1).

Burke, R. C., Gauthier, M. Y., Rouleau, N., & Persinger, M. A. (2013). Experimental demonstration of potential entanglement of brain activity over 300 Km for pairs of subjects sharing the same circular rotating, angular accelerating Magnetic fields: verification by s_LORETA, QEEG measurements. *Journal of Consciousness Exploration & Research*, 4(1).

Chalmers, D. J. (1995). Facing up to the problem of consciousness. *Journal of Consciousness Studies*, 2(3), 200-219.

Cifra, M., Fields, J.Z., & Farhadi, A.(2011).Electromagneticcellularinteractions. *Prog. Biophys. Mol. Biol.* 105, 223–246.doi:10.1016/j.pbiomolbio.2010.07.003

Dennett, D. C. (1993). Consciousness explained. Penguin UK.

Dennett, D.C. (2001). Are we explaining consciousness yet?. *Cognition*, 79(1), 221-237.

Dennett, D. C., & Kinsbourne, M. (1992).Time and the observer: The where and when of consciousness in the brain. *Behavioral and Brain Sciences*, 15, 183-247.

Dietrich, C. J., & Morad, M. (2010). Synaptic acidification enhances GABAA signaling. *The Journal of Neuroscience*, 30(47), 16044-16052.

Dolan, R. J., & Fletcher, P. C. (1997). Dissociating prefrontal and hippocampal function in episodic memory encoding. *Nature*, 388(6642), 582-585.

Dotta, B. T., Saroka, K. S., & Persinger, M. A. (2012). Increased photon emission from the head while imagining light in the dark is correlated with changes in electroencephalographic power: Support for Bókkon'sbiophoton hypothesis. *Neuroscience Letters*, 513(2), 151-154.

Dotta, B. T., Karbowski, L. M., Murugan, N. J., & Persinger, M. A. (2013). Incremental Shifts in pH Spring Water Can Be Stored as “Space-Memory”: Encoding and Retrieval Through the Application of the Same Rotating Magnetic Field. *NeuroQuantology*, 11(4).

Eccles, J.C. (1992). Evolution of consciousness. Proc. Natl. Acad. Sci., 89, 7320-7324.

Einstein, A., Podolsky, B., & Rosen, N. (1935). Can quantum-mechanical description of physical reality be considered complete?. *Physical Review*, 47(10), 777.

Engert, F., & Bonhoeffer, T. (1999). Dendritic spine changes associated with hippocampal long-term synaptic plasticity. *Nature*, 399(6731), 66-70.

Gabrielli, E.,Huitu, K.,& Roy, S.(2006).Photon propagation in magnetic and electric fields with scalar/pseudoscaler couplings: a new look. *Phys. Rev. D* 74,1–21. doi:10.1103/physrevd.74.073002

Gödel, K. (1931). On formally undecidable propositions of principia mathematica and related systems. *Monatshefte fur Math. u. Physik*, 38, 173-198.

Hameroff, S., & Penrose, R. (1996). Orchestrated reduction of quantum coherence in brain microtubules: A model for consciousness. *Mathematics and Computers in Simulation*, 40(3), 453-480.

Hari, S. D. (2008). Eccles's Psychons Could be Zero-Energy Tachyons. *NeuroQuantology*, 6(2).

Jung, C. C. G. (1981). The archetypes and the collective unconscious (Vol. 9). Princeton University Press.

Kotwicki, V. (1991). Water in the Universe. *Hydrological Sciences Journal*, 36(1), 49-66.

Laws, V., & Perry, E. (2010). Near death experiences: A new algorithmic approach to verifying consciousness outside the brain. *NeuroQuantology*, 8(2).

Malenka, R. C., & Bear, M. F. (2004). LTP and LTD: an embarrassment of riches. *Neuron*, 44(1), 5-21.

Meador, K. J., Ray, P. G., Echauz, J. R., Loring, D. W., & Vachtsevanos, G. J. (2002). Gamma coherence and conscious perception. *Neurology*, 59(6), 847-854.

McFadden, J. (2007). Conscious electromagnetic (CEMI) field theory. *NeuroQuantology*, 5(3).

McFadden, J. (2002). Synchronous firing and its influence on the brains electromagnetic field. *Journal of Consciousness Studies*, 9(4), 23-50.

Nagel, T. (1974). What is it like to be a bat?. *The Philosophical Review*, 83(4), 435-450.

Nagel, T. (1979). Mortal Questions (Canto). Cambridge: Cambridge University Press.

Penrose, R., & Hameroff, S. (2011). Consciousness in the universe: Neuroscience, quantum space-time geometry and Orch OR theory. *Journal of Cosmology*, 14, 1-17.

Persinger, M.A. (2013). Billions of human brains immersed within a shared geomagnetic field: Quantitative solutions and implications for future adaptions. *The Open Biology Journal*. 6, 8-13.

Persinger, M. A. (2012). Brain electromagnetic activity and lightning: potentially congruent scale-invariant quantitative properties. *Frontiers in Integrative Neuroscience*, 6(19), 1-7.

Persinger, M. A. (2010). The Harribance effect as pervasive out-of-body experiences: NeuroQuantal evidence with more precise measurements. *NeuroQuantology*, 8(4).

Persinger, M. A. (1999). Is there more than one source for the temporal binding factor for human consciousness?. *Perceptual and Motor Skills*, 89(3f), 1259-1262.

Persinger, M. A., & Koren, S. A. (2007). A theory of neurophysics and quantum neuroscience: implications for brain function and the limits of consciousness. *International Journal of Neuroscience*, 117(2), 157-175.

Persinger, M. A., & Lavallee, C. F. (2010). Theoretical and experimental evidence of macroscopic entanglement between human brain activity and photon emissions: implications for quantum consciousness and future applications. *Journal of Consciousness Exploration & Research*, 1(7).

Persinger, M. A. (2014). Quantitative Convergence Between Physical-Chemical Constants of the Proton and the Properties of Water: Implications for

Sequestered Magnetic Fields and a Universal Quantity. *International Letters of Chemistry, Physics and Astronomy*. 2, 1-10.

Phillips, D. F., Fleischhauer, A., Mair, A., Walsworth, R. L., & Lukin, M. D. (2001). Storage of light in atomic vapor. *Physical Review Letters*, 86(5), 783.

Popp, F.-A. (1979).“Photon storage in biological systems,” in Electromagnetic Bioinformation, eds F.A. Popp, G. Becker, H.L. Konig, W. Pescha (Munich: Urban and Schwarzenberg),123–149.

Popper, K. R. (1977). Some remarks on panpsychism and epiphenomenalism. *Dialectica*, 31(1-2), 177-186.

Pyatnitsky, L. N., & Fonkin, V. A. (1995). Human consciousness influence on water structure. *Journal of Scientific Exploration*, 9, 89-106.

Rouleau, N. & Dotta, B.T. (2014). Electromagnetic fields as structure-function zeitgebers in biological systems: environmental orchestrations of morphogenesis and consciousness. *Frontiers in Integrative Neuroscience*, 8(84), 1-9.

Strawson, G. (2006). Realistic monism: Why physicalism entails panpsychism. *Journal of Consciousness Studies*, 13(10;11), 3.

van Bibber, K., Dagdeviren, N. R., Koonin, S. E., Kerman, A. K., & Nelson, H. N. (1987). Proposed experiment to produce and detect light pseudoscalars. *Physical Review Letters*, 59(7), 759.

vanHeerden, P. J. (1963). Theory of optical information storage in solids. *Applied Optics*, 2(4), 393-400.

Whittington, M. A., Cunningham, M. O., LeBeau, F. E., Racca, C., & Traub, R. D. (2011). Multiple origins of the cortical gamma rhythm. *Developmental Neurobiology*, 71(1), 92-106.

(Published in Journal of Signal and Information Processing, 2014)

Chapter 2: Cerebral Networks of Interfacial Water: Analogues of the Neural Correlates of Consciousness in a Synthetic Three-Shell Realistic Head Model

Abstract

The physical properties of water, particularly the nature of interfacial water and pH shifts associated with dynamics of the hydronium ion near any surface, may be a primary source of the complex electromagnetic patterns frequently correlated with consciousness. Effectively all of the major correlates of consciousness, including the 40 Hz and 8 Hz coupling between the cerebral cortices and hippocampal formation, can be accommodated by the properties of water within a specific-shaped volume exposed to a magnetic field. In the present study, quantitative electroencephalographic activity was measured from an experimental simulation of the human head constructed using conductive dough whose pH could be changed systematically. Spectral analyses of

electrical potentials generated over the regions equivalent to the left and right temporal lobes in humans exhibited patterns characteristic of Schumann Resonance. This fundamental and its harmonics are generated within the earth-ionospheric cavity with intensities similar to the volumetric intracerebral magnetic (~2 pT) and electric field (~6 $\times$ 10^{-1} $V \cdot m^{-1}$) strengths. The power densities for specific pH values were moderately correlated with those obtained from normal human brains for the fundamental (first) and second harmonic for the level simulating the cerebral cortices. Calculations indicated that the effective pH would be similar to that encountered within a single layer

of protons near the plasma membrane surface. These results reiterate recent measurements in a large population of human brains showing the superimposition of Schumann power densities in QEEG data and indicate that intrinsic features of proton densities within cerebral water may be a fundamental basis to consciousness that can be simulated experimentally.

Introduction

Neuroanatomical organization of a sufficient complexity is thought to be a necessary condition of consciousness (Deamer, 2011) wherein neural networks form and the resulting structure dictates the function of the organ (McIntosh, 2000). Neurons, composed mainly of water and proteins (Alberts et al., 1994), communicate by means of electrochemical signalling with direction and magnitude which result in cognitive states and behaviours. However, as the convolutions which constitute the structure of the brain became increasingly complex, so did the intervening negative spaces—including the extracellular environment. Studying consciousness exclusively within cells is problematic when considering that the medium between cells is primarily composed of water with ions (Alberts et al., 1994) and that solutions such as these are able to store and release electromagnetic energy (Persinger & Dotta, 2011). The implication is that the proteinaceous structure of the brain itself is an epiphenomenon which operates simultaneous to a covert system where neurons express activity from the local environment in an integrated network of aqueous boundary conditions.

That the relatively stable microstructual patterns, at the level of the synapse, function to maintain the temporal consistency of the conditions that correlate with

consciousness, is a viable, alternative possibility. Water molecules adjacent to a surface exhibit all of the major properties attributed to the plasma cell membrane. Interfacial water, compared to bulk water, displays about ten times the viscosity. The resulting exclusion zone is associated with a narrow zone of protons. The generated potential difference ranges in the order of 100 mV which is the same order of magnitude as the resting membrane potential traditionally attributed to the disparity in concentration of cations and anions across the membrane space. Within the exclusion zone generated by ordinary water adjacent to a surface, electromagnetic fields can be retained for protracted periods of time (Persinger, 2014).

Water displays universal properties derived from fundamental physical parameters. For example its diffusivity (0.8×10^{-7} $m^2 \cdot s^{-1}$) is obtained by dividing the magnetic moment of a proton (1.41×10^{-26} $A \cdot m^2$) by the unit charge (1.6×10^{-19} $A \cdot s$). When this quotient is multiplied by the typical viscosity of water (1.0×10^{-3} $kg \cdot m^{-1} \cdot s^{-1}$) at 20˚C the resulting force is 8.8×10^{-11} $kg \cdot m \cdot s^{-2}$ (Persinger, 2014). When applied across the width of two O-H bonds (1.92×10^{-10} m) the energy is about 1.7×10^{-20} J. This value is within the measurement error of the energy for the second shell hydrogen bond that reflects proton mobility in water (Decoursey, 2003). We think it is relevant that ~1.7×10^{-20} J is within the range of energy associated with effects of a typical neuronal action potential upon a unit charge and the energy required to stack one nucleotide onto an RNA sequence (Persinger, 2010). In other words, the most fundamental increment of energy associated with the neuronal correlate of consciousness and cognition, the action potential, and energy required to add different nucleotides, the determinant of the protein patterns of memory, is the same value as that associated with the movements of protons through water.

The proton is a primary candidate to mediate information within brain space. According to DeCoursey (2003) the proton is unique among cations in being interchangeable with the protons that form water. There is a five-fold higher conductivity for H^+ in water compared to other cations such as K^+ and there are more proton channels than the sum of channels from all other ions combined. Even when one considers the numbers of free protons within the hydronium atom is about 40 nM (compared to the 110 M of hydrogen in water), the numbers become significant when one appreciates that most of the brain volume is water. During a 100 pA outward H^+ current between 10^8 and 10^9 H^+ leave the typical cell. The importance and prevalence of protons and proton channels has been attributed to the evolutionary necessity of quickly dissipating the intracellular diminished pH associated with interactions between organic acids.

Shifts in pH along neuronal membranes accompany action potentials and occur as transients with intervals between 10 and 40 ms (Brevan, 1998). Highstein *et al.* (2014) showed that protons act as neurotransmitters with shifts of ~0.2 pH near synaptic clefts. Recently Murugan *et al.* (2010) observed that continuous exposure of spring water with ion concentrations similar to biological fluids to physiologically-patterned magnetic fields produced frequent temporal shifts of small increments in pH whose durations were between 20 and 40 ms. The relevance of this increment, which is the ~40 Hz activity associated with higher functions for cerebral activity such as consciousness, is well known. Llinas and Ribary (1993) found that cohesive integrative waves displaying phase modulation moved as recursive phenomena in a rostral to caudal direction every 20 to 25 ms. Several authors have noted the “coincidence” that the time required for bulk velocity action potentials to move through the hippocampal,

thalamic, cerebral “circuits” displays durations of approximately 20 to 25 ms. This reiterates our approach that the

structure of pathways through which consciousness is mediated are arranged to ensure the specific timing of the circuit to match intrinsic features of water.

Persinger (2013) proposed that the Earth’s quasi-static main magnetic field is a potential medium by which all brains can be unified at a fundamental level. Although speculative and potentially interesting, the solution for the individual brain is particularly relevant. Assuming an average volume of 1350 cc which is ~945 cc (70% water), there would be 55.5 M of water (18 cc per M). This would involve 3.16×10^{25} water molecules. The magnetic energy from the static geomagnetic field, assuming an average of 5×10^{-5} T, would be in the order of 0.945×10^{-6} J or 2.9×10^{-32} J per water molecule (Murugan et al., 2014). The equivalent frequency, obtained by dividing Planck’s constant (6.626×10^{-34} J·s) would be ~40 Hz. Even neural correlates of consciousness have been attributed to synchronous gamma activity (Crick & Koch, 1990). The fundamental theta (4 to 8 Hz) frequency of the hippocampal formation, the “gateway to memory”, exhibits superimosed ~40 Hz ripples that may be fundamental to interaction between cerebral cortical and parahippocampal regions (Bear, 1996).

The extremely-low frequency (ELF) component of the Earth’s electromagnetic radiation spectrum is generated by a resonance phenomenon between its surface and the ionosphere with a fundamental operating frequency of 7.8 Hz (Schlegel & Füllekrug, 2002). Originally characterized by Schumann (1952), this fundamental and its harmonics (14.1 Hz, 20.3 Hz, 26.4 Hz, and 32.5 Hz) are a result of global lightning discharges where the fundamental mode is determined by the circumference of the Earth. The wave forms and temporal structures associated with the Schumann

frequencies are remarkably similar to the classic delta, theta, and alpha patterns attributed to cerebral cortical activity (König, 1971). The magnetic field strength of these resonances is in the order of 1 to 3 pT, which is within the range of the operating magnetic field within the human cerebrum. If the typical 0.2 μV change associated with a single ion channel is applied to a unit charge (1.6×10^{-19} A·s), the increment of energy is 0.3×10^{-25} J. The square root of this value divided by the mass of a proton is ~4.5 m·s–1 which is the typical velocity of the rostral-caudal waves or bulk velocity of the integrated cerebral electromagnetic fields. Assuming the average circumference of a human skull to be 60 cm, the standing wave would be between 7.5 to 7.8 Hz. Schumann resonance frequencies are thought to influence brain activity as well as blood pressure (Cherry, 2002; 2003) and other biological processes (König, 1971).

The hippocampal formation and parahippocampal gyrus in particular are thought to be strongly coupled to the Schumann resonance (Persinger, 2008). The observation that the low-frequency oscillations which characterize the typical human electroencephalographic profile overlap significantly with the fundamental Schumann resonance frequency (7.8 Hz) and the paired harmonics might not be coincidental. Layers II and III within the entrorhinal cortices of the parahippocampal gyrus, which provides the bi-directional interactions between the cerebral cortices and hippocampal formation (Alonso & Klink, 1993), exhibit a near-continuous subthreshold oscillation of ~8 Hz. The mean amplitude of these oscillations was 2.6 (±0.5) mV.

Geomagnetic storms are associated with altered human cognition and behaviour (Stewart & Persinger, 2000), suggesting some intrinsic relationship between the brain and the electromagnetic environment. Whereas it is possible that some recondite third factor is influencing both systems, experimental inductions of altered brain function

using artificially generated electromagnetic fields indicate that the brain is a magnetoreceptive organ (Stewart & Persinger, 2000). Though electromagnetic cellular interactions have been studied in detail (Cifra et al., 2011), the negative brain-space of the extra-cellular environment wherein subtle physical phenomena might be occurring must be further considered as a contributing source of variance.

A negative space brain system might function by absorption and emission of electromagnetic energies as has been demonstrated in paradigms involving spring water (Gang et al., 2011), and cell cultures (Dotta et al., 2011). In both cases, externally applied stimuli were involved, suggesting that non-cerebral sources of electromagnetic energies could potentially interact with the brain by means of interaction with water. The discovery that induced, subtle shifts in pH within the synaptic cleft in C. elegans were sufficient to alter post-synaptic firing indicates the importance of proton- based neurotransmission (Beg et al., 2008). Synapses, consisting effectively of parallel plates, operate within parameters sufficient to generate Casimir forces (Burke & Persinger, 2013), suggesting that these interfaces are more than just transitional zones through which molecular neurotransmitters traverse. The same authors have calculated that the wavelength equivalent of the energy associated with these forces applied over 10 nm—a value approximating the width of the synaptic cleft and the neuronal membrane—would approximate the width of neutral hydrogen.

Together, these findings have suggested that classical mechanisms, although essential and highly reliable, do not accommodate the variety of processes observed involving neuronal signalling. Additionally, these works indicate that the proton is of central importance with regards to the functioning of the nervous system. We hypothesized that perhaps an external force or zeitgeber is ordering neural activity

wherein the sum of the cellular units are necessary although insufficient to produce the resulting function in much the same way a radio receiver is necessary but insufficient in radio transmission. Whereas brain structure would be essential to brain function, the output of the brain would not be explained by cellular structures alone. As neurons would be receptive to this extra-cerebral force, it follows that the energies involved in such a process are subject to experimental measurement and quantification. Here, we present an experimental detection of what is potentially extra-cerebral information which could explain a subset of brain function normally ascribed to synchronous cellular activity.

Materials & Methods

Synthetic Three-Shell Realistic Head Model

A three-shell experimental model of the human head was constructed (Figure 2.1) based upon theoretical models which are assumed in the dynamic neuroimaging technique of quantitative electroencephalography (QEEG; Berg & Scherg, 1994; Ermer et al., 2001). The inner and outer surfaces of a plastic, replica human skull (Figure 2.2; Human Skull-Standard, WSP-01 by Skulls Unlimited International) were lined with an electroconductive dough (ED) in order to simulate the anatomical organization of the cortex, skull, and scalp. The replica, measuring 20 cm in length, 13.5 cm in width, and 15.5 cm in height, features anatomically accurate sutures, foramina, canals, fissures, condyles, and other cranial features. The organization can be described as a relative non-conductor placed between two conductors. The conductive material consists of an open-source amateur electronics recipe by Squishy Circuits. This material is typically used as an educational tool to demonstrate the principles of electrical systems (Figure

2.3). The dough is fabricated by mixing 237 cc of water, 355 cc of flour, 59 cc of salt, 15 cc of vegetable oil, 2 cc food

coloring, and various concentrations of a proton donor (lemon juice) together in a pot over a heated surface while stirring until partially solidified. The ball of dough is then covered in 10 cc of flour, kneaded, and applied at a constant thickness of ~5 mm in order to approximate the average human cortical thickness.

Figure 2.1. Synthetic three-shell realistic head model consisting of electroconductive dough which lines the inner and outer surfaces of a replica human skull. Lateral (left), rostral (right) views of the model showing the scalp layer.

Figure 2.2. Replica human skull. Ventral (left) and dorsal (right) aspects of the internal cranial vault are shown. Realistic, non-symetrical cranial features are present includng processes, fossa, condyles, ridges, tuberosities, and sutures.

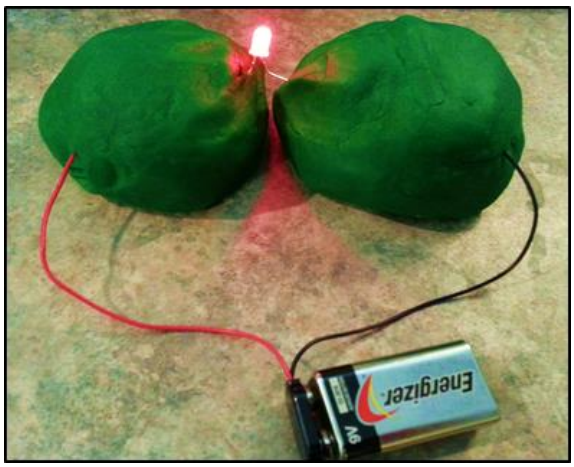

Figure 2.3. Squishy Circuits electroconductive dough coupled to a 9V DC battery and a light-emitting diode (LED). This material lined the inner and outer aspects of a replica human skull to simulate the three-shell realistic head model.

Three dough recipes were prepared which differed only by concentration of the proton donor: 44 cc (low), 133 cc (medium), and 222 cc (high). Measurements were obtained in order to quantify the relative pH and total protons associated with each recipe as a function of this experimental manipulation. A pH sensor coupled to a Dr. DAQ data logger relayed information to a Lenovo laptop running PicoLog data acquisition software. The scan time of the pH meter was set to measure every 50 ms, averaging values which were then recorded at a 1 Hz sampling rate. Each concentration of lemon juice was measured within the fixed volume of 237 cc of water within a glass beaker. pH measurements were obtained for 120 seconds and averaged across the trial to obtain the value associated with the recipe.

The high concentration condition was associated with a pH value of 2.47 whereas the medium and low concentration conditions were associated with pH values of 2.52 and 2.66 respectively. Hydrogen ion concentration (HIC) was then calculated $[H^+]= 10^{-pH}$ which results in M/L. These values are then adjusted for volume and multiplied by Avagadro's number ($6.02 \bullet 10^{23}$ mol/M). It was determined that the total hydrogen ions as a function of the donor were ~10^{21} for the high concentration condition and ~10^{20} for the medium and low concentration conditions. Although the difference was slightly less than a factor of ten, the total unit difference between the conditions exceeds 10^{20} proton units.

Procedure

QEEG measurements of ED baseline activity were obtained (n=12) with an associated sampling rate of 250 Hz and a notch-filter set to exclude frequency contributions between 45 and 75 Hz. A Mitsar 19-channel QEEG system coupled to a HP ENVY laptop running Windows 8 served as the data logging equipment; however only four sensors (T3, T4, T5, and T6) were used due to the highly homogeneous activity of the ED across small spatial distances ($r= 0.99$, $p<0.001$). These sensors correspond to those typically placed over areas that overlay the middle and posterior portions of the temporal lobe as per the 10-20 International System of Electrode Placement. Sensors were referenced to an average of sensor-clips positioned on either side of the ED.

Alternative geometrical configurations were measured within the three recipes which included the two conductive layers of the three-shell realistic head model (i.e. cortex and scalp) as well as two extra-cranial measurements. Sphere and disk shaped structures were formed with the ED using the same volumes of materials applied intra-

skeletally (180 cc). The surface area of the disk condition (400 cm^2) was equivalent to that of the scalp layer of the three-shell head model.

Five (n=5) eyes-open baseline QEEG profiles were randomly selected from a laboratory database containing hundreds of participants. These data served as baseline measures which could be statistically compared to the electrical activity associated with the ED. Although 19 sensors were involved in all human measurements, only sensors T3, T4, T5, and T6 were used for the current paradigm. Whereas human measurements were consistently within the 100 – 200 μV/cm range, ED activity was increased to approximately 200 – 300 μV/cm.

Computing Additional Variables

Electrodes were clustered into left and right montages as well as a global montage incorporating all four sensors. QEEG measurements (uV^2/Hz) were z-scored, spectral analyzed, and averaged across trials. Transformed variables were then re-combined to generate new factors. An intra-skeletal condition was generated by averaging (interfering) the spectral output of the scalp and cortex layers. An extra-skeletal condition was generated by the same process involving the disk and sphere configurations. Variables were generated for low, medium, and high HIC between and within the geometrical conditions.

Results

There was a moderate, positive correlation between intra-skeletal and human spectral densities within the narrow subset of gamma from 30-50Hz, $r=0.60$, $p<0.001$ corresponding to an effect size of 36% (Figure 2.4). It was determined that the layer

which contributed to this significant relationship was that of the cortex, r= 0.55, p<0.001. Extra-skeletal spectral densities (Figure 2.5) as well as the scalp layer of the three-shell model did not show this relationship.

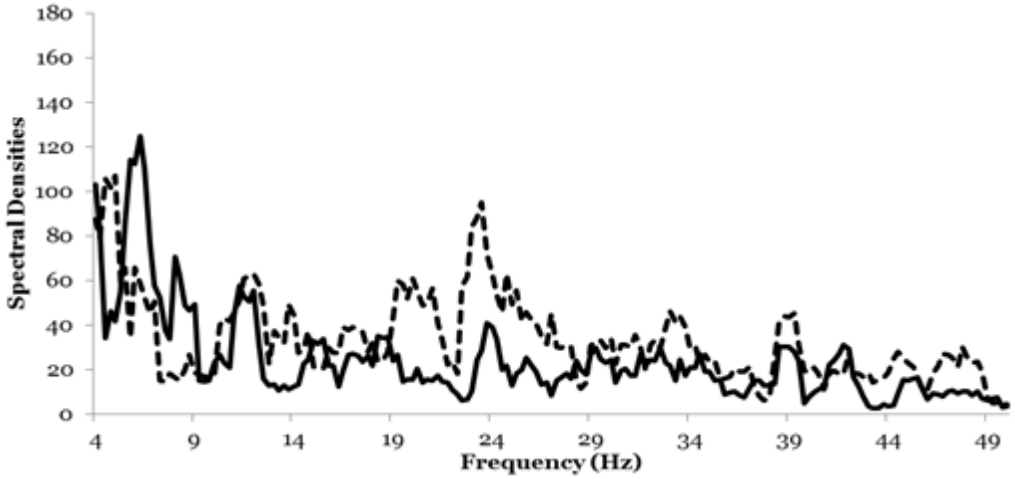

Figure 2.4. Spectral characteristics of z-transformed QEEG measurements of human baseline activity (dotted line) and intra-skeletal ED activity (solid line). The intra-skeletal condition is a composite of measurements obtained over the cortex and scalp layers (ED) bound to the replica skull which, together, forms the three-shell realistic head model.

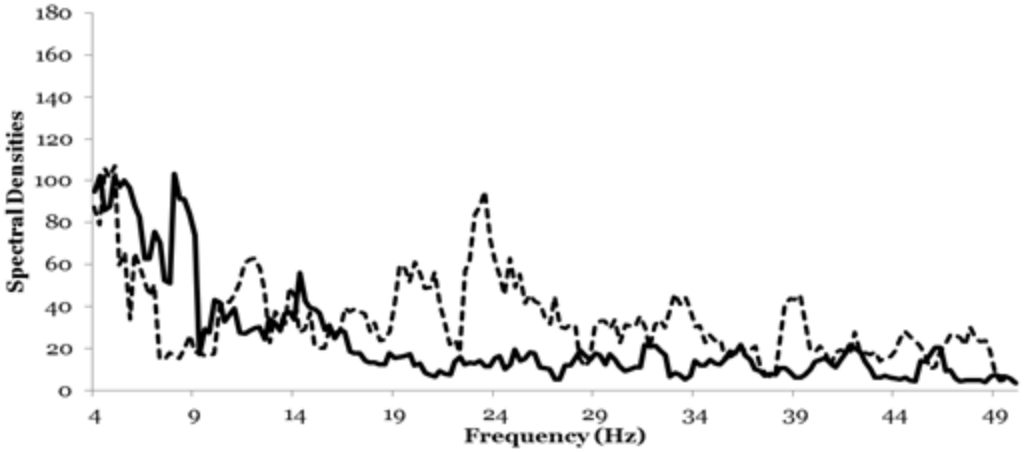

Figure 2.5. Spectral characteristics of z-transformed QEEG measurements of human baseline activity (dotted line) and extra-skeletal ED (solid line). The extra-skeletal condition consists of a composite of measurements obtained over a ball and a disk of ED placed on a flat surface.

Correlational analyses performed for cases associated with Schumann frequency bands revealed a moderate, positive relationship between human and intra-skeletal spectral densities within the fundamental of ~8 Hz ($r= 0.59$, $p<0.005$) as well as the first harmonic or 14 Hz, $r= 0.53$, $p<0.01$. When performing the analysis separately upon the two conductive layers of the three-shell model, spectral densities of the cortex moderately correlated with human spectral densities for the fundamental Schumann frequency ($r= 0.59$, $p<0.005$); however, the scalp layer was not significantly correlated ($r= 0.30$, $p>0.05$). Extra-skeletal spectral densities did not correlate with those of the human sample within the first three frequency bands; however, within the frequency band corresponding to the fourth harmonic (33Hz), extra-skeletal and human spectral densities were moderately correlated, $r= 0.58$, $p<0.005$. The cortex layer spectral densities were also correlated with human spectral densities within the frequency band corresponding to the fourth harmonic ($r= 0.52$, $p=0.01$). This relationship was not observed for the spectral densities derived from the electrical activity of the scalp layer alone or in combination with the cortex layer.

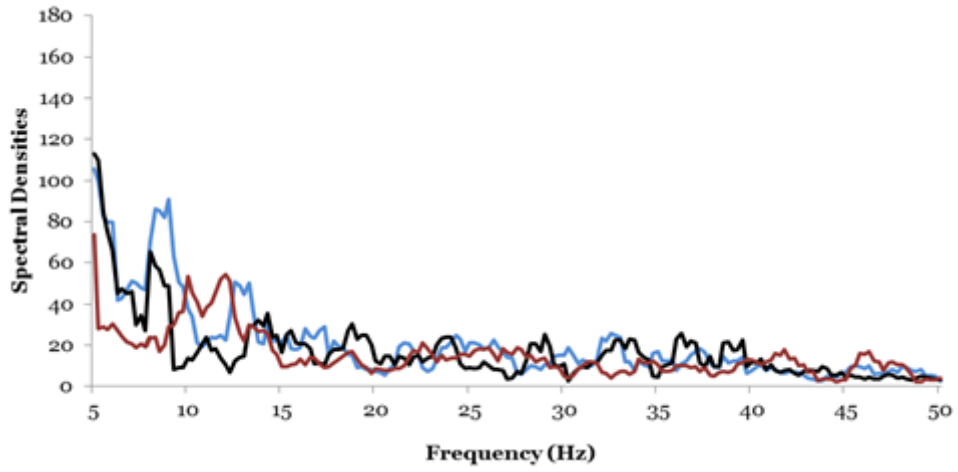

Figure 2.6. Spectral characteristics of ED recipes with high (black), medium (blue), and low (red) hydrogen ion concentrations. ED containing high hydrogen ion concentrations displays peaks typical of the Schumann resonance including 8Hz,14Hz, and ~19Hz. A phase-shifted series of subsequent peaks separated by a relatively constant interval are present.

ED containing high ($r=0.50$, $p<0.001$) and medium ($r=0.48$, $p<0.001$) proton concentrations showed moderate, positive correlations with human spectral densities between 30-50Hz which were not apparent for the low concentration conditions, $r= -0.01$, $p>0.05$. The observed correlations were not significantly different, $zF = -0.16$, $p>0.05$. Figure 2.6 shows that the spectral characteristics emergent of the high hydrogen ion concentration condition (black) displays peaks of increased oscillatory activity within frequency bands associated with the Schumann resonance. The low hydrogen ion condition (red) displayed relatively equal contributions of power under most frequency bands (i.e. increased noise) with the exception of the 10-13 Hz range.

Examining the simulated cortex layer only for each proton concentration condition for the typical waking, human electroencephalographic bandwidth (4-50Hz) revealed a moderate positive correlation between spectral densities of the high hydrogen ion concentration cortex condition and human spectral densities ($r= 0.60$, $p<0.001$). Figure 2.7 shows spectral densities associated with the high hydrogen ion concentration cortex condition with human spectral densities. This relationship, although observed, was significantly diminished for the low and medium hydrogen ion concentration cortex conditions, $zF > 1.96$, $p< 0.01$. There was also a significant difference between the correlation coefficient illustrated in Figure 2.8 and the significant but weak correlations between human spectral densities and those of the ED sphere ($r= 0.38$, $p<0.001$) and ED disk ($r=0.41$, $p<0.001$), $zF > 1.96$, $p<0.001$. Figure 2.8 and 9 show the ED that were

shaped as a sphere or a disk paired with human spectral densities. These results suggest that the intrinsic oscillatory activity of the cortex layer within the “high” hydrogen ion concentration condition was more strongly associated with human spectral densities than any other condition.

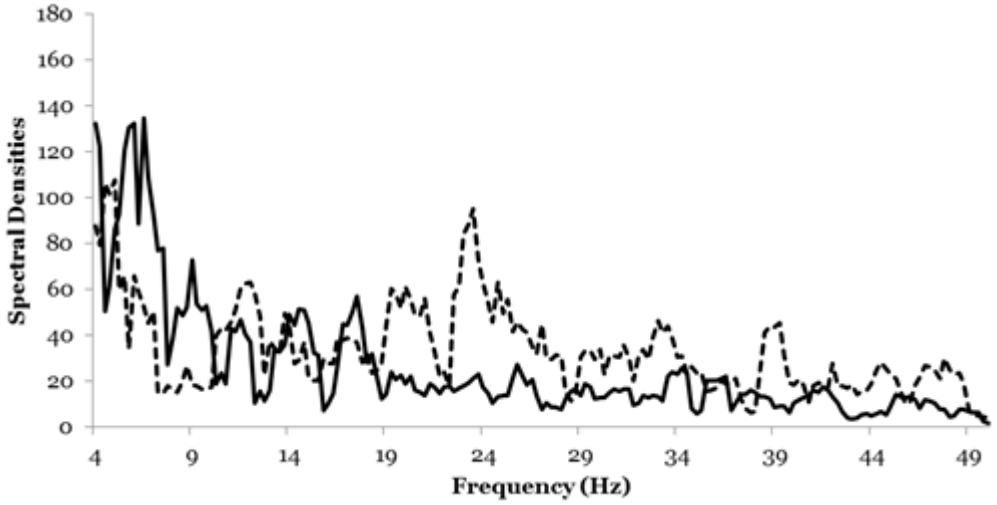

Figure 2.7. Spectral characteristics of z-transformed QEEG measurements of human baseline activity (dotted line) and activity associated with the cortex layer of the three-shell head model within the high hydrogen ion concentration condition (solid line).

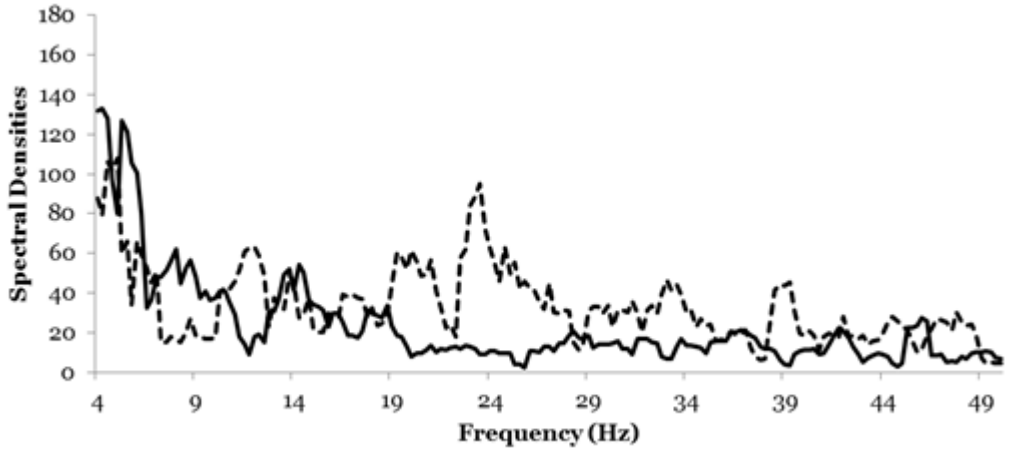

Figure 2.8. Spectral characteristics of z-transformed QEEG measurements of human baseline activity (dotted line) and activity associated with ED as a sphere placed on a flat surface (solid line).

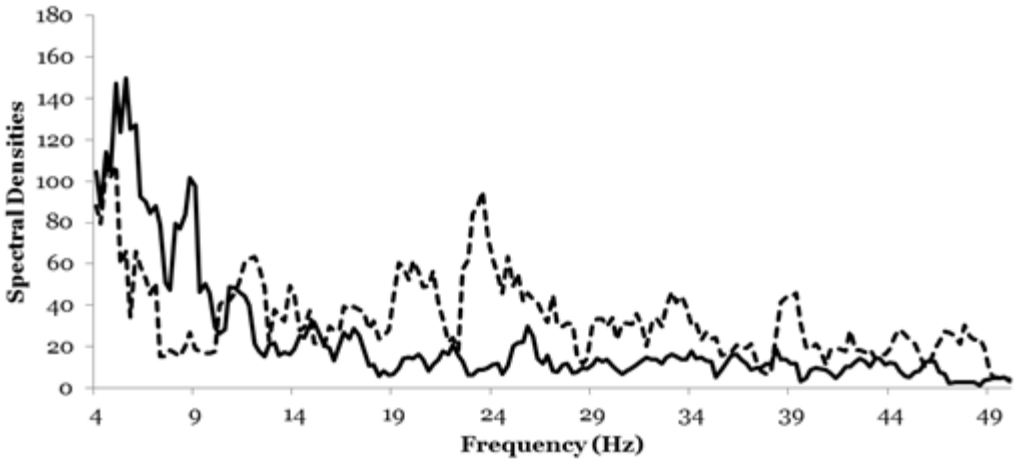

Figure 2.9. Spectral characteristics of z-transformed QEEG measurements of human baseline activity (dotted line) and activity associated with ED as a disk placed on a flat surface (solid line).

Discussion

The "spontaneous" spectral densities for an electro-conductive medium (ED) occupying the approximate volume of the human cerebral cortices and containing "high" (pH=2.47) or "medium" (pH=2.52) proton concentrations showed a significant overlap with human spectral densities which were not present for the "low" (pH=2.66) concentration condition. Other geometries, such as a flat disk or solid spherical shape did not display these significant cross-correlations with actual human cerebral cortical spectral densities.

The fact that a critical number of protons were required strongly indicates the moderate strength correlation between spectral densities observed from passive measurement of the ED and those of actual human brains was not an artefact of the QEEG or our procedures. If procedural artefacts were present then the moderate strength correlations should have been evident when all concentrations of protons were

employed. However, the significant correlations were only evident for the pH values <2.53.

The direct application of these results and this model to actual brain function may appear to be limited by the marked discrepancy in pH. The typical levels of pH in intracellular space during neuronal activity are around 7.0 with shifts of about 0.2 pH units. On the other hand the pH levels within our ED simulation was much more acidic, about pH=2.5. The most parsimonious solution to this apparent discrepancy involves the numbers of H+ within the functional volume. The ionic source of the resting membrane potential for plasma cell membranes for soma around 10 μm in width is about the width of a Bohr radius or $5.6 \cdot 10^{-9}$ cm (Persinger, 2012). The shell (assuming a sphere) occupied by this additional volume is $1.8 \cdot 10^{-14}$ cc. The numbers of H^+ (M=10-pH) within this volume with a pH=2.5 would be $3.16 \cdot 10^{-3}$ M multiplied by $9.8 \cdot 10^{-16}$ cc ($1.8 \cdot 10^{-14}$ cc divided by 18 cc per M) or $31 \cdot 10^{-19}$ M. When multiplied by Avogadro's constant, the numbers of H+ would be about 1.9×10^6 molecules.

On the other hand, the volume occupied by a shell that extends 1 μm from the cell, where experimental pH levels are typically taken, would involve a volume of $3.8 \cdot 10^{-10}$ cc or $2.1 \cdot 10^{-11}$ cc ($3.82 \cdot 10^{-10}$ divided by 18 cc per M). For a pH of 7 the numbers of H+ would be the same order of magnitude (about 10^6) as that calculated for the more acidic pH within a single layer of charges. Interesting this is the estimated numbers of charges required to maintain the resting plasma membrane potential (Persinger, 2010). This convergence suggests that the functional concentration of H+ along the proximal surface that markedly influences the resting cell membrane potential is much more acidic than typically assumed and more typical of what we employed in the ED model. The primary difference between the ED "cerebral cortex" and the natural human

cerebral cortex is that the thin shell of protons would line an extraordinarily complex surface structure along the membrane of neuronal soma, dendrites and axons within the ~3 mm thick cortical shell.

The convergent of numbers of H^+ for the measured neuronal environment when the single layer of charge along the plasma cell membrane is considered has significant implication for mechanisms of consciousness. According to Bordag et al. (2001) only the surface layer of atoms or charges can be considered a continuum. It is this continuum that interacts with an electromagnetic field. The Casimir effect, which emerges in space-times with nontrivial topology (such the cerebral cortex) is the interaction between a pair of parallel conducting plates due the disturbance of the vacuum of the electromagnetic field. Bordag et al. (2001) describes this process as a pure quantum effect. This connects the Casimir effect to the existence of Zero Point Fluctuations and the forces coupled with Gravity (Puthoff, 1989).

That gravity is relevant to consciousness is illustrated by the solution for the potential energy for a human brain's mass. Gravitational energy is classically defined as $G \bullet kg^2 \bullet m^{-1}$, where G is the Newtonian Gravitational Constant ($6.67 \bullet 10^{-11}$ $m^3 \bullet kg^{-1} \bullet s^{-2}$), kg is the mass of the human brain (assume 1.5 kg) and m is the average length (assume 12 cm). The resulting energy is $1.25 \bullet 10^{-9}$ J. Assuming an increment of energy of $\sim 2 \bullet 10^{-20}$ J for the effects of an action potential (120 mV) upon a unit charge ($1.6 \bullet 10^{-19}$ A•s) with the average frequency of 10 Hz, the gravitational energy would have the potential to be equivalent to about 10^{10} neurons, which is with the order of magnitude of functioning cells within the human cerebral cortices (Persinger, 2010).

For the entire volume, we suggest the value of $\sim 10^{21}$ units represents a critical threshold – a necessary condition – at which point Schumann-type oscillations are

present in the spectral profile of the ED. Assuming the hydron isotope of a proton (H+) with an associated mass of $1.67 \bullet 10^{-27}$ kg, the mass equivalency of $\sim 10^{21}$ protons is $1.5 \bullet 10^{-6}$ kg. Because the typical cell is 1 nanogram or 10^{-12} kg, the number of cells associated with this mass-equivalency of the hydron threshold is $\sim 1.5 \bullet 10^{6}$ cells or between 1 and 2 million. This is the approximate number of cells which constitute the hippocampus (Levy et al., 2004), a body which is linked to Schumann activity (Persinger, 2008). The value of 10^{6}-10^{7} neurons also constitutes the typical discrete cluster of cells associated with a "thought" (Levy et al., 2004).

We pursued the idea that hydrogen ion matrices composed of a minimum of $\sim 10^{21}$ units are intrinsic receptive structures associated with the Schumann resonance. The volume of the human neocortex is $\sim 5 \bullet 10^{2}$ ml on average with considerable variability within and between sexes (Pakkenberg, 1997). Converting to grams, ~60% of the mass is water or $3 \bullet 10^{2}$ g. This mass can be further reduced to its hydrogen component which is 11% by proportional mass or a total of 33 g. If the molar mass of H_2O is 18 g/M, this volume represents 1.83 M that, when multiplied by Avagadro's number gives $1 \bullet 10^{24}$ units within the human cerebral cortex of available hydrogen to dissociate. If the ED and the cerebral cortex are responding in the same way due to microstructural similarity in hydron content, the suggestion would be that a critical threshold of hydron units is needed to resonate with the ionosphere and express the Schumann pattern.

Spectral densities associated with the intra-skeletal condition optimally correlated with human baseline brain activity. This was primarily due to the cortex layer of the model, which suggests an intrinsic role of the shape of the skull in the representation of Schumann patterns in QEEG profiles. Nunez (1995) has presented

works which demonstrate that the bulk velocity of action potentials within the cerebral cortices (4.5 $m \cdot s^{-1}$) applied over a skull with a 60 cm circumference would generate a standing wave of approximately 7.5 Hz – a value approximating the fundamental Schumann resonance frequency. A recent quantitative analysis of Earth-Brain interactions has revealed multiple convergences which suggest a profound relationship between the two structures (Persinger, 2014). Where neurons contained within the skull provide structure, the chemical and geometrical orientation of the space surrounding neurons are the primary interfaces for phenomena which precede the action potential. In the absence of neurons, the lattice of the dough might provide a similar network of structures along which signals might propagate in the presence of an external electromagnetic stimulus.

In this study, synchronous gamma oscillations within the 40Hz range were measured in a three-shell realistic head model which was constructed to simulate the basic organization of the human cortex, scalp, and skull. As a neural correlate of consciousness, the expression of synchronous gamma in an intra-skeletal organization of ED does not indicate that the experimental apparatus was conscious. The only suggestion here is that a neural correlate of consciousness which operated within parameters similar to that observed in humans was disembodied from any neuronal substrate in a geometrical and chemical approximation of the components of the brain measured by the QEEG. These distinct, physiologically-patterned oscillations were not present in the same material shaped as a sphere or disk placed outside of the skull.

One theoretical solution involves a transmission theory of brain activity whereby an external signal is filtered by the brain and intermediate tissues (James, 1898). Coherent oscillations across spaces which do not accommodate typical structural connections

would be accommodated as receptive fields and would respond similarly to the application of the external stimulus. These responses, although simultaneous and independent, would be coherent and perhaps vulnerable to intra-cerebral resonance phenomena. Synchronous activity across brain-space is intrinsically linked to the binding problem (Meador, 2002). If the three-shell model is operating as an antenna and receiving signals from the environment, this project lends experimental validity to the metaphor of consciousness and other brain functions as transmitted information.

Kuhn (1962) argued that paradigm shifts are necessary and are brought about by a growing sense that existing models, albeit once optimally useful in pursuit of further knowledge, have malfunctioned in some fundamental way. In order to accommodate the observations that consciousness has avoided the traditional neuroscientific line of inquiry involving localization of function in brain-space, the idea of extra-cerebral signals and the information contained within them must be seriously considered as a potential source for the neural correlates of consciousness.

Conclusion

Here we present results indicating oscillatory electrical activity in a non-human model of the human head displays spectral densities that correlate with those of human subjects obtained over the scalp using QEEG technology. Quantification suggests a central role of the proton in relation to the physical dimensions of the cell. Further experiments are required which would parcel out the environmental contributions to the neural correlates of consciousness and other functions typically ascribed to the brain. In particular, the capacity for this preparation to show simulations of “memory”,

that is the representation of previous stimuli no longer present, and learning, the more or less permanent change in responsiveness due to experience, should be demonstrable.

References

Alberts, B., Bray, D., Lewis, J., Raff, M., Roberts, K., & Watson, J. D. (1994) Molecular Biology of the Cell, .Garland, New York, 50-56.

Alonso, A., & Klink, R. (1993). Differential Electroresponsiveness of Stellate and Pyramidal-Like Cells of Medial Entorhinal Cortex Layer II. *Journal of Neurophysiology*, 70(1), 128-143.

Bear, M. F. (1996). A Synaptic Basis for Memory Storage in the Cerebral Cortex. *Proceedings of the National Academy of Sciences*, 93(24), 13453-13459.

Schlegel, K., & Füllekrug, M. (2002). 50 Years of Schumann Resonance. *Physik in unserer Zeit*, 33(6), 256-264.

Beg, A. A., Ernstrom, G. G., Nix, P., Davis, M. W., & Jorgensen, E. M. (2008). Protons Act as a Transmitter for Muscle Contraction in C. elegans. *Cell*, 132, 149-160.

Berg, P., & Scherg, M. (1994). A Fast Method for Forward Computation of Multiple-Shell Spherical Head Models. *Electroencephalography and Clinical Neurophysiology*, 90, 58-64.

Bevan, S. (1998) Proton-Gated Ion Channels in Neurons. In: Kaila, K. and Ransom, B.R., Eds., pH and Brain Function, Wiley-Liss, New York, 447-476.

Bordag, M., Mohideen, U. & Mostepanenko, V. M. (2001). New developments in the Casimir effect. *Physics Reports*, 353, 1-205.

Burke, R. C., & Persinger, M. A. (2013). Convergent Quantitative Solutions Indicating the Human Hippocampus as a Singularity and Access to Cosmological Consciousness. *NeuroQuantology*, 11(1).

Cherry, N. (2002). Schumann Resonances, a Plausible Biophysical Mechanism for the Human Health Effects of Solar. *Natural Hazards*, 26, 279-331.

Cherry, N. (2003). Human Intelligence: The Brain, an Electromagnetic System Synchronised by the Schumann Resonance signal. *Medical Hypotheses*, 60, 843-844.

Cifra, M., Fields, J. Z., & Farhadi, A. (2011). Electromagnetic Cellular Interactions. *Progress in Biophysics and Molecular Biology*, 105(3), 223-246.

Crick, F., & Koch, C. (1990). Towards a Neurobiological Theory of Consciousness. *Seminars in the Neurosciences*, 2, 263-275.

Deamer, D. (2011). Consciousness and Intelligence in Mammals: Complexity Thresholds. *Journal of Cosmology*, 14.

Decoursey, T. E. (2003). Voltage-Gated Proton Channels and Other Proton Transfer Pathways. *Physiological Reviews*, 83(2), 475-579.

Dotta, B. T., Buckner, C. A., Lafrenie, R. M., & Persinger, M. A. (2011). Photon Emissions From Human Brain and Cell Culture Exposed to Distally Rotating Magnetic Fields Shared by Separate Light-Stimulated Brains and Cells. *Brain Research*, 1388, 77-88.

Ermer, J. J., Mosher, J. C., Baillet, S., & Leahy, R. M. (2001). Rapidly Recomputable EEG Forward Models for Realistic Head Shapes. *Physics in Medicine and Biology*, 46, 1265.

Gang, N., St-Pierre, L. S., & Persinger, M. A. (2012). Water Dynamics Following Treatment by One Hour 0.16 Tesla Static Magnetic Fields Depend on Exposure. *Water*, 3, 122 – 131.

Highstein, S. M., Holstein, G. R., Mann, M. A., & Rabbitt, R. D. (2014). Evidence That Protons Act as Aeurotransmitters at Vestibular Hair Cell–Calyx Afferent Synapses. *Proceedings of the National Academy of Sciences*, 111(14), 5421-5426.

James, W. (1898). Human immortality: Two Supposed Objections to the Doctrine. Boston: Houghton Mifflin.

König, H. (1971). Meteorological Cycles: Biological Effects of Extremely Low Frequency Electrical Phenomena in the Atmosphere. *Biological Rhythm Research*, 2, 317-323.

Kuhn, T. S. (1962). The Structure of Scientific Revolutions. University of Chicago Press, 1-15.

Levy, I., Hasson, U. & Malach, R. (2004). One Picture is Worth at Least a Million Neurons. *Current Biology*, 14(11), 996-1001.

Llinas, R., & Ribary, U. (1993). Coherent 40-Hz Oscillation Characterizes Dream State in Humans. *Proceedings of the National Academy of Sciences*, 90(5), 2078-2081.

McIntosh, A. R. (2000). Towards a Network Theory of Cognition. *Neural Networks*, 13, 861-870.

Meador, K. J., Ray, P. G., Echauz, J. R., Loring, D. W., & Vachtsevanos, G. J. (2002). Gamma Coherence and Conscious Perception. *Neurology*, 59, 847-854.

Murugan, N.J., Karbowski, L.M., Persinger, M.A. (2014). Serial pH Increments (~20 to 40 milliseconds) in Water During ExPosures to Weak, Physiologically Patterned Magnetic Fields: Implications for Consciousness. *Water*, 6, 45-60.

Nunez, P.L. (1995). Neocortical Dynamics and Human EEG Rhythms. Oxford University Press, New York.

Pakkenberg, B., & Gundersen, H. J. G. (1997). Neocortical Neuron Number in Humans: Effect of Sex and Age. *Journal of Comparative Neurology*, 384, 312-320.

Persinger, M. A. (1976). Day Time Wheel Running Activity in Laboratory Rats Following Geomagnetic Event of 5–6 July 1974. *International Journal of Biometeorology*, 20, 19-22.

Persinger, M. A. (2008). On the Possible Representation of the Electromagnetic Equivalents of all Human Memory Within the Earth's Magnetic Field: Implications for Theoretical Biology. *Theoretical Biology Insights*, 1, 3-11.

Persinger, M. A. (2010). 10^{-20} Joules as a Neuromolecular Quantum in Medicinal Chemistry: An Alternative Approach to Myriad Molecular Pathways?. *Current Medicinal Chemistry*, 17(27), 3094-3098.

Persinger, M. A. (2012). Brain Electromagnetic Activity and Lightning: Potentially Congruent Scale-Invariant Quantitative Properties. *Frontiers in Integrative Neuroscience*, 6(19), 1-7.

Persinger, M. A. (2013). Billions of Human Brains Immersed Within a Shared Geomagnetic Field: Quantitative Solutions and Implications for Future Adaptations. *Open Biology Journal*, 6, 8-13.

Persinger, M. A. (2014). Quantitative Convergence Between Physical-Chemical Constants of the Proton and the Properties of Water: Implications for

Sequestered Magnetic Fields and a Universal Quantity. *International Letters of Chemistry, Physics and Astronomy*, 1(10), 1-10.

Persinger, M. A., & Dotta, B. T. (2011). Temporal Patterns of Photon Emissions Can Be Stored and Retrieved Several Days Later From the" Same Space": Experimental and Quantitative Evidence. *NeuroQuantology*, 9(4), 605-613.

Puthoff, H. E. (1989). Source of Vacuum Electromagnetic Zero-Point Energy. *Physical Review A*, 40(9), 4857.

Schumann, W. O. (1952). On the Free Oscillations of a Conducting Sphere Which is Surrounded by an Air Layer and an Ionosphere Shell. *Z. Naturforschaft*. 7A, 149-154.

Stewart, L. S., & Persinger, M. A. (2000). Pretraining Exposure to Physiologically Patterned Electromagnetic Stimulation Attenuates Fear-Conditioned Analgesia. *International Journal of Neuroscience*, 100, 91-98.

West, M. J., & Gundersen, H. J. G. (1990). Unbiased Stereological Estimation of the Number of Neurons in the Human Hippocampus. *Journal of Comparative Neurology*, 296(1), 1-22.

(Submitted to Brain Research)

Chapter 3: Simultaneous and Trace Conditioning are Reflected in Spectral Power Densities of Potential Differences and Microstructural Reorganization of Constituents in Brain pH Dough

Abstract

An electrically conductive material composed of carbohydrates, proteins, fats, ions, water, and trace amounts of vitamins and minerals was classically conditioned as inferred by quantitative electroencephalographic (QEEG) measurements. Spectral densities during the display of a conditioned stimulus (CS) probe were strongly congruent with those displayed during the CS-UCS. The neutral stimulus consisted of the pulsed light from a LED. The unconditioned stimulus (UCS) was an alternating current. Interstimulus intervals >130 ms did not result in conditioned responses. Microscopic analysis of the chemically-fixed substratum revealed 10-200 μm wide 'vessel structures' within samples exposed to a stimulus. Greater complexity (increased fractal dimensions) was clearly discernable by light microscopy for stained sections of fixed samples that had been conditioned compared to various controls. The denser pixels indicated greater concentration of stain and increased canalization. Implications for learning, memory formation, and the natural selection of primitive nervous systems are discussed.

Keywords: associative learning, classical conditioning, trace conditioning, memory, neural simulation, neural evolution

Introduction

Associative learning is a feature of the nervous system that has been studied extensively (Pavlov, 1927; Skinner, 1938) and represents one of many ways by which the microstructure of the brain can accommodate functional modifications. The storage or more accurately the representation and release or "retrieval" of information within brain-space as memory can be separated by great intervals of time. This property allows organisms to operate functionally beyond the specious present and to access the representation of events not present within the immediate sensory environment. Mechanisms underlying these processes have been characterized at the cellular and subcellular levels in biological organisms (Hawkins et al., 1983; Malenka & Bear, 2004). However, the observation that ferromagnetic materials can be conditioned (Cragg & Temperley, 1955) suggests a fundamental physical basis to learning which can perhaps be generalized to other systems.

Classical conditioning is a type of associative learning which involves pairing stimuli in space-time (space-time contiguity) to elicit responses using previously neutral stimuli (Gormezano, Kehoe, & Marshall, 1983). A stimulus must elicit a physiological response and necessarily be an event to which the organism is receptive. There are many forms of energy which can be sequestered by an organism. There are also innumerable events, many of cosmic origin, that do not constitute stimuli at all. In classical conditioning, the neutral stimulus becomes a conditioned stimulus (CS) after being paired with an unconditioned stimulus (UCS). The presentation of the CS elicits a conditioned response (CR). The CR reflects major features of the UCR but is rarely identical to the UCR with respect to major properties, such as amplitude. The net effect

of learning is that a previously neutral stimulus – generating no specific response – becomes capable of generating a response which it would not have generated if space-time contiguity of the CS and UCS had not occurred.

A variety of learning procedures have been developed which are collectively termed classical conditioning. Simultaneous conditioning involves presenting and terminating the CS and UCS during the same temporal interval (Burkhardt & Ayres, 1978). The two stimuli therefore overlap entirely, requiring a narrow time-frame of reception on the part of the organism. Trace conditioning, however, involves presenting and terminating the neutral stimulus before the onset of the UCS (Beylin et al., 2001). A short interval of time devoid of any stimulation occurs between the two stimuli. This hiatus is traditionally labelled the "interstimulus" or trace interval. A represented trace of the neutral stimulus within the subject is therefore required to effectively pair it with the UCS. This demands a capacity to store short-term traces of information for the minimum time of the interstimulus interval. Simultaneous conditioning is a classical method by which the learning capacity of an organism can be determined whereas trace conditioning represents a method by which one can determine its temporal range.

Recent work has demonstrated electrical activity characteristics, as inferred by quantitative electroencephalography, of the neural correlates of consciousness in electroconductive dough. The phenomenon was most conspicuous when the pH of the dough was similar to the equivalent proton concentrations adjacent to the neuronal cell membrane (Rouleau & Persinger, 2014). The material displayed spectral densities within frequency bands characteristic of human brain activity, but only when the specific chemical and geometrical conditions were present. The potentially shared

sources of variance between this model and the brain were considered by these authors to involve the proton within the hydronium ion. The most likely mechanism involved cerebral networks of interfacial water are critically important for modulating functions. The magnitude and the reliability of our results suggested that there could be information storage capacity for this material and that it might be able to "maintain the representation" of relevant stimuli. In other words, it might be "conditionable".

The aim of the current study was to induce a conditioned response in an inanimate object whose properties exhibited the major chemical characteristics of brain tissue. The two most important components appear to be the geometry of the medium and the narrow band of proton concentrations (pH) in aqueous solutions containing physiological-like concentrations of ions. To this end, two primary experiments were designed. Experiment 1 involved exposing the dough to an electric shock (UCS) paired simultaneously with an LED (CS) as a pulse pattern (10Hz). After a temporal delay, a probe (CS) was displayed in order to elicit a potential CR. Electrical potentials were recorded throughout the trials using traditional QEEG equipment. Experiment 2 involved pairing the same UCS and CS with inter-stimulus delays of varying durations in order to discern the temporal sensitivity of the material. A confirmed CS-CR pattern was operationalized as a display of spectral densities within a probe period (CS only) which significantly correlated with the spectral density profile of the UCS-UCR as measured by QEEG during the training phase. In other words, the electrical patterns displayed by the dough when it was being shocked should, in principle, be displayed during the probe phase if the LED-shock pairing was effective. These same patterns should not be present

during the pre-training baseline. The presentation of the LED pattern alone, initially, did not elicit a UCR ($p>.05$) and was therefore classified as a neutral stimulus.

Samples of the dough, exposed to various combinations of the UCS and CS, then underwent chemical fixation, processing, and paraffin embedding procedures that we typically utilize for histological studies. After staining sections of the dough, quantification of microstructures within the dough was performed using light microscopy. The purpose of this structural analysis was to compliment the functional analysis of the CS-CR relationship using QEEG. Together, these measures demonstrated the structure-function relationships which are characteristic of learning except they occurred in an "inanimate" object.

Results

Experiment 1: Simultaneous Conditioning

An examination of the spectral profile of the QEEG data associated with the stimulation period (UCS-UCR) during the training phase revealed a clear 10Hz peak which defines the CR (Figure 1). Harmonics at 20Hz and 30Hz were noted with an emerging sub-harmonic at ~1Hz, confirming the effectiveness and effect of the 10Hz stimulus. All simultaneous conditioning experiments involved the 10Hz stimulus as the effective UCS-UCR. Consequently, the 9Hz to 11Hz band was selected as the window within which spectral densities across periods were correlated for simultaneous conditioning trials.

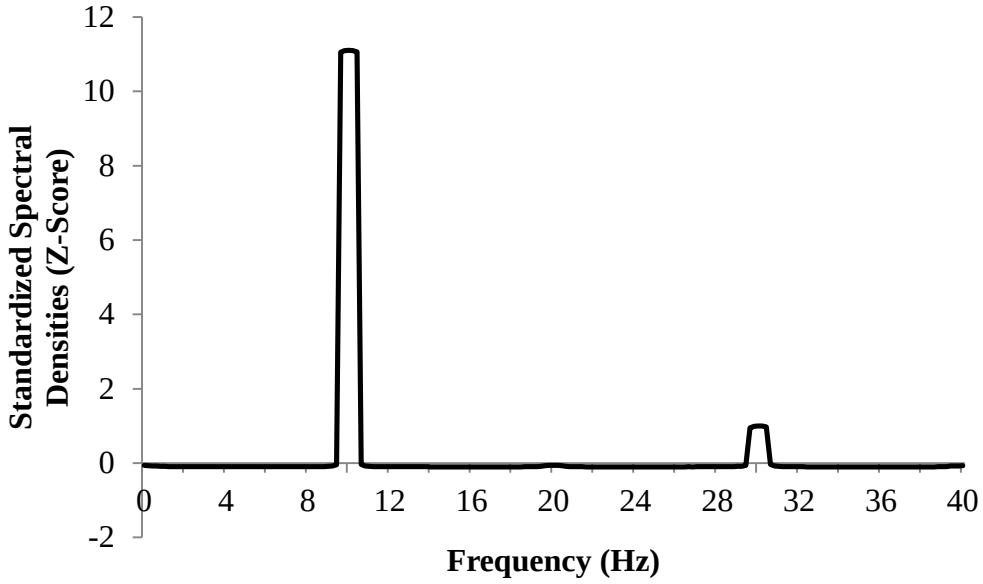

Figure 3.1. Mean standardized (z-score) spectral densities of the training phase (CS-UCS) displaying a clear peak (z>10) at approximately 10Hz. Harmonics are present at both 20Hz and 30Hz.

Trials associated with a training phase consisting of five (5), 10s periods of 10Hz stimulation revealed significant correlations between spectral densities associated with electrical potentials recorded during the probe period (CR) and the training phase (CS-UCS) after a 5 minute delay immediately following the training phase, rho= -.71, $p<.05$. This relationship persisted after a 10 minute delay, rho= -.92, $p<.001$. Pre-training electrical potentials did not exhibit spectral content reflective of the UCS-UCR ($p>.05$). Ten (10), 10s periods of 10Hz CS-UCS pairings resulted in a significant correlation between spectral densities of electrical potentials during the training phase (CS-UCS) and probe period (CR) after a 5 minute delay following the training phase, rho= -.92, $p<.001$. However, spectral densities of electrical potentials obtained during the pre-exposure baseline also correlated with the probe period (CR) following a 5 minute delay post-training phase, rho= .80, $p<.01$.

Experiment 2: Trace Conditioning

A systematic analysis of potential CRs as a function of the duration of the interstimulus delay was revealing. Interstimulus intervals between 3ms and 500ms were examined. Probe period (CR) and training phase (CS-UCS) spectral densities were significantly correlated after a 1 minute delay following the training phase for the 3ms (rho= -.78, p<.05), 25ms (rho= .73, p<.05), 100ms (rho= .85, p<.005), and 130ms (rho= -.75, p<.05) interstimulus interval conditions. This was not the case for 150, 170, 200, 300, and 500ms conditions (p>.05). These results are represented in Figure 2.

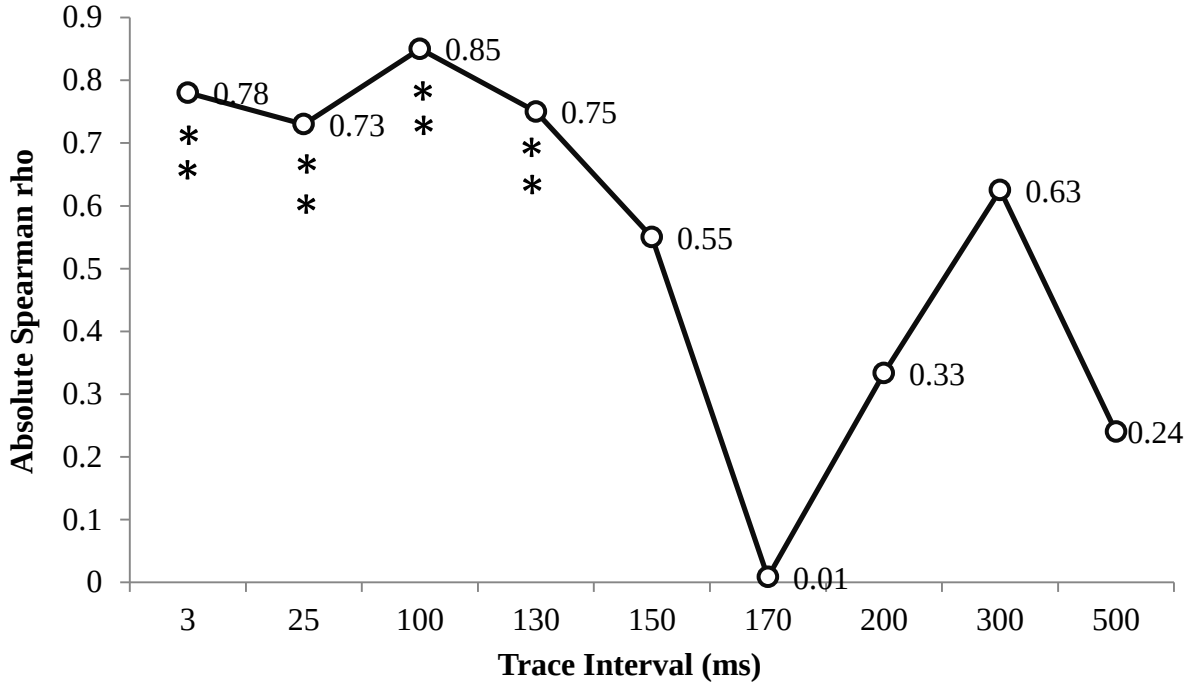

Figure 3.2. Plotted absolute non-parametric correlation coefficients (Spearman rho) demonstrating the systematic relationship between the spectral densities of the training phase (UCS-UCR) and the probe period (CS-CR).

Figure 3 demonstrates the relationship between the CR and the CS-UCS for the 3ms interstimulus interval condition as standardized spectral densities, displaying approximately z= 2.0 deviations (with opposite direction) as a function of the frequency peak associated with the UCR within the 17Hz to 19Hz band. This frequency band is relevant because the combined duration of the CS (25ms), UCS (25ms) and interstimulus delays (3ms) between the stimuli result in a cycle equivalent to 17.9Hz or ~18Hz. The true shift in raw μV values associated with the probe period was equivalent to a change of approximately 10 μV. As a relative comparison, the standardized shifts in spectral densities presented in Figure 3 associated with the training phase (for any trace condition) are equivalent to actual shifts of 1000 – 2500 μV.

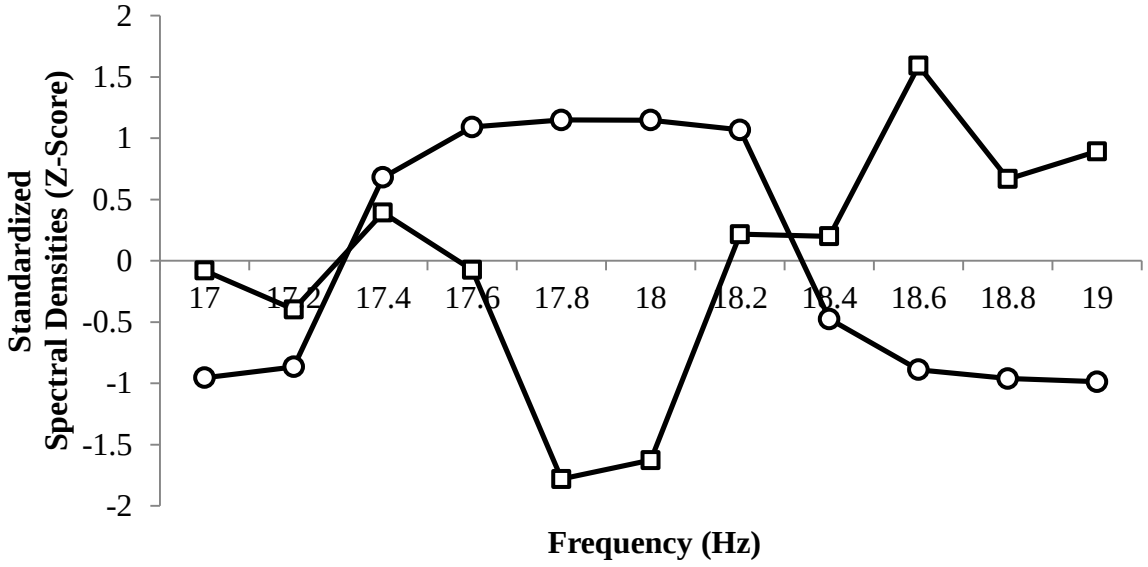

Figure 3.3. Mean standardized spectral densities (z-scores) computed from measurements obtained during the probe period (CR; squares) for the 3ms trace interval trials involving a 1 minute delay following the training phase with 0.2Hz increment deviations within the 17Hz to 19Hz band. Condition-matched data for the training phase or UCS-UCR (circles) is also plotted.

Probe period (CR) and training phase (CS-UCS) spectral densities were significantly correlated after a 5 minute delay post-training phase for the 3ms (rho= -.85, $p<.05$), 25ms (rho= -.75, $p<.05$), 100ms (rho= .82, $p<.005$), 130ms (rho= -.68, $p<.05$), and 170ms (rho= -.68, $p<.05$) interstimulus interval conditions. This was not the case for 150, 200, 300, and 500ms conditions ($p>.05$). Pre-training spectral densities were also correlated with the training phase for the 130ms (rho= -.87, $p<.005$) and 170ms (rho= -.97, $p<.001$) interstimulus interval conditions. These results suggested an intrinsic property within the dough whereby an interval between the two events of less than 130 ms or the equivalent of 7.7 Hz could be associated.

Microscopy Data

Complexity measures for slides of paraffin-embedded sections of the fixed dough stained with Toluidine Blue O and Periodic Acid-Schiff were positively correlated (r= .53, $p<.01$, rho= .56, $p<.005$), demonstrating reliability of the tools. Only TBO-associated data (n= 40) are presented for simplicity, although it should be noted that effects were comparable for both stain types. An ANOVA revealed differences in complexity between exposure conditions prior to chemical fixation, $F(4,39)= 6.10$, $p=.001$, explaining 41% of the variance. Conditioned dough displayed increased complexity relative to controls, $t(14)= 2.99$, $p=.01$, $r^2 = .39$. Similarly, conditioned dough displayed increased complexity relative to conditioned dough that had been crushed before being chemically fixed, $t(14) = 4.29$, $p=.001$, $r^2= .57$. Comparing complexity scores for controls and conditioned-crushed dough as well as controls and light-exposed dough revealed no significant differences ($p>.05$). However, shock-exposed dough was

marginally more complex relative to controls, t(14)= 2.61, p<.05, explaining 30% of the variance. Complexity scores associated with light- and shock-exposed dough were significantly greater than those of conditioned-crushed dough, explaining 33% and 67% of the variance respectively. Conditioned dough, light-exposed dough, and shock-exposed dough displayed comparable levels of complexity (p>.05). These results are summarized in Figures 4 and 5.

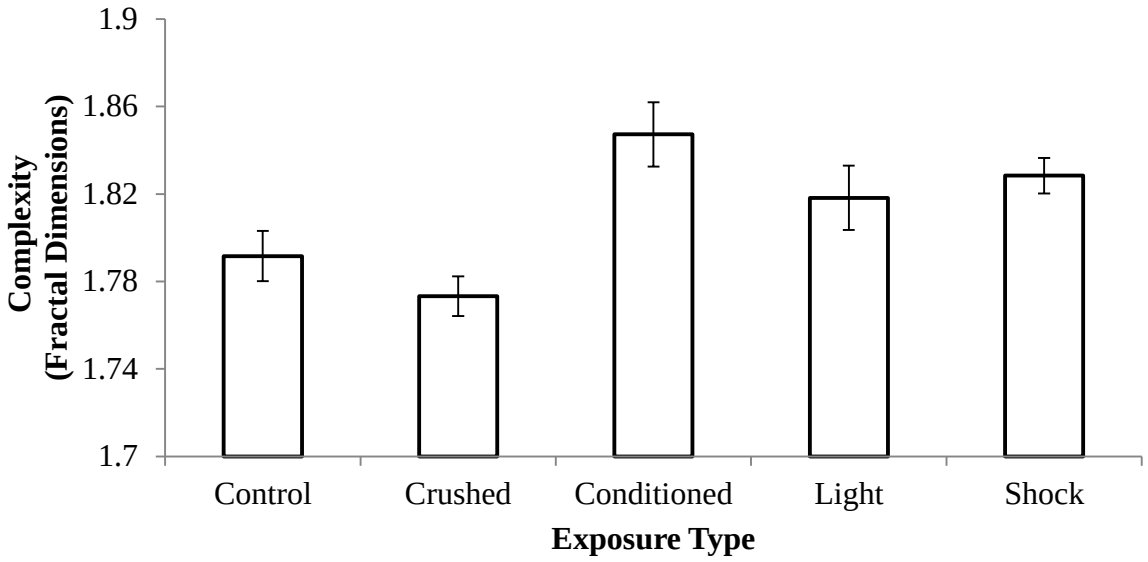

Figure 3.4. Mean complexity (fractal dimension) scores extracted from 8-bit, binary images of sectioned dough stained with TBO, plotted as a function of exposure type prior to chemical fixation. Standard error bars are provided.

Statistically significant differences in the average number of blue pixels contained within photographs of stained slides (Figure 5), a measure of TBO staining, were observed as a function of the exposure conditions [F(4,39)= 3.38, p<.05, explaining 29% of the variance]. A similar effect was noted for cyan pixels, F(4,39)= 6.91, p<.001, explaining 44% of the variance. Conditioned dough was associated with a greater

number of cyan pixels than controls or non-treated dough [t= 2.99, p<.05, r^2= .39]. Conditioned dough was similarly associated with a greater number of cyan pixels relative to conditioned-crushed dough, t= 2.61, p<.05, r^2= .33. Blue and cyan pixel counts were not significantly different when comparing controls and conditioned-crushed dough. However, controls were associated with less blue pixels relative to light-exposed dough, t(14)= -2.71, p<.05, r^2= .34. Controls were also associated with less cyan pixels relative to light-exposed dough, t(14)= -3.81, p<.005, r^2= .51. Differences were only obtained when examining cyan pixel counts when comparing controls to shock-exposed dough, t(14)=-2.96, p<.05, r^2= .38. Conditioned dough , as well as light- and shock-exposed dough did not demonstrate any differences across blue or cyan pixel counts (p>.05).

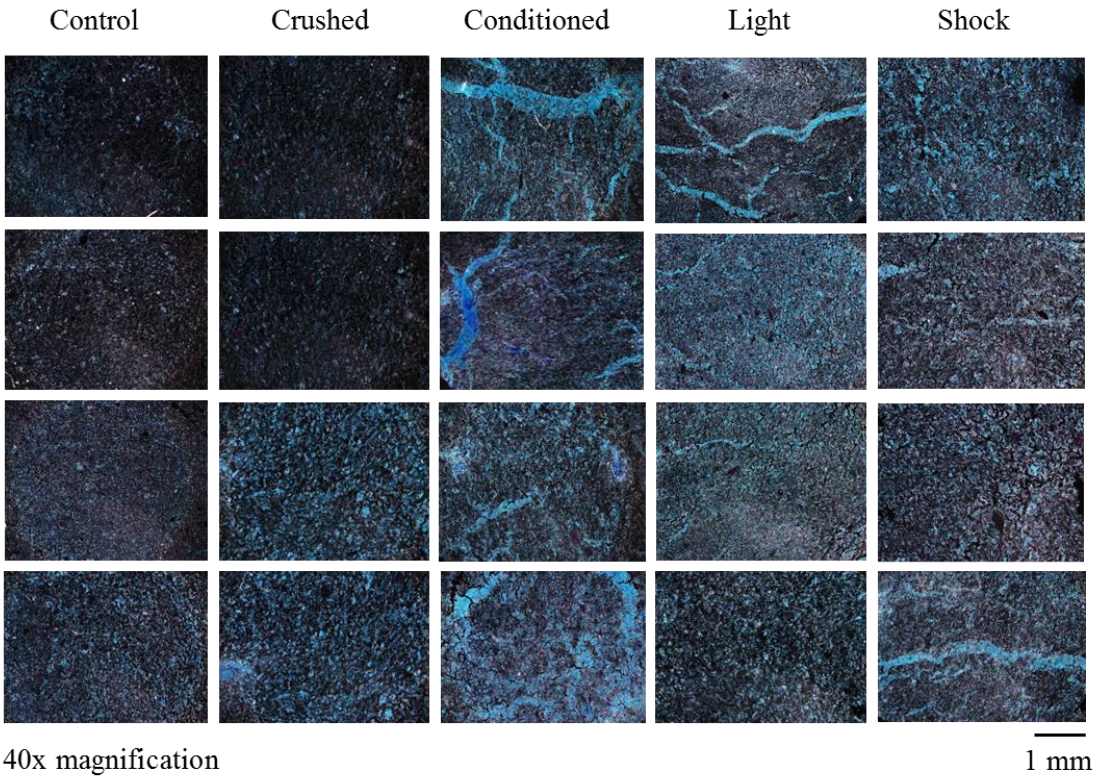

Figure 3.5. Samples stained with TBO, imaged at 40x magnification under Phase 2 contrast light

microscopy classified by exposure type prior to chemical fixation. 'Vessel structures' were measured to be 10-200 μm wide.

Three (n= 3) independent observers were asked to count the total number of 'vessel structures' for each slide. Inter-rater measures indicated moderate to strong reliability. An ANOVA was then computed in order to identify any differences in total identified 'vessel structures' between conditions. A statistically significant difference was found [$F(4,117)= 20.90$, $p<.001$, $\Omega^2= .43$] between the groups. Post hoc analyses indicated three distinct groups. The first consisted of Control (M= .38, SE= .15), Crushed (M= 2.58, SE= 1.00), and Shock (M= 4.36, SE= 1.46). The second group consisted of Shock (M= 4.36, SE= 1.46) and Light (M= 7.63, SE= 1.24). The third subset involved the Conditioned (M= 12.54, SE= .98) dough alone. Post-hoc t-tests confirmed that the major source of the difference was due to the significant differences between the control and crushed samples, the light without pairing with shock samples, and the conditioned (light after light+ shock) samples. These results are presented in Figure 6.

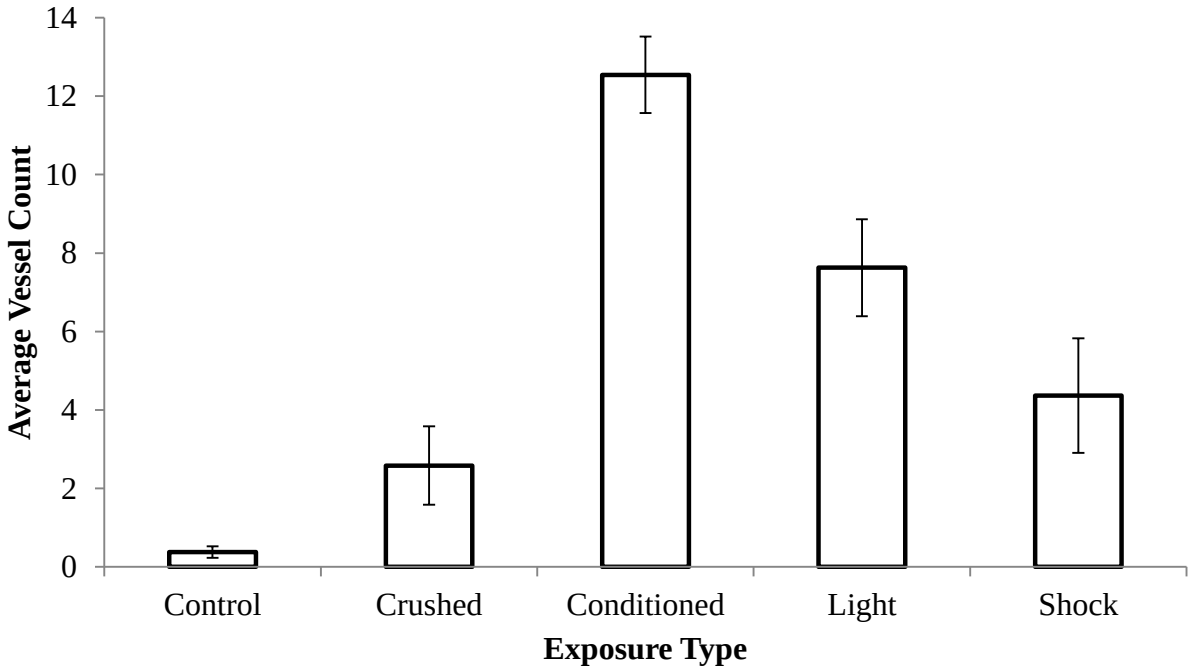

Figure 3.6. Mean vessel structure counts by exposure type for slides stained with TBO. Standard error bars are provided.

Discussion

Although memory can be considered to involve complex processes for the representation of information within a brain or its simulated arrangements (the computer) the operation is much more universal. The symbolic representation of "memory" can be defined as a induction of some subset of Set A within Set B such that long after Set A is no longer adjacent or existent, that representation of Set A remains in Set B. This operation can be found in most of the traditional scientific disciplines and includes the concepts such as memory, genetic history, culture, and tradition. The

microstructural changes within membranes and receptors of the cells that compose the immune system would be another classic example of “chemical memory” with referencing brain function.

Most experiments involving conditioning and learning in non-mammalian systems such as plants or inanimate objects such as the domains within iron exposed time-varying and static magnetic fields have employed direct measurements of discrete events. In the present study we employed the spectral power densities of the range of frequency variations within the special preparation of dough to compare similarities between alterations from current induction only (the UCS), simply the presentation of the light from an LED, or the response to this light after it had been paired with the UCS. The fact that the “conditioned” dough after it had been exposed to the light only displayed a power spectral density that was most similar to the SPD elicited by electric current only is consistent with learning.

The congruence with the “conditioned” pattern of “power” density for the distributions of background potential differences in the dough and the “unconditioned” pattern of power densities due to the electrical stimulation suggests that comparisons of the temporal structures or the “field” properties of conditioned and unconditioned stimuli could add additional information to what lays at the bases of association through space-time contiguity. That this effect was not an artefact was indicated by the absence of this marked congruence of SPDs in response to the light only in condition dough if the delay between the CS and UCS had been more than 130 ms.

Solving for frequency or f= 1/T, the lower limit frequency of stimulus presentation which resulted in a paired association was 7.7Hz. This could suggest that

implicit variations between 333 Hz to 7.7 Hz are an optimal range to effectively pair the CS-UCS in this pH-brain simulated dough. It could be relevant that the operating frequency of the hippocampus, a deep temporal lobe structure critically involved in mammalian trace conditioning (Beylin et al., 2001), is the theta (4 to 7 Hz) range and particularly ~8Hz (Fries, Nikolic & Singer, 2007). Temporal lobe atrophy and associated memory deficits are linked to the emergence of increased sub-theta (<7Hz) neural activity as inferred by QEEG (Gambardella, Gotman, Cendes & Andermann, 1995). This convergence upon intrinsic patterns of neural activity associated with learning in the mammal is supportive of a fundamental principle of temporal architecture of learning based upon contiguity which might not be restricted to living tissues.

The structural changes within the dough in response to conditioning that were evident with classical histological methods suggest there was a physical correlate to the changes in SPD. Complexity of the material was highest when exposed to a stimulus, and lowest when unexposed or when mechanically ablated. Light and shock, both independently and in combination, produced 10-200 μm 'vessel structures'. However, only after being paired with the UCS (AC current; shock) did the neutral stimulus (LED; light) display the definition of a CS by eliciting a CR In other words, stimuli with a history of space-time contiguity with a separate stimulus impinging upon the mass was sufficient to alter the internal structure in a different manner than if the stimuli had never been associated.

The range of width associated with these structures is within the typical diameter of most human cells. These microstructures were accompanied by increased blue and cyan pixel counts, indicative of increased stain uptake. Toluidine Blue is an acidophilic

stain with a high affinity for nucleic acids (Sridharan & Shankar, 2012), and is thought to heavily penetrate malignant epithelial tissue due to widening of intracellular canals (Epstein, Scully, & Spinelli, 1992). We do not know if these structures are indicative of accreted molecules or increased spaces within the organizational matrix. However boundary conditions were formed that could serve as the physical correlate or even the "substrate" for the CR to simple light flashes but only after the conditioning had been completed.

What is clear is that significant energy was required within the mixture of constituents that comprised the dough to produce such visible obvious changes. Direct measurements indicated a potential difference of 50 mV across the dough. The resistance was 15 kΩ and the electric stimulus (UCS) was between 1000 and 2500 μV. Hence the passive current would have been about 1.6×10^{-7} A. The equivalent across 5 cm would be 0.3×10^{-5} A/m. The equivalent voltage would be 0.5×10^{-1} V/m resulting in 0.15×10^{-6} W per m^2. The CS (light) was 43 Lux (or 5×10^{-2} W per m^2) on the surface of the dough. Considering a conservative estimate of attenuation of a factor of 100 to 1000 of the incident light within the deeper regions of the dough, there would a possible convergence of flux density within the constituents for both the light and the electric current. The estimates of capacitance from the physical dimensions of the "vessel structures" could be associated with capacitance of about 10^{-7} F per cm^2. If the resistance was about 3.75×10^5 Ω cm^2 the time constant would be about 40 ms which is within the range of optimal duration for pairing of the CS and UCS for the dough. If concept is applicable to cerebral function then the relationship between the theta rhythms, the 8 Hz pulsatile cells within the second layer of the entorhinal cortices and

the persistent 1 μm width of a synaptic cleft, width of a node of Ranvier and typical interspine distance on a dendritic shaft may share a physical source.

Conditioning as an intrinsic feature of space-time contiguity of stimuli (defined as packets of energy) could modify our presumptions concerning abiogenesis, the production of biological phenomena from inorganic or inanimate precursors. Persinger (2012) demonstrated the many ways by which lightning can be quantitatively described as a scale-invariant analogue of the action potential. Both the average energy densities (10^{-7} J/s·m^3), and current densities (~10^5 A/m^2) of lightning over the surface of the planet are remarkably similar to the values calculated to occur within cerebral volumes and along axons during action potentials. If discrete displays of current presented for transient periods during abiogenesis were preceded (more frequently) by photons of specific wavelengths, the possibility of conditioning being represented as a fundamental process within the most elementary living systems might be considered. Miller (1953) experimentally demonstrated that early atmospheric conditions in combination with electrical discharges – simulating lightning – were sufficient to synthesize amino acids *de novo*. In principle, these experiments show that complex biological processes can be replicated by physical-chemical interactions in nature.

Suppose a natural event involving a burst of photons paired with the flow of electric charge across a matrix of ions contained within a proteinaceous mass was sufficient to generate microstructures of the type reported here within early organisms on the planet. Interactions resultant of the initial lightning strike and point of contact would likely be too destructive to accommodate subtle structural modification. Residual current might be sufficient to generate structures which would allow a previously

homogeneous mass to respond differentially to presented stimuli. It was perhaps lightning that forged the first nervous systems, imbuing some biomass with a matrix of boundary conditions and a capacity to interact with stimuli from which it had previously been isolated. A natural replication of these experiments is entirely possible given an abundance of lightning strikes over billions of years.

The experiments resulted in some clear technical patterns which should be addressed. The increased representation of negative correlations between spectral densities associated with the CS-UCS period and the CS probe period requires further consideration. One potential explanation involves the method of information encoding. Negative-images or castings represent one method by which an object or information source can be effectively replicated and stored within a novel space. This is perhaps one of the simplest forms of information storage. In the case of negative-images, 0101 is stored as 1010 and, assuming maximum efficiency, the relationship between the original signal and stored information would be equivalent to a correlation coefficient of r= -1.0, rho= -1.0. Figure 3 demonstrates what might represent the relationship between the original signal and its stored counterpart, released upon display of a CS. Both signals center upon a common frequency with identical relative amplitude.

There is evidence to suggest any stored information was localized rather than isotropically distributed. Consider the relationship between the primary sensor (Cz) and the references (Figure 7). An averaged reference over four (4) sensors, two of which are a means of grounding the system, provide a comparator by which potential differences are calculated over Cz. If electrical activity was strictly homogeneous throughout the entire mass, the potential differences would be effectively or near zero. It was

demonstrated that this was not the case. Therefore, any information detected as a signal was not being expressed everywhere simultaneously. If it were, potential differences would be zero and no effect would be discernible

Materials and Methods

Electroconductive Dough

The content of the conductive material, which is effectively unleavened dough with a proton donor, has been described elsewhere (Rouleau & Persinger, 2014). A bleached, all-purpose flour was mixed with tap water, table salt, vegetable oil, and lemon juice as per an open-source recipe by Squishy Circuits which is typically used as a pedagogical tool to demonstrate basic principles of circuit formation. Rouleau & Persinger (2014) reported that the material displayed electrical activity which expressed spectral densities that correlated with human brain activity as inferred by QEEG within band ranges typically associated with neural correlates of consciousness and Schumann Resonance. These patterns were only evident for the material when the pH of the precursor solution was <2.53. It was calculated that this pH was representative of the spatially discrete, extracellular environment immediately adjacent to the cell where a monolayer shell of protons extending out by a Bohr radius or $5.6 \cdot 10^{-9}$ cm maintains the resting membrane potential. For the purposes of the present experiments, only dough associated with a pH <2.53 was used. The authors proposed that the capacity for the material to express the most fundamental patterns associated with "memory" should be demonstrable if the brain can be functionally described as a network of interfacial water punctuated by a complex spatial distribution of quasi-stable units (i.e. dendrites).

Confirming this prediction could involve identifying the equivalent of a conditioned response elicited by the dough.

QEEG

A Mitsar, 19-channel quantitative electroencephalograph (QEEG) was employed to measure subtle, relative shifts in the electrical activity of the dough during conditioning trials. The montage consisted of a single electrode (Cz) placed at the apex of the spherical dough mass, referenced to an average of activity measured at sensor locations placed over left and right lateral extremities of the mass. The sampling rate was set to 250Hz, with a 45-75Hz notch filter to exclude ambient electromagnetic noise.

Conditioning Apparatus and Stimuli

The conditioning apparatus was constructed to manually administer stimuli with the capacity to systematically alter the interstimulus interval which separated the CS and UCS. An Arduino Uno R3 microcontroller coupled to an electronic breadboard received uploaded signal files via USB 2.0 from an HP ENVY laptop running Windows 8. Leads from the microcontroller ran current through a red light emitting diode (LED) placed 5 mm away from the dough. The LED had an associated emission wavelength of 620-625nm and an intensity of 150-200 millicandela. Direct leads to and from the dough completed the circuit, allowing for simultaneous or lagged electrical shocks and light stimulation (see Figure 7). The program determined the temporal delay between the administration of the shock and the light stimulation. Once the files were uploaded, a reset button on the microcontroller was used to initiate the stimuli.

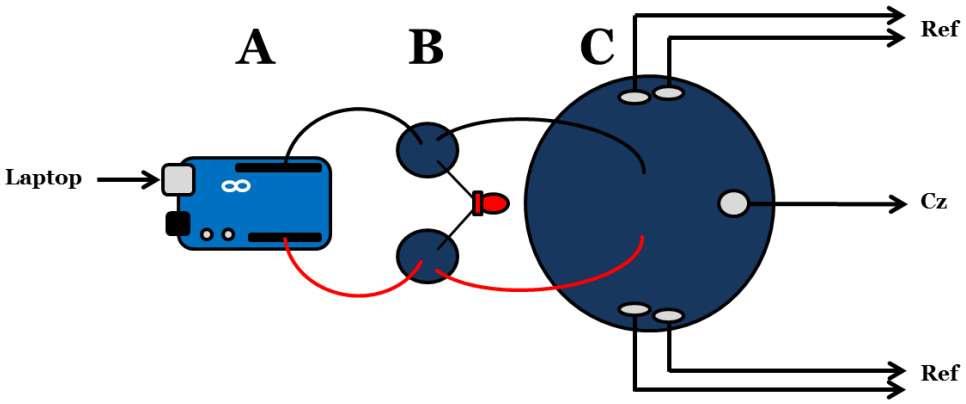

Figure 3.7. Conditioning apparatus. Stimuli are presented by a digital-to-analog microcontroller operating at 5V (A) into bilateral pieces of electroconductive dough which holds an LED (B) in parallel and further still into the conditioning focus (C) which is referenced to its own lateral extremities (Ref) in a monopolar QEEG montage with the Cz sensor mounted at the apex of the spherical mass.

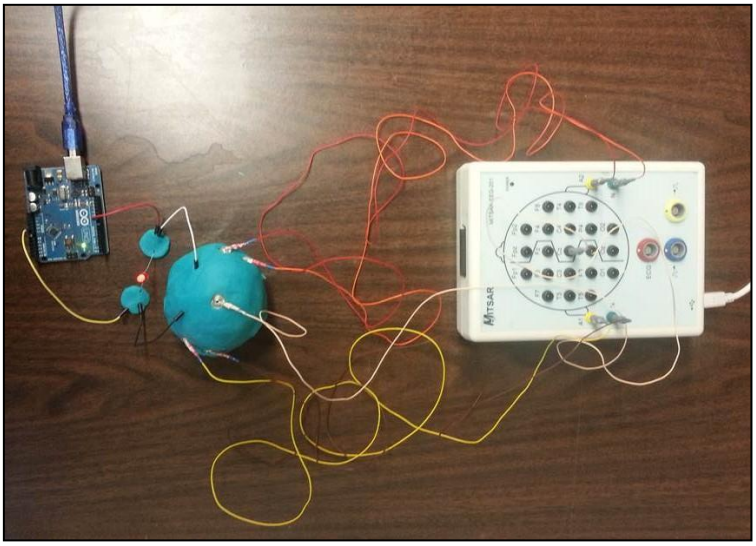

Figure 3.8. Conditioning and recording equipment sending and receiving signals to and from the spherical dough mass.

The unconditioned stimulus consisted of an all-or-none shock (1-5 V) administered directly into the dough. The lead, which was a standard electronic jumper

cable, extended 0.5 cm into the dough. The duration of the direct stimulation was either 25ms or 50ms, contingent upon the procedure type described elsewhere. The neutral stimulus, as indicated by no discernable change in QEEG activity upon display, consisted of a 25ms or 50ms pulse of visible light from a red LED.

Procedure: Simultaneous Conditioning

Four (n=4) samples of dough, weighing approximately 70g each, were trained and later exposed to a CS while being monitored for CRs using QEEG. A total of twenty-four (n= 24) trials were conducted using the same dough samples. The training phase consisted of 5 or 10 brief, 10 second periods of 10Hz CS-UCS pairings presented sequentially and separated by 60 seconds. The simultaneously presented stimuli, with associated frequencies of 10Hz, are generated by presenting the LED and shock for 50ms with 50ms delays between each stimulus. Each cycle was therefore 100ms, which over 1000ms or 1s, gives 10 cycles of 10Hz. After the training phase, there was a short delay of 1 or 5 minutes followed by a probe (CS) in order to elicit a CR. QEEG recordings were obtained throughout all phases of the experiment.

All samples of dough were mechanically ablated after a given trial, recycling the material. This involved crushing the dough so as to remove any potential microstructures resultant of the treatment that might contribute to differences between the dough samples. In other words, the dough samples were 'reset' for every new trial, but the material involved was not tested more than once within the same experimental condition in order to eliminate any potential redundant variance.

Procedure: Trace Conditioning

Four (n=4) samples of dough, weighing approximately 23g each, were trained and later exposed to a CS while being monitored for CRs using QEEG. The training phases consisted of 5 brief 10 second periods of CS-UCS pairings where the interstimulus interval changed systematically across conditions. The duration of each LED or shock stimulus was 25ms. Nine (9) trace conditions were employed with the following interstimulus intervals: 3ms, 25ms, 100ms, 130ms, 150ms, 170ms, 200ms, 300ms, and 500ms. After the training phase and a 1 or 5 minute post-training delay, the samples of dough were exposed to a probe (CS). QEEG recordings were obtained throughout all phases of the experiment. A total of 81 trials were completed. All samples of dough were recycled using the method described for the simultaneous conditioning experiments.

Histological Technique

Twenty (n=20) 1 cm^3 samples of dough exposed to five conditions underwent histological processing. The first and second conditions involved exposure to simultaneous conditioning training protocols described elsewhere; however, the second condition was mechanically ablated. The third and fourth conditions involved exposures to light only and electrical shocks only, respectively. The fifth condition was that of a control wherein the dough samples were naïve to the training or any other protocol.

Samples were fixed in a solution of ethanol-formalin-acetic acid (EFA) for 7 days before systematic dehydration, and further chemically processed. The penetrated specimens were then embedded in paraffin wax blocks and sectioned into 10μm slices. Samples were then stained with Toluidine Blue O or Periodic Acid-Schiff and mounted.

QEEG Data Processing

Raw microvolt (μV) data were extracted in 5 second chunks and spectral analyzed. Baseline, stimulation, and probe period spectral densities were correlated within the narrow bandwidths associated with the respective UR periodicities. Based upon measurements obtained during the training phase (CS-UCS), frequencies coinciding with the greatest spectral density peak were selected as the defined conditioned response. Employing this method, a selected spectral peak $z>2.0$ would be defined with cases for +/- 1Hz included. The narrow band data (9 cases per band) then underwent non-parametric correlational analysis where pre-exposure baseline, stimulation, and probe period spectral densities were simultaneously analyzed.

Microscopy Data Processing

Mounted samples of stained dough (n=80) were photographed at 40x magnification with phase 2 contrast. A standardized method was used to capture the images whereby the upper left, upper right, and lower center extremities of the sample were photographed as internal measures of reliability, for a total of 240 images. Images were then uploaded to ImageJ and processed by Fractal Box Counting (FBC) and Colour Pixel Counter (CPC), methods which measure complexity as a function of scale and number of pixels of a given colour (e.g. red, blue, cyan, etc.). Whereas coloured Bitmaps (.bmp) were used for the CPC method, images undergoing FBC were converted to 8-bit format and grey-scaled before processing. To eliminate redundant variance, mean complexity and pixel measures were computed from the 3 images, reducing the cases to n=80. Total pixels remained consistent across all images ($\sim 2 \cdot 10^6$ pixels).

References

Beylin, A. V., Gandhi, C. C., Wood, G. E., Talk, A. C., Matzel, L. D., & Shors, T. J. (2001). The role of the hippocampus in trace conditioning: temporal discontinuity or task difficulty?. *Neurobiology of Learning and Memory*, 76(3), 447-461.

Cragg, B.G. & Temperley, H.N.V. (1955). Memory: The analogy with ferromagnetic hysteresis. *Brain*, 78(2), 304-316.

Epstein, J. B., Scully, C., & Spinelli, J. (1992). Toluidine blue and Lugol's iodine application in the assessment of oral malignant disease and lesions at risk of malignancy. *Journal of Oral Pathology & Medicine*, *21*(4), 160-163.

Fries, P., Nikolić, D., & Singer, W. (2007). The gamma cycle. *Trends in Neurosciences*, 30(7), 309-316.

Gambardella, A., Gotman, J., Cendes, F., & Andermann, F. (1995). Focal intermittent delta activity in patients with mesiotemporal atrophy: a reliable marker of the epileptogenic focus. *Epilepsia*, 36(2), 122-129.

Gormezano, I., Kehoe, E. J., & Marshall, B. S. (1983). Twenty years of classical conditioning with the rabbit. *Progress in Psychobiology and Physiological Psychology*, 10, 197-275.

Hawkins, R. D., Abrams, T. W., Carew, T. J., & Kandel, E. R. (1983). A cellular mechanism of classical conditioning in Aplysia: activity-dependent amplification of presynaptic facilitation. *Science*, 219(4583), 400-405.

Malenka, R. C., & Bear, M. F. (2004). LTP and LTD: An embarrassment of riches. *Neuron*, 44(1), 5-21.

Miller, S. L. (1953). A production of amino acids under possible primitive earth conditions. *Science*, 117(3046), 528-529.

Pavlov, I. P. (1927). Conditioned reflexes: An investigation of the physiological activity of the cerebral cortex. In G.V. Anrep, Trans. (Ed.). Dover Publications, Inc., New York.

Persinger, M. A. (2012). Brain electromagnetic activity and lightning: potentially congruent scale-invariant quantitative properties. *Frontiers in Integrative Neuroscience*, 6(19), 1-7.

Rouleau, N., & Persinger, M. (2014). Cerebral Networks of Interfacial Water: Analogues of the Neural Correlates of Consciousness in a Synthetic Three-Shell Realistic Head Model. *Journal of Signal and Information Processing*, 5(4), 143-154.

Skinner, B.F. (1938). The behavior of organisms: An experimental analysis. Appleton-Century-Crofts, New York.

Sridharan, G., & Shankar, A. A. (2012). Toluidine blue: A review of its chemistry and clinical utility. *Journal of Oral and Maxillofacial Pathology: Journal of Oral and Maxillofacial Pathology*, 16(2), 251.

(Pubished in Journal of Biophysical Chemistry, 2014)

Chapter 4: Non-Local pH Shifts and Shared Changing Angular Velocity Magnetic Fields: Discrete Energies and the Importance of Point Durations

Abstract

Macroscopic productions of "non-locality" or "excess correlations" of dynamic changes within media between two spaces could be utilized as alternative communication systems. Previous experiments have shown that injections of a weak acid within one of two volumes of spring water sharing the same patterned circular magnetic fields with changing angular accelerations separated by non-traditional (5 m) distances were associated with opposite (basic) shifts in pH within the non-injected, non-local volume. In the present experiments, employing a different technology, pairs of beakers separated by 1 m containing either 25 cc, 50 cc, or 100 cc of spring water were placed within toroids generating weak (30, 300 nT) changing acceleration magnetic fields with 1 ms, 2 ms, or 3 ms point durations or a field whose point durations changed. When a proton source (weak acid) was injected into one beaker (local) pH shifts in the other (non-local) beaker exhibit increased acidity for the 3 ms point duration but increased alkalinity for the 1 ms duration. Neither intermittent point durations nor variable point durations for the same volumes of water placed between the two magnetic field-coupled beakers exhibited significant changes from baseline. Contingent upon the point duration of the applied field, the pH shift was consistent with a fixed quantity of decreased free protons (increased pH) or increased protons (decreased pH) in the non-local beakers. The opposite directions of the pH shifts at 1 ms and 3 ms that correspond to quantitative

cosmological solutions for electrons and protons suggest these results may reflect a fundamental physical process.

Introduction

A means by which information could be inexpensively exchanged over large distances without the requirement for classic "transmission" and the escalating expense of equipment would substantially alter the concept and form of communication. The concept of "non-locality" and "excess correlation" has been considered by many as the quintessential property limited to quantum phenomena. As indicated by Hofmann *et al.* (2012), "observers of two or more entangled particles will find correlations in their measurements that cannot be explained by classical statistics". Two-photon, three dimensional entanglements may be capable of applied quantum communication (Vaziri et al., 2002). Such quantum energy "teleportation" may not be limited by distance (Hotta et al., 2014).

Although from some perspectives photons will remain the only means of quantum communication because of the technical requirements (Vaziri et al., 2002), Julsgaard *et al.* (2001) experimentally entangled two macroscopic entities, each containing ~10^{12} atoms of caesium gas, for which the entanglement was maintained for 0.5 milliseconds. Dotta and Persinger (2012) hypothesized that "excess correlation" might be facilitated by exposing two spaces at non-traditional distances (5 m) to the same circularly generated ("rotating") magnetic fields with intensities of ~1 μT and changing angular velocities. These same intensities when applied strategically produced robust photon emissions from aggregates of cells. Dotta and Persinger (2012) demonstrated that if the group and phase velocity of these rotating magnetic fields were

dissociated, conspicuous excess correlations in photon emission as measured by photomultiplier tubes were evident. If both loci were exposed to the same computer-generator fields, the simultaneous injections of small aliquots of hydrogen peroxide into hypochlorite solutions at both loci "doubled" the photon emission from one locus. The "excess correlation" was as if both loci were transposed to the same space.

The effect was equivalent to injecting twice the aliquot of peroxide into any one locus without the presence of the field. However, it was only evident for a specific order of presentation of the field configurations and was maintained for about 8 minutes. Considering the numbers of molecules involved with the solutions from which the photons were emitted this duration was consistent with values for a smaller number of molecules reported by Julsgaard *et al.* (2001) and suggested a type of "mass action". The effect was similar to that observed for pairs of cell cultures or human brains separated by non-traditional distances but exposed to the same magnetic field configurations and parameters (Dotta et al., 2009; Dotta et al., 2011). To test if the effect could be produced in other systems, Dotta *et al.* (2013) measured pH changes in different quantities of spring water separated by 5 m. They shared the same configuration and parameters of magnetic fields which produced the excess correlation of photon emissions. After the required period of exposure injection of a small amount of protons (weak acid) into one beaker which produced a clear shift towards acidic pH, the pH in the other beaker that shared the same patterned, rotating magnetic field exhibited discrete increases towards basic pH. The antithesis of the response, that is the decrease in pH in the active (injected) solution and the increase in pH in the non-local (non-injected) solution, was consistent with the excess correlation associated with "entangled" photons whereby the

change in polarity of one photon is associated with a comparable (opposite) shift in the other even at extraordinary distances (Persinger & Koren, 2013).

Here we present evidence that the shift in pH with the same patterned magnetic field during the phase associated with excess correlation or entanglement was specific to the point durations of the voltages generated by computer software that produced the field. Unlike previous studies where the changing angular velocities of the magnetic field were generated within circular arrays of solenoids, computer-generated, software driven shifts within toroids were employed. Fixed point durations of 1 ms or 3 ms, solutions from cosmological conditions involving Planck's lengths (Persinger & Koren, 2007), an intermittent value of 2 ms and a field with changing point durations were selected.

Experimental Details

Equipment

The experiment consisted of seventy-two (n = 72) trials separated over several weeks with 6 trials completed per session. Each trial involved four beakers. The four beakers were placed in a row with equal separation along the axis. The two most lateral beakers were separated by 1 m and placed within the center of toroidal coils as described by Burke *et al.* (2013). The schematic is shown in Figure 4.1. Each beaker within the same trial contained either 25 cc, 50 cc, or 100 cc of spring water. The constituents of

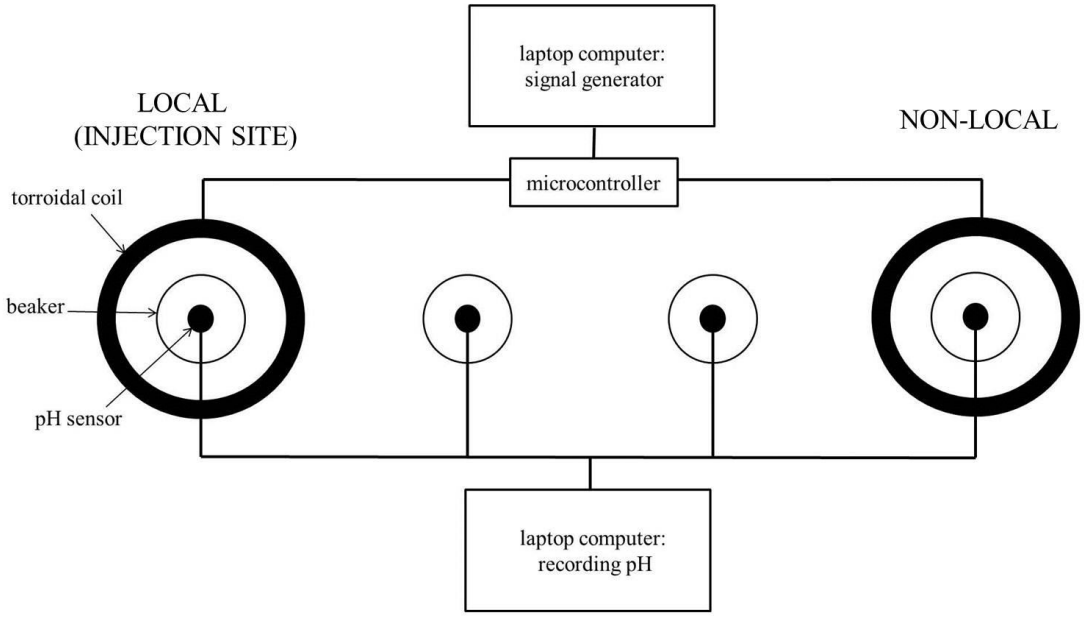

Figure 4.1. Schematic of the apparatus employed to produce "entanglement" or "excess correlation" in pH shifts within two separate containers of water. The dark circles refer to the toroids that generate the shared fields with changing angular velocities. The two cirlces representing beakers in the center were "controls" to ensure there were no indirect field effects upon pH shifts.

the spring water have been reported elsewhere (Burke et al., 2013). Different volumes of water were employed to discern the quantity of potential energy that could be involved, per molecule, from a fixed amount associated with the shared magnetic fields. To verify that the magnetic field intensity was the primary correlate of the energy that mediated the effect of the "entanglement" between the volumes of water, two intensities were generated: 30 nT or 300 nT, within the space occupied by the beakers. These intensities were elected for theoretical (Dotta et al., 2013; Persinger & Koren, 2007) reasons and for potential practical applications so that more extensive applications only required the output from conventional laptop computers.

The coils were connected to an electronic breadboard receiving signals from an Arduino UNO microcontroller which generated synchronized, patterned electromagnetic fields (Figure 4.1). The shape of the primary pulse, whose durations could be varied experimentally, generated from the Arduino directly and within each toroid is shown in Figure 4.2. All signals were generated by an Arduino UNO microcontroller receiving uploaded patterns from a Sony Vaio laptop computer running Arduino v1.01 software on a Windows 7 operating system via USB 2.0. Low intensity (30 nT) and high intensity (300 nT) conditions, as measured by an AC MILLIGAUSS METER model UHS by AlphaLab, Inc. (USA), were included. The low intensity was just discernable above the 60 Hz background. The present of the signals and their fidelity were verified by listening to an acoustic amplifier connected to a small solenoid (telephone coupler). Whereas the 5 V output from the USB to the microcontroller defined the low intensity condition, the high intensity condition was achieved by coupling a 9 V (800 mA) Nexxtech power adaptor to the breadboard as an external power source.

Maintaining the Integrity of the Specifications

The procedure involved exposing a local and non-local beaker to synchronized, counter-clockwise rotating, electromagnetic fields for a total of 18 minutes. A similar procedure using different technologies for generating the fields was described by Dotta *et al.* (2013). Two field patterns were presented in series, both consisting of looped, 7-point pulses with points lasting 1, 2, or 3 ms in duration. The first field (the "primer field"), presented from minute 0 to minute 6, was a phase modulated pattern wherein the temporal delay between points (beginning with 20 ms) successively increased by 2 ms as a function of time (*i.e.* decelerating). The second field (the "excess correlation

field"), presented from minute 6 to minute 18, was characterized by a temporal delay between points that successively decreased by 2 ms as a function of time (*i.e.* accelerating). In both cases, the temporal delay returned to 20 ms after a 7-point pulse, defining the loop.

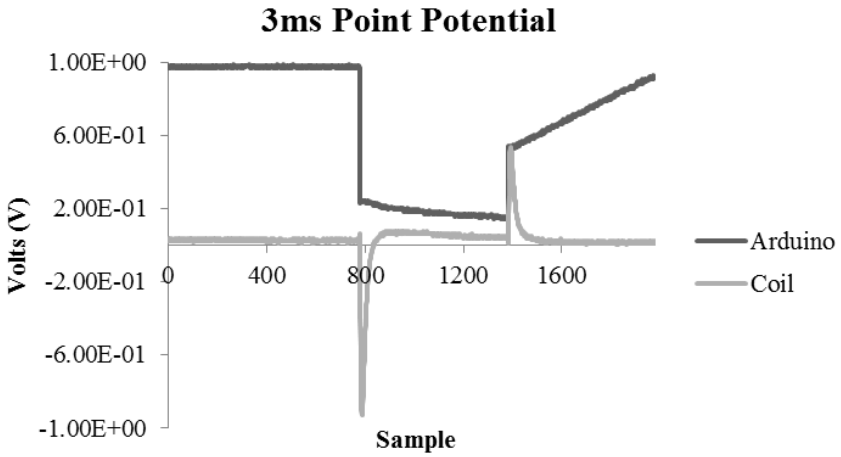

Figure 4.2. The 2D representation of the 3 ms point durations measured at the level of the Arduino (dark line) and coil (light line) that composed the shape of the field generated within the toroids. The other point durations were similar in shape but were presented for either 1 ms or 2 ms. Here, the x-axis represents samples recorded by an Agilent Technologies MSOX3012A oscilloscope where the time equivalent between peaks is equal to 3 ms.

The fourth point condition (delta) was an exception to this procedure in that the delays between points remained fixed (100 ms) whereas the points themselves defined the phase modulation. Consequently, cycled through the wave pattern, the point durations started at 20 ms and then either decelerated or accelerated by 2 ms
until returning to 20 ms. The rationale was to insure that the critical feature for entanglement was the change in angular velocity of fixed point durations of electromagnetic energy or "quantum wells". A proton source (5% acetic acid) was

injected into one of the two magnetic fields exposed beakers at fixed intervals throughout the trials. The pH values were recorded for all beakers. Shifts in pH, as measured by probes inserted into the water, relayed information to a Lenovo laptop computer running Pico Technology (UK) via Dr. Daq boards with USB 2.0. The system sampling rate was set to 1 Hz and programmed to terminate recording after 1080 samples. On average, starting pH values ranged from 7.0 to 7.5 which indicated accurate calibration of the instruments. The two center beakers served as controls; pH shifts were monitored but no injections were administered. At minute 4 of the trial, 68 μL of 5% acetic acid was injected into the local beaker using a micropipette. Subsequent to the switch from the first field to the second, injections were made continuously from minute 7 to minute 15 of the experiment. All conditions were triplicated to ensure reliability of the phenomenon. To reiterate, the local beaker was the only flask to receive a chemical manipulation (*i.e.* injections of a proton donor).

Results

25 cc Volumes

The mean shifts in pH in the 25 cc volumes by the end of the 6th minute of exposure to the decelerating magnetic field are shown in Figure 4.3. There was a marginally significant shift towards alkalinity for the 1 and 3 ms point (fixed) durations for the 30 nT conditions compared to the same strength magnetic field whose point durations increased while the time between points remained constant. On the other hand, during the "excess correlation" component, that is when the same magnetic field with fixed point durations was accelerated within the toroid, the mean shift in pH was significantly different for both the 3 ms and 1 ms point durations compared to the delta

and 2 ms intervals. The volumes of water exposed to the 3 ms durations shifted towards acidity while the 1 ms point duration-exposed volumes shifted towards alkalinity.

The shift in pH in the specific directions exhibited an asymptote at about 2 min after the onset of the accelerating field (see Figure 4.4). The mean values for the shifts that demonstrated the "excess correlation" are shown in Figure 4.5.

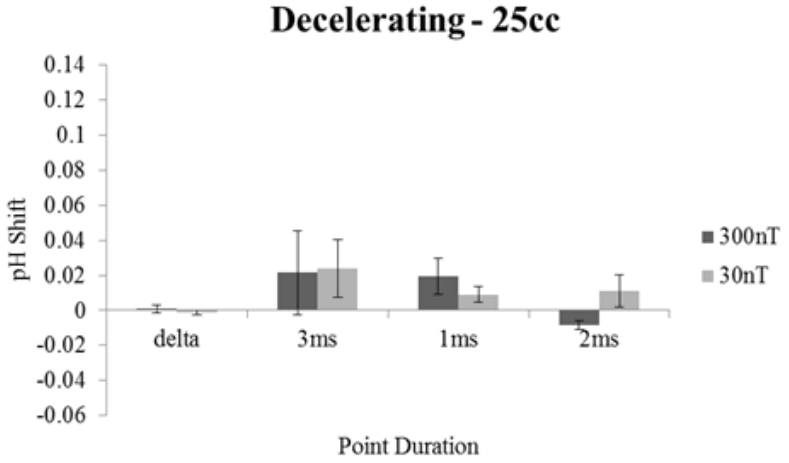

Figure 4.3. Means and standard errors of the mean for the shift in pH in the 25 cc volumes as a function of the fixed point durations for the applied decelerating magnetic field configurations for the two intensity conditions. Delta indicates a field with changing point durations but no deceleration.

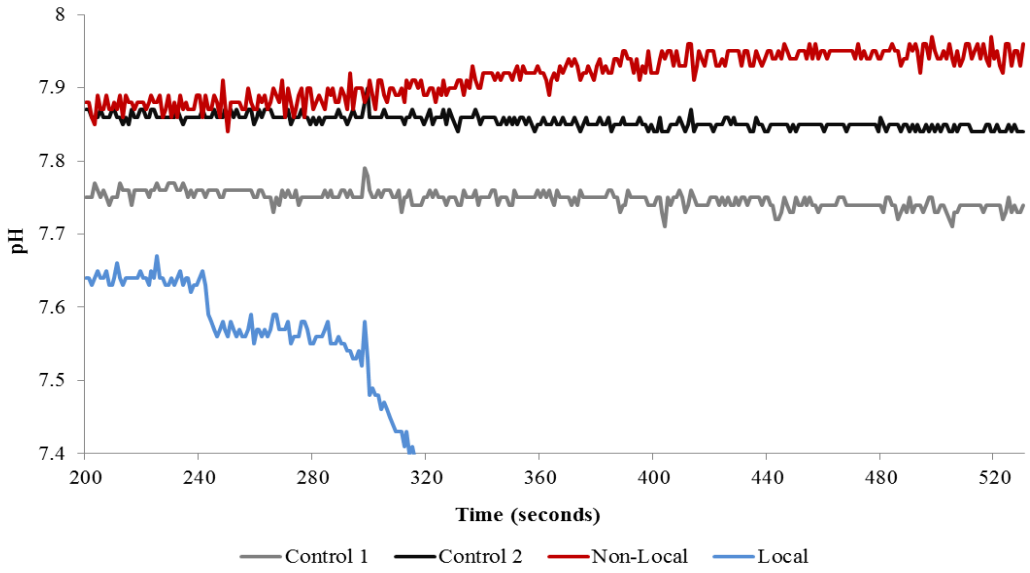

Figure 4.4. A typical example of non-Local and local pH shifts during a trial involving electromagnetic fields composed of 1ms point durations with an associated intensity of 30 nT. The pH for the control beakers remains static throughout the exposure. Note the first injection of acid at 240 seconds within the local beaker. The non-local shift asymptotes ~100 seconds after the onset of the accelerating field at 360 seconds.

There was no significant difference between the two intensities of the field applications from baseline for either the same accelerating field with 2 ms point durations or for the field whose point durations cycled by 2 ms from a base of 20 ms to 34 ms throughout the sequence of the field application while the time between points remained fixed at 100 ms. When selecting for only those trials involving beakers containing 25 cc of spring water, significant differences in pH shifts across point duration conditions were observed from the 6th to the 18th minute of the exposure for the non-local beaker, $F(3,26) = 5.31$, $p < 0.01$, Ω^2 estimate = 0.42. The local as well as the two control beakers did not differ across point duration conditions when considering the same selection criteria ($p > 0.05$). There was greater inter-experiment variability for

the shifts in pH associated with the 300 nT intensities compared to the 30 nT intensities. The effect size of the latter was about 0.82. In other words about 82% of the variance in pH in the volumes exposed to the 30 nT fields at the various point durations could be explained by these temporal features. *Post-hoc* analysis revealed the major sources of this effect were the marked differences in pH shifts associated with 1 ms (M = 0.04, SE = 0.02) and 3 ms (M = −0.04, SE = 0.01) point conditions, $t(4) = -4.59$, $p = 0.01$, $r^2 = 0.92$. Control beakers for these same trials did not differ across point conditions within the 30 nT intensity ($p > 0.05$).

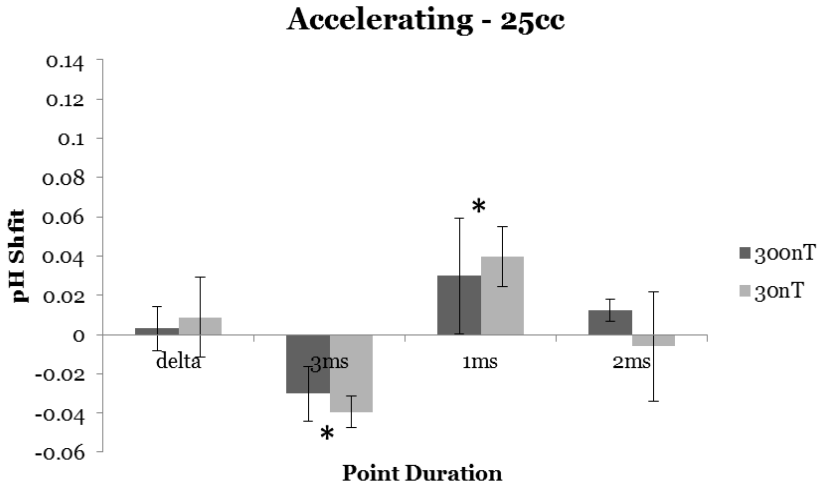

Figure 4.5. Means and standard errors of the mean (vertical lines) for the mean shift in pH in the 25 cc volumes during the "excess correlation" phase of the experiment as a function of the different fixed point durations. Delta indicates a field with changing point durations but no acceleration. Significant differences across point duration are indicated asterisks.

Within the 50 cc volumes, there were no significant deviations from baseline during the priming (decelerating) phase (Figure 4.6). During the excess correlation phase there was an increased in alkalinity for both the 1 ms and 3 ms point durations for the 30 nT condition in particular (Figure 4.7). Figure 4.8 and Figure 4.9 show the results

for the 100 cc volumes. Again, there were no significant changes in pH from baseline for any of the experimental conditions during the priming phase. During the presentation of the accelerating field phase, there was a marginally significant increased alkalinity for water exposed to the 1 ms point durations.

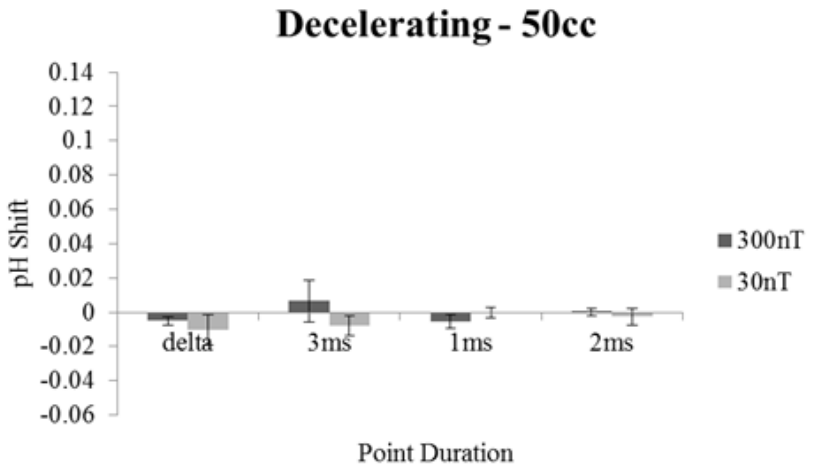

Figure 4.6. Means and standard errors of the mean for the shift in pH in the 50 cc volumes as a function of the fixed point durations for the applied decelerating magnetic field configurations for the two intensity conditions. Delta indicates a field with changing point durations but no deceleration

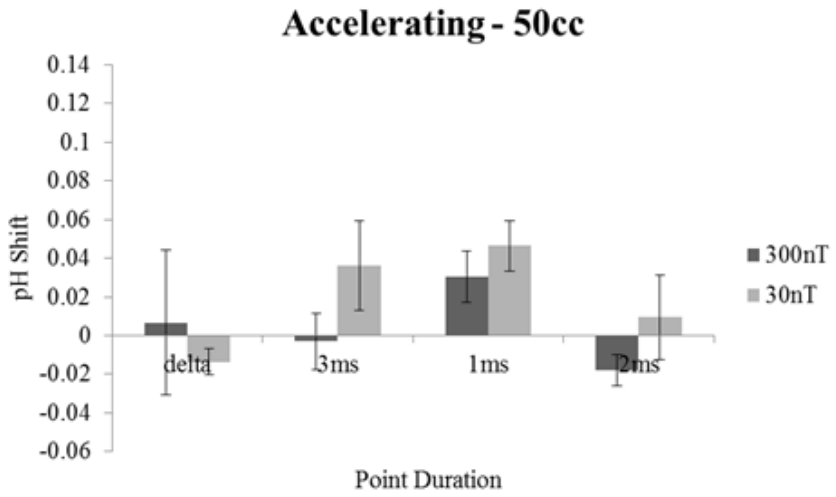

Figure 4.7. Means and standard errors of the mean (vertical lines) for the mean shift in pH in the 50 cc volumes during the "excess correlation" phase of the experiment as a function of the different fixed point durations. Delta indicates a field with changing point durations but no acceleration.

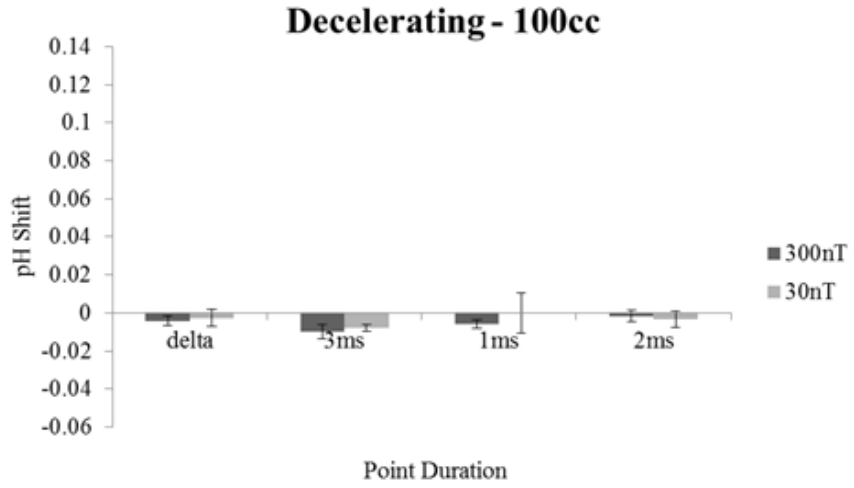

Figure 4.8. Means and standard errors of the mean for the shift in pH in the 100 cc volumes as a function of the fixed point durations for the applied decelerating magnetic field configurations for the two intensity conditions. Delta indicates a field with changing point durations but no deceleration.

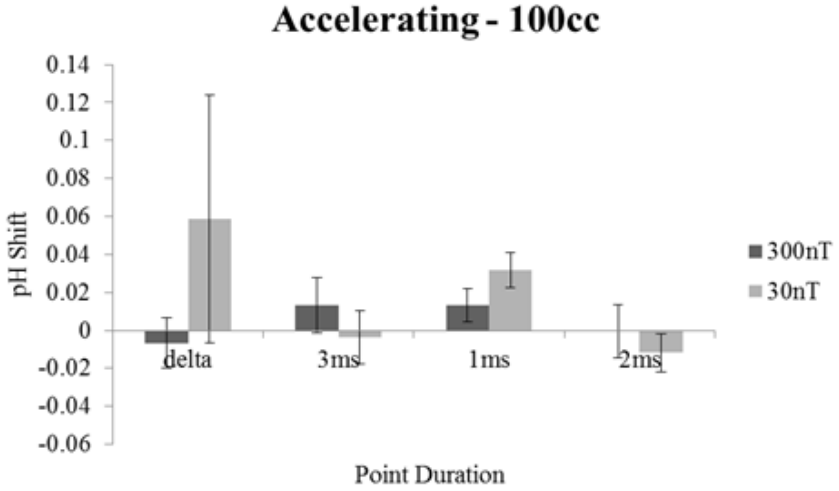

Figure 4.9. Means and standard errors of the mean (vertical lines) for the mean shift in pH in the 100 cc volumes during the "excess correlation" phase of the experiment as a function of the different fixed point durations. Delta indicates a field with changing point durations but no acceleration

Discussion

In this experiment, pH values were recorded continuously during EM field exposures. It is reasonable to propose that the digital pH meters were not affected by process of electromagnetic induction. The most compelling result was that the primary effect was associated with the low intensity (30 nT) condition. If an induction effect sufficient to alter the functioning of the pH meters had occurred, the condition expected to express these effects would be the high intensity condition (300 nT). This was not the case. Further, it should be noted that fields composed of delta and 2 ms point durations were not associated with the reported effects. If there had been an inherent confounding variable or artefact that produced these shifts in pH, the delta and 2 ms conditions applied at intensities identical to those conditions which demonstrated an effect should have demonstrated comparable shifts. It should be noted that all of the fields were associated with the same pulsed all-or-none potentials while only the 3 ms and 1 ms conditions demonstrated an effect primarily within a specific volume of water. This suggests that the presence of an EM field of the type described here is not a sufficient condition which would alter the basic function of the pH meters. For these reasons, we are confident that the results presented here were a function of the experimental manipulation.

The results of these experiments are consistent with those reported by Dotta *et al.* (2013) who employed a different technology and distances. They utilized digital-to-analogue (DAC) software generating magnetic fields through discrete shifts in voltages from 256 discrete increments between −5 and +5 V through a circular array of 8 solenoids. Two complex, physiological patterns were generated. The first exhibited a decelerating feature while the second exhibited an accelerating feature.

Here the fields were generated by machine code through toroid arrangements. The pattern was not complex. Instead the time between the fixed point duration (e.g., 1 ms, 2 ms, 3 ms) either increased in 2 ms increments from a base of 20 ms or increased in 2 ms increments. In both studies the movement of the magnetic field around the circular geometry displayed the same discrete decreased (the priming phase) and increased (the "excess correlation" phase) angular accelerations.

In the Dotta *et al.* experiments (2013), the shift in pH in spring water within the non-local volume of water opposite (increased alkalinity) to the acidity in the local volume due to injections of successive small aliquots of acetic acid injection in the local volume occurred only during the "excess correlation" phase as we found here. This increased (alkalinity) pH was maximum in the 25 cc volumes and also involved the 1 ms point duration. The 3 ms point duration was not employed in those studies. The strength of their field was about 1000 nT rather than 300 nT and 30 nT. The results of the Dotta *et al.* study (2013) and the present experiments both exhibited minimum changes in pH during the first phase involving the decelerating angular movement of the field. The conspicuous shifts in pH occurred during the second accelerating phase.

For both experiments the effects were most obvious in 25 cc of water rather than larger volumes. The shift in pH during the excess correlation phase of the Dotta *et al.* experiments that employed 1000 nT intensities was 0.07, 0.03, and 0.01 units within the 25 cc, 50 cc, and 100 cc volumes, respectively. In the present studies the net values of the changes for the two intensities of the field (30 and 300 nT) and critical point durations (1, 3 ms) were about 0.04 units, 0.03 units, and 0.01 units, respectively. The changes during the priming phase were effectively zero. The consistency and maximum

magnitude of the effect within the 25 cc volumes compared to larger volumes suggests a discrete amount of energy that is diluted with volume.

The phenomena we measured with this method of generating circular magnetic fields with changing angular velocities was the creation of the opposite effect upon the pH shift depending upon the point duration of the field. When both volumes of water were surrounded by the field with the 1 ms duration, the successive injections of acetic acid produced an increased alkalinity in the non-injected (non-local) volume. This would suggest a decrease in the availability of free protons, or, potentially an increase in free electrons such as OH^-. When both volumes of water were surrounded by the field with the 3 ms durations, the successive injections of acetic acid produced increased acidity. This suggests an increased availability of free protons (H^+).

One potential source of the energy associated with the excess correlations might be the magnetic field generated by the toroids within the water. This can be estimated by $J = B^2(2 \times 4\pi \times 10^{-7}\ N{\cdot}A^{-2})^{-1}\ V$ where B is the strength of the magnetic field and V is the volume. For 25 cc of volume, the energy from the 30 nT magnetic field within the volume would be 3×10^{-18} J. Within the 25 cc beaker the shift in pH was associated with a decrease or increase of 0.05. For the 3 ms point durations the shift, which displayed an asymptote after about 2 minutes following activation of the accelerating field, the average pH for 6 different experiments was 7.53. The maximum change levelled at pH = 7.58. Employing the classic $H+ = 10^{-pH}$, the difference would be $3{\times}10^{-9}$ M. Given that 25 cc contains 1.39 M and there are 6.023×10^{23} molecules per Mole, there would be a change (decrease) of $\sim 10^{14}$ protons.

This means that there would be $(3 \times 10^{-18}\ J) \times (2.5 \times 10^{14}\ H^+)^{-1}$ or $1.2 \times 10^{-32}\ J{\cdot}H^{+-1}$. If there are an average of $0.8 \times 10^{12}\ H^+$ (per hydronium ion) s^{-1} then there would

be 1×10^{-20} J·s^{-1} and over a period of 100 s, the approximate temporal delay observed for the asymptote, the total energy within the system would equal 10^{-18} J. This value represents an energy equivalent of the total transferred material. According to these calculations, the energy associated with the magnetic field within the 25 cc volume is conserved. However, if the energy were not applied over this temporal interval the total energy involved would equal ~1×10^{-20} J. This range of quantum has been considered to be a fundamental value that exists throughout the fabric if space (Persinger, 2014). It is also within the range of the energy of the second shell hydrogen bonds that diminish and return in the path of proton movements. Obviously, there are other explanations for this quantitative convergence. What is clear is that larger volumes, such as 50 cc or 100 cc, would result in markedly different energy densities with quantitative solutions beyond this range.

The concept of an implicit and cosmological association of the proton with the 3 ms point duration and the electron with the 1 ms duration was developed by Persinger and Koren (2007) several years ago while attempting to estimate local values for Hubble's parameter. Assuming a median value of 2.4×10^{-18} s^{-1} for Hubble's expansion parameter H, multiplication by any extent or length produces a term of velocity and when divided by Planck's length results in a specific duration. For the proton with a classic width of 2.5×10^{-15} m, the duration, is about 3 ms. For the electron, with an estimated length of 4.86×10^{-15} (*i.e.*, twice the classic radius), the value is about 1 ms.

We (Persinger & Koren, 2007) have interpreted these two intervals as the "time" required for the proton or electron to expand one Planck's length. Because the total force within the universe when divided by the numbers of Planck voxels results in an energy of 10^{-20} to 10^{-19} J when applied over the distance of the neutral hydrogen line

(Persinger et al., 2008), we suggest that if excess correlation is being displayed in a cosmological sense within our experiments, the congruence between the two critical point durations of the accelerating fields, the specific energy available from that field, and the congruence with a fundamental universe quantum, may be required to produce the phenomena. The specific test will be the extent or distance in space for which the "excess correlation" occurs. Some physical experiments with pair photon shifts in polarity have occurred over approximately 100 km (Fedrizzi et al., 2009).

References

Burke, R.C., Gauthier, M.Y., Rouleau, N., *et al.* (2013) Experimental Demonstration of Potential Entanglement of Brain Activity over 300 Km for Pairs of Subjects Sharing the Same Circular Rotating, Angular Accelerating Magnetic Fields: Verification by sLORETA and QEEG Measurements. *Journal of Consciousness Exploration and Research*, 4, 35-44.

Dotta, B.T., Buckner, C.A., Lafrenie, R.M., *et al.* (2011) Photon Emissions from Human Brain and Cell Culture Exposed to Distally Rotating Magnetic Fields Shared by Several Light-Stimulated Brains and Cells. *Brain Research*, 388, 77-88. http://dx.doi.org/10.1016/j.brainres.2011.03.001

Dotta, B.T., Mulligan, B., Hunter, M.D., *et al.* (2009) Evidence of Macroscopic Quantum Entanglement during Double Quantitative Electroencephalographic (QEEG) Measurements of Friends and Strangers. *NeuroQuantology*, 7, 548-551. http://dx.doi.org/10.14704/nq.2009.7.4.251

Dotta, B.T., Murugan, N. J., Karbowski, L.M. *et al.* (2013). Excessive correlated shifts in pH with distal solutions sharing the phase-uncoupled angular accelerating magnetic fields: macro-entanglement and information transfer. *International Journal of Physical Sciences*, 8, 1783-187.

Dotta, B.T. and Persinger, M.A. (2012) Doubling of Local Photon Emissions from Two Simultaneously Separated, Chemiluminescent Reactions Share the Same Magnetic Field Configurations. *Journal of Biophysical Chemistry*, 3, 72-80. http://dx.doi.org/10.4236/jbpc.2012.31009

Fedrizzi, A., Ursin, R., Herbst, T., *et al.* (2009) High-Fidelity Transmission of Entanglement over a High-Loss Free- Space Channel. *Nature Physics*, 5, 389-392. http://dx.doi.org/10.1038/nphys1255

Hoffmann, J., Krug, M., Ortegel, N., *et al.* (2012) Heralded Entanglement between Widely Separated Atoms. *Science*, 337, 72-75. http://dx.doi.org/10.1126/science.1221856

Hotta, M., Matsumoto, J. and Yusa, G. (2014) Quantum Energy Teleportation without a Limit of Distance. *Physical Review*, 89, 012311-1-012311-6.

Julsgaard, B., Kozhekin, A. and Polzik, E.S. (2001) Experimental Long-Lived Entanglement of Two Macroscopic Objects. *Nature*, 413, 400-403. http://dx.doi.org/10.1038/35096524

Persinger, M.A. (2014) Discrepancies between Predicted and Observed Intergalactic Magnetic Field Strengths from the Universe's Total Energy: Is It Contained within Submatter Spatial Geometry? *International Letters of Chemistry, Physics and Astronomy*, 11, 18-23.

Persinger, M.A. and Koren, S.A. (2007) A Theory of Neurophysics and Quantum Neuroscience: Implications for Brain Function and the Limits of Consciousness. *International Journal of Neuroscience*, 117, 157-175. http://dx.doi.org/10.1080/00207450500535784

Persinger, M.A. and Koren, S.A. (2013) Dimensional Analyses of Geometric Products and the Boundary Conditions of the Universe: Implications for a Quantitative Value for the Latency to Display Entanglement. *The Open Astronomy Journal*, 6, 10-13. http://dx.doi.org/10.2174/1874381101306010010

Persinger, M.A., Koren, S.A. and Lafreniere, G.F. (2008) A Neuroquantological Approach to How Human Thought Might Affect the Universe. *NeuroQuantology*, 6, 262-271. http://dx.doi.org/10.14704/nq.2008.6.3.182

Vaziri, A., Weihs, G. and Zeilinger, A. (2002) Experimental Two-Photon, Three Dimensional Entanglement for Quantum Communication. *Physical Review Letters*, 89, 240401-1-240401-4.

(Published in Journal of Electromagnetic Analysis and Applications, 2015)

Chapter 5: Local Electromagnetic Fields Exhibit Temporally Non-Linear, East-West Oriented 1 - 5 nT Diminishments within a Toroid: Empirical Measurement and Quantitative Solutions Indicating a Potential Mechanism for Excess Correlation

Abstract

States of excess correlation have previously been achieved at macroscopic levels by simultaneously exposing two non-local spaces to weak electromagnetic field patterns, generated by toroids, presented in a sequence such that the angular velocity of the field is modulated by changes in frequency over time. Here we systematically investigated effects upon the local space at the center of a single toroid generating the excess correlation sequence. The results indicated that a 1 - 5 nT diminishment in field intensity on the Y- or east-west axis was characteristic of the excess correlation sequence which was not indicated for control conditions. Statistically significant shifts in field intensity approximately 40 to 60 s before the onset of the first field associated with the excess correlation sequence indicated a temporally non-linear effect which converged upon the ratio of g and the rotational velocity of the Earth for the local space where Coriolis-like forces were inferred. Intensity shifts associated with the excess correlation sequence but not controls were quantitatively convergent upon parameters of the hydrogen line (1.42 GHz). Implications for these findings were discussed in relation to Mach's principle and, in particular, to the electron as a physical unit which was found to relate classical and quantum systems.

Introduction

The experimental treatment of two non-local spaces such that they behave as if they were the superimposed and had become the "same space" has theoretical and practical applications. Excess correlations, a frequently employed analogue for "entanglement" (Vedral, 2003), were once exclusively relegated to quantum and subatomic levels. However, demonstrations of excess correlations within gaseous (Calsamiglia, 2005), chemiluminescent reactions (Dotta & Persinger, 2012), and photon emissions from cells (Dotta & Buckner, 2011) separated by non-traditional distances have indicated this class of phenomena may exhibit analogues at macrolevels. The most consistent of these demonstrations required two loci that were simultaneously exposed to frequency (phase)-modulated magnetic fields displaying changing angular velocities within either a circular array of solenoids or toroids. The excess correlations between the two reactions within the two loci were enhanced when sequences of changing angular velocities were opposite to the increasing or decreasing frequency or phase modulated magnetic fields that were rotated. Our theoretical approach suggests that the rotational features of the Earth and its magnetic field should contribute to conditions that produce these excess correlations. Hence a component of this "excess" correlation would require an alteration of subtle magnetic intensities along the axis of rotation. Here we have presented experimental support for the contention that very small, approximately 1 to 5 nT steady-state shifts in the east-west component of the local magnetic field precipitated by magnetic fields generated within toroids by the current during creation of the time-varying magnetic fields (whose angular velocities were increased with decreased frequency modulation and then decreased with increased

frequency modulation), may reveal a possible mechanism by which excess correlations might be explained.

Based upon the conclusions by Tu et al (2005) that photons may exhibit non-zero rest masses and hence would display a dissociation between group and phase velocities, Dotta et al (2009) exposed pairs of human beings (each pair separated by 10 m) to circumcerebral, complex weak magnetic fields. The rotating magnetic fields were applied through a circular array of 8 solenoids equally spaced around the head at the level of the temporal lobes of each subject. The pattern generated by computer software through the solenoids could be accelerated or decelerated. Dotta and his colleagues (2009) found that under optimal conditions when both members of a pair were exposed to the rotating magnetic fields with changing angular velocities, flashing light into the face of one subject sitting within a closed Faraday Cage was associated with the release of photons ($\sim 10^{-11}$ $W \cdot m^{-2}$) as measured by photomultiplier tubes from the right hemispheres of the other member of the pair who was sitting in complete darkness in another room. A similar effect was measured for pairs of cell cultures separated by this distance and exposed to the same field parameters simultaneously.

In order to discern if photons, per se, were involved rather than processes associated with living systems Dotta and Persinger (2012) placed small amounts of hypochlorite solutions in two loci separated by 10 m. When the same amount of hydrogen peroxide was injected into each container the photon emissions were consistent and predictable. If the two areas shared a specific sequence of circularly rotating magnetic fields, simultaneous injection of the same amount of hydrogen peroxide produced twice the response (a doubling of the photon emission duration) as if

twice the amount had been injected into the single volume of hypochlorite. The reactions within the two loci under these conditions behaved as if they had been superimposed. This robust phenomenon was clearly observed when the two sites of reactions were separated by 3 km and the magnetic fields were generated by separate sets of equipment.

This "doubling of the photon duration" (Dotta & Persinger, 2012), as if the reaction had received twice the amount of reactant, only occurred if the two loci containing the hypochlorite were situated in the center of a circular array of solenoids where the angular velocity of the field was first accelerated in conjunction with a decelerating (phase) modulated pattern for a few minutes followed by fields with an accelerating (phase) modulated pattern whose rotational (group) velocity was decreasing. The effect was maintained for about 8 minutes. This conspicuous excess correlation was not measured if the order of the presentations was reversed (decelerating angular velocity, increasing frequency-phase modulation followed by accelerating angular velocity, decreased frequency-phase modulation). If the increasing or decreasing phase-frequency modulated magnetic fields were employed without the changing angular velocity, the effect was not evident as well. To discern if the effect generalized to other fundamental systems Dotta et al (2013) exposed separate beakers of spring water to the same field parameters for changing angular velocities and magnetic field patterns. When small quantities of protons (a weak acid) were added to one quantity of spring water during this approximately 8 minute window, discrete increases in alkalinity were noted in the non-local reaction (the other beaker) within which nothing had been injected.

The circular array of eight-solenoids that produced the discrete bursts of magnetic fields with changing angular velocities was operated by Complex © software and required custom-constructed Digital-to-Analogue Converters (DAC). A more accessible technology was required. After Burke et al (2013) showed statistically significant convergence in LORETA (Low Resolution Electromagnetic Tomography) of cerebral activity between pairs of subjects separated by 400 km wearing toroids operated by Arduino systems, Rouleau et al (2014) employed the same technology to replicate the pH shifts in spring water reported by Dotta et al (2013). Rouleau et al (2014) found that the Arduino-generated phase and frequency-modulated magnetic fields generated through the same toroids as those employed in the present study resulted in very similar non-local shifts in pH that reflected excess correlations. In that study the most powerful excess correlation between the two loci involved intensities for the frequency-modulated field that was within the 30 nT range or approaching the background values for power (60 Hz) frequencies. Stronger intensities (300 nT) for the phase modulations displayed less intense excess correlations.

However, in the process of measuring the static components of what is primarily the Earth's magnetic field by a magnetometer in the three axial planes (X, N-S; Y, E-W, and Z, vertical), we noted an interesting anomaly that was consistent with the magnitude and direction of potential variations in G (ΔG), the gravitational constant, and "geomagnetic" static intensity in the Y-axis. Typical daily fluctuations in G are within the range of ~3 x 10^{-3} of the average value. Recently Persinger and St-Pierre (2014) confirmed the relationship measured by Vladimirsky and Bruns (1998) over 25 years ago that approximately 5 nT increases in ambient geomagnetic activity were

associated with decreases in ΔG such that an increment of 10^{-9} T and 10^{-14} m^3 kg^{-1} s^{-2} might share the same source of variance. The energy equivalence for the ΔG and this magnitude of magnetic field intensity within 1 L of space converged to be ~3 x 10^{-14} J (Persinger, 2014). This is effectively the energy equivalent of the rest mass of an electron. We had also shown in other experiments that comparable, small decreases in ambient geomagnetic intensity of about 5 nT were associated with increases in photon emissions from the right hemisphere of human brain during specific cerebral activity (Persinger et al., 2013). Other experiments demonstrated this inverse effect between geomagnetic changes and photon emissions from cultures of melanoma cells habituating to room temperature after removal from standard incubatory conditions (Dotta et al., 2014).

Methods & Materials

Equipment

Each toroid core was a plastic ring with a diameter of 25.4 cm (circumference=79.8 cm). It was wrapped with 225 turns of 16 gauge wire (stereo speaker copper wire). The coil was wrapped in black, vinyl electrical tape. The elevation from the surface upon which the toroid rested and its top (i.e., the diameter of the ring around which the wire was wrapped) was 3.81 cm. An actual picture of the toroid is shown in Figure 5.1.

Figure 5.1. A picture of the toroid employed in the present study.

A MEDA FVM-400 Vector Magnetometer sensor was placed at the center of the toroid. Fluctuations in background electromagnetic field intensity (nT) were measured. The probe's X-axis was oriented to magnetic north, positioning the Y-axis within the perpendicular horizontal plane, and the Z-axis within the vertical plane (Figure 5.2). The entire apparatus was placed on a wooden table positioned 3 m away from and was connected to a Lenovo ThinkPad data logging laptop computer running Windows 7. Raw nT values were collected with an associated sampling frequency of 1 Hz.

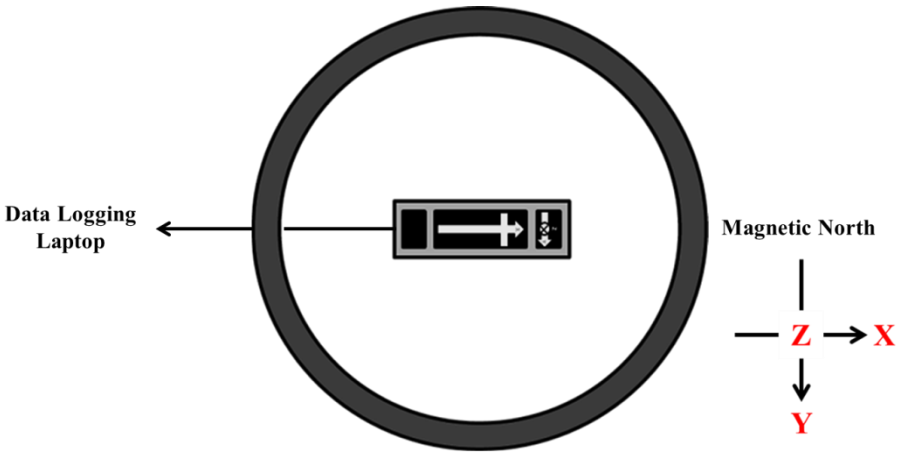

Figure 5.2. The sensor was placed at the center of the toroid, with the X-axis oriented toward Magnetic North. Corresponding Y- and Z-axes are labeled. The sensor cable exited away from Magnetic North in the X-axis and was plugged into a laptop 3m away from the center of the coil.

The same laptop provided digital-to-analog output to an Arduino Uno R3 microcontroller which carried a patterned current through the toroidal coil. The 5V output sequence and its associated electromagnetic field has previously demonstrated a capacity to establish states of 'excess correlation' between beakers of spring water separated by 1 m (Rouleau et al., 2014) as well as brains separated by 300 km (Burke et al., 2013) such that quantitative fluctuations at point A fluctuated at point B with convergent amplitudes of effect. Leads from the microcontroller to the toroid entered by way of the X-axis of the sensor orientation, parallel to data logging cables. A more specific schematic is shown in Figure 5.3.

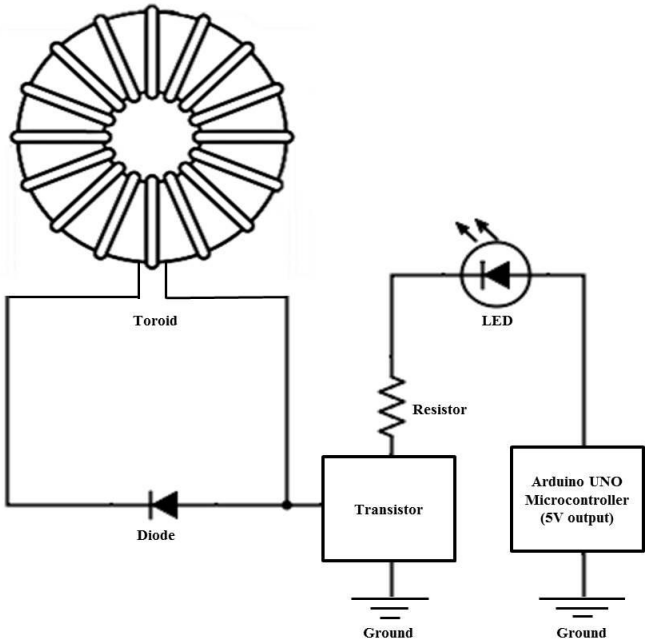

Figure 5.3. Schematic of the Arduino-toroid circuit employed in the present experiments.

Measurement Protocol

A 300 s pre-exposure baseline recording was obtained before the initiation of the first field pattern in the sequence. Once initiated, the first field – a temporally decelerating pattern – looped continuously for 360 s. A temporally accelerating field was initiated at the 660 s mark, exposing the space within which the sensor was placed for an additional 660 s. The second field pattern was then terminated and 480 s of post-exposure baseline data were collected. This protocol, similar to that employed by Dotta and Persinger (2012) and the Rouleau et al (2014) pH shift experiments was called the "Excess Correlation" procedure (Figure 5.4). The time required for the completion of single pattern sequence during the accelerating phase was 128 ms; for the decelerating field the duration was 203 ms.

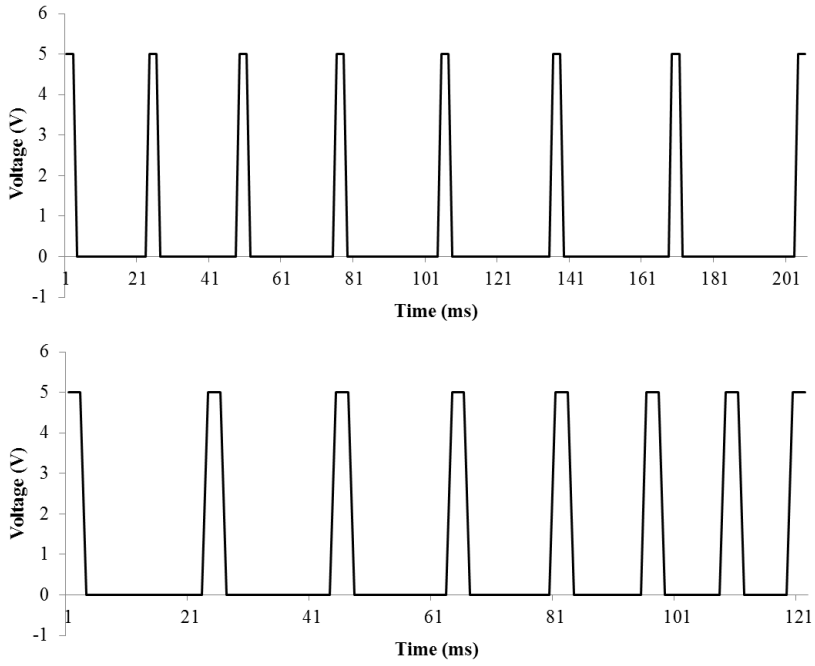

Figure 5.4. Two-dimensional representation of the decelerating (top) and accelerating (bottom) field patterns as output from the microcontroller. Note the sequences of 3 ms potentials followed by incrementally longer or shorter intervals of time.

Two variants of this protocol were performed as comparators in order to control for non-specific artifacts from the generation of magnetic fields. The first protocol variant (Reverse) involved a reversal of the temporal pattern associated with the first and second field exposure such that the accelerating field preceded the decelerating field. The exposure times of the first and second field remained consistent. The second variant (Control) was a control protocol wherein 1800 s of baseline data are collected without the initiation of any field.

All protocols were repeated 6 times for a total of 18 trials. No two trials were completed on the same day. However, all trials were completed between 9PM-2AM local

time in order to control for diurnal variations in background electromagnetic field intensities. Once collected, raw data were extracted and new variables were computed. First, a 60 s average of field intensity was computed from the center of each exposure phase. For example, the mean and standard deviation for the pre-exposure baseline phase were computed by averaging second-by-second nT values from minute 2.5 of each trial (n=18) during pre-exposure baseline phase and computing grand averages within each exposure protocol for X-, Y-, and Z-axes. Shifts in intensity (nT) were then computed by subtraction in order to infer net changes in intensity as a function of experimental manipulation. Running 30 s intensity averages were then calculated for all axes and incremental nT shifts were computed in order to infer fine-scale changes.

Results

An ANOVA revealed statistically significant differences in nT shifts from the pre-exposure baseline phase to the first field phase along the Y-axis only as a function of exposure protocol [$F(2,15)= 7.20$, $p<.01$], explaining 53% of the variance. *Post-hoc* tests revealed the source of variance to be a subtle negative shift (decrease) in field intensity associated with the Excess protocol ($M= -2.77$, $SEM= .37$) relative to Control protocol ($M=-.34$, $SEM= .60$), [$t(8)=3.45$, $p<.01$, $r^2=.60$]. Similarly negative shifts were observed from pre-exposure baseline to the first field exposure in Excess protocol trials relative to Reverse trials ($M= .35$, $SEM= .72$), [$t(9)= -3.61$, $p<.01$, $r^2= .59$]. There were no significant differences in shifts from pre-exposure baseline to the first field exposure between Control and Reverse protocols along the Y-axis ($p>.05$). These results are

presented in Figure 5.5. No further differences were noted within X-, Y-, or Z-axes across all shift phases.

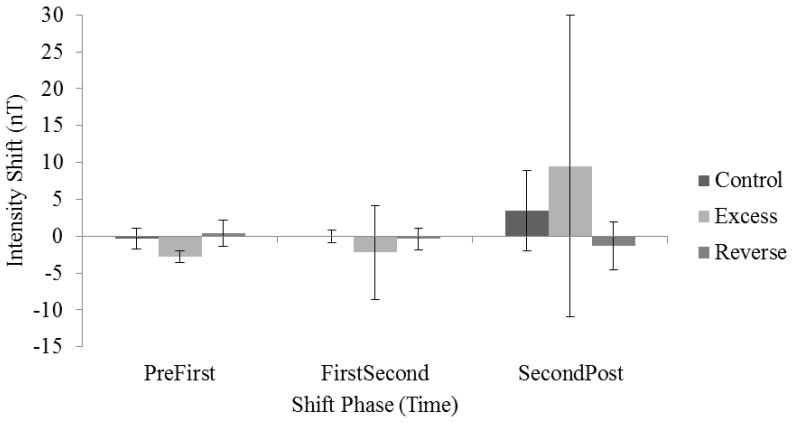

Figure 5.5. Shifts in intensity (nT) as a function of shift phase by exposure protocol. PreFirst refers to shifts from the pre-exposure baseline condition to the first field exposure. FirstSecond refers to shifts from the first field exposure to the second. SecondPost refers to shifts from the second field exposure to the post-exposure baseline.

In order to discern the temporal characteristics of this shift as a function of exposure protocol, multiple independent t-tests were generated examining incremental shifts from minute 2.5 to 3.0, 2.5 to 3.5, 2.5 to 4.0, etc. The differences between Excess and Control protocols were first noted when examining the shift from minute 2.5 to 4.0, $t(10)=3.20$, $p<.05$. This incremental shift difference between Excess and Control protocols persisted for 120 s until the shift from minute 2.5 to 6.5, $t(10)= 2.03$, $p>.05$. There were no significant differences noted for incremental shifts between Control and Reverse protocols. Differences between Excess and Reverse protocols were transient,

however, and were comparable to those observed for Excess and Control comparisons. These results are reported in Figure 5.6.

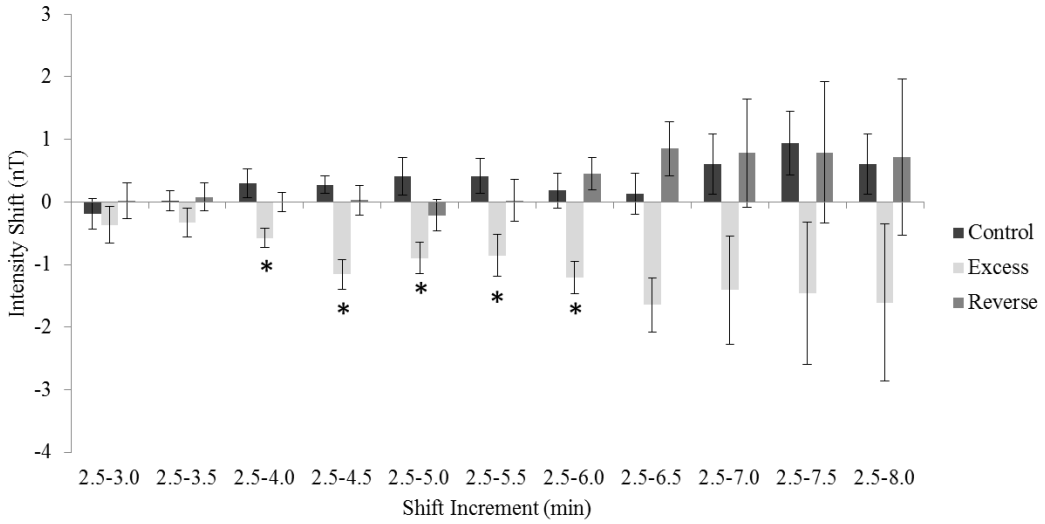

Figure 5.6. Incremental shifts in field intensity (nT) across protocol type. Shift increments are indicated in minutes, where 2.5-3.0 refers to a nT shift occurring between the beginning to the end of the second half of the second minute. Increments of time with significant differences between conditions are indicated.

Correlational analyses were completed to discern any relationship between the aforementioned 30 s-by-30 s serial nT shifts and time. Serial nT shifts along the Y-axis (n=58) positively correlated with time ($r = .68$, $p < .001$) for the Excess protocol only. These correlations for the Y-axis were not statistically significant for the Control or Reverse trials ($p > .05$). No further significant relationships were revealed. These results are presented in Figure 5.7.

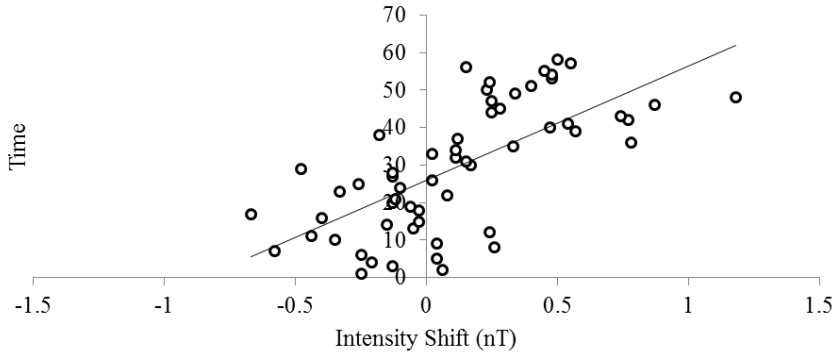

Figure 5.7. A moderate, positive correlation between serial shifts in field intensity (nT) across the Excess protocol for the Y-axis and time.

Calculations & Implications

The contribution from the energy from the rotation of the Earth to the east-west magnetic shift measured in our experiments for only the excess correlation procedure should have quantitative consistency. Assuming the mass of the earth to be 5.98×10^{24} kg and the velocity to be 4.63×10^{2} m s^{-1}, the total energy of the system would be 1.27×10^{30} J distributed over a spatial field equivalent to the surface area of the earth (5.1×10^{14} m^2), or, about 0.25×10^{16} $J \cdot m^{-2}$. When applied to the area occupied by an electron as a particle (6.15×10^{-30} m^2 per electron), the average energy would be about 1.5×10^{-14} J per electron. This energy is remarkably similar (the same order of magnitude) to the mass equivalent of an electron.

The energy of a system from a magnetic field can be estimated by B^2 divided by 2μ when this quotient is multiplied by the volume involved. In this instance μ_o is magnetic permeability ($4\pi \times 10^{-7}$ N A^{-2}) and B is the strength of the field. From Figure 5.5 the shift (diminishment) of the east-west component of the static field during the

"excess correlation" procedure, but not during the reverse or control procedures, was an average of ~1.5 nT. If volume were solved instead:

$$m^3 = (J \times B^{-2}) \times 2\mu_o \quad (1),$$

the value would be 0.96 x 10^{-2} m^3, or a linear distance of 21 cm. This value is important because it reflects the approximate width of the toroid (25 cm). It is also the approximate wavelength of the most copious standing wave in the universe, the neutral hydrogen line (1.42 GHz). If a procedure were to be developed to capture this condition of excess correlation over non-traditional distances, the hydrogen line would be expected to be involved.

The phenomena may have occurred because of the circumference of the toroid. We had selected these parameters in order to place the toroid over or around the average human head. According to conventional calculations of inductance (L):

$$L = \mu_o N^2 A (2\pi r)^{-1} \quad (2),$$

where N is the numbers of turns around the toroid, A is the torus' cross-sectional area and r is the radius of the toroid. For our equipment these values were 225, 3.7 x 10^{-4} m^2, and 1.3 x 10^{-1} m. The inductance of the toroid would have been 2.9 x 10^{-5} H.

Application of dimensional analysis for values potentially relevant for a type of universal entanglement suggests that the product of inductance ($kg \cdot m^2 \cdot A^{-2} \cdot s^{-2}$), unit charge ($A \cdot s$), and the square of frequency (s^{-2}), in this case the neutral hydrogen line, would be relevant. Consequently the product of 2.9 x 10^{-5} H, 1.9 x 10^{-19} A s, and (1.42 x 10^9 Hz)^2 results in 9.4 x 10^{-6} V. In experiments with human brain activity we had considered this an important range because of its congruence with the change of voltage

associated with the conduction within a single ion channel in the plasma membrane of a neuron. In the present application the product of this potential difference and the unit charge is associated with a quantity of energy ~ 1.5 x 10^{-24} J. The value is clearly recognizable because its quantum frequency obtained by dividing it by Planck's constant (6.626 x 10^{-34} J·s) is within error of measurement of the 1.42 GHz hydrogen line.

Because the Earth is rotating in an east-west direction and the current within the toroid was rotating as well there would be the potential for Coriolis-like forces to contribute. In the balance of probabilities if they interacted the interface of the process should be manifested by the relationship between the axial drift velocity of the current in the toroid and intrinsic frequency at this latitude as define by the angular velocity of the system and the latitude. Drift velocity is classically defined as:

$$v=I \times (n\ A\ q)^{-1} \quad (3),$$

where v is velocity, I is the current in the toroid, n is the molar density of the material (in this instance copper), A is the area (of the wire) and q is the unit charge. Both direct measurements of the circuit during the generation of the frequency-modulated magnetic fields during the excess correlation protocol and calculations from the Arduino-toroid circuit indicate that the nominal current was 0.55 mA during the decelerating phase and 0.85 x 10^{-3} A during the accelerating phase.

Assuming 9.0 gm·cm^{-3} density for copper, 6.023 x 10^{23} molecules per mole and 1 electron per atom, this product when divided by copper's atomic weight (64 gm per mole) shows the numbers of free electrons would be 8.5 x 10^{28} m^{-3}. When multiplied by the cross-sectional area of the 16 gauge copper wire (1.32 x 10^{-6} m^2) and the unit charge

1.6×10^{-19} A·s for the unit charge, the value is 17.95×10^{3} $A \cdot (s \cdot m^{-1})^{-1}$. When divided into the 0.55×10^{-3} A (decelerating phase) to 0.85×10^{-3} A (accelerating phase) measured in the circuit, the median drift velocity would between ~3.1 and 4.7×10^{-8} m s^{-1}. This would occur for a steady current. However our current was oscillating. We assumed that this temporal component could facilitate the drift by the factor $f \times v$, where f is the intrinsic frequency of the oscillations. For the 3 ms intervals employed here, the equivalent f is 3.33×10^{2} Hz. For a unit second this results in an enhancement to a "dynamic" drift value between 1.0 to 1.6×10^{-5} $m \cdot s^{-1}$.

If the forces of interaction between the angular velocity of the system (the Earth) and the internal rotation of the toroid are similar in relation to Coriolis forces, then the radius of the "circular" rotation generated by the toroid can be estimated by:

$$r = v \times f^{-1} \quad (4),$$

where v is the drift velocity and f is the Coriolis parameter at the specific latitude (46.39 N) which is determined by the angular velocity of the system. In this instance we assumed the average of the velocity for the decelerating (205 ms) and accelerating (128 ms) cycle completions around the circumference of the toroid, or, 5.1 $m \cdot s^{-1}$. The value would be 8.6×10^{-5} s^{-1}. When the dynamic drift velocity, v, was divided by the Coriolis parameter, the resulting radius for the "circular motion" or "inertia of the circle" would be between ~11 cm and 18 cm. The diameter for this "circular inertia" would be within the range of the 21 cm hydrogen wavelength. However the nature of the coefficients required for the congruence is not obvious at this time. Higher current intensities and stronger measured magnetic fields within the toroid would solve for different drift velocities and hence different solutions. This may explain the efficacy of the ~30 nT and

associated current (mA level) time-varying fields in the excess correlation condition compared to the 300 nT strengths applied in the same manner (Rouleau et al., 2014). The latter required the addition of an amplifier to the circuit.

If the adjustment for time-variation had not been made within the original drift velocity the radius of the inertia of the circle would have been between 3.1 and 4.7 x 10^{-4} m or a circumference of 1.9 to 3 mm with a corresponding frequency, if electromagnetic, of 1.6 x 10^{11} Hz to 1 x 10^{11} Hz. When multiplied by Planck's constant and divided by the Boltzmann constant of 1.38 x 10^{-23} J $°K^{-1}$, the equivalent temperature approaches within a factor of 2 the cosmic background microwave levels. We cannot exclude the possibility at this time that some static component of the current induction, even though it was time varying by the Arduino circuit, occurred. The diminishment of the E-W component of the "geomagnetic" field within the center of toroid was not phasic but constantly persistent for several minutes and occurred only when the excess correlation protocol was applied.

The Coriolis force involved with our parameters for the latitude at which the experiments were conducted according to classic calculations would be 4.32 x 10^{-4} $m{\cdot}s^{-2}$. The energy associated with the mass of an electron (9.11 x 10^{-31} kg) for this acceleration spread along the circumference of the toroid (0.8 m) would be ~3.15 x 10^{-34} J. This is remarkably similar to the energy from a unit frequency for Planck's constant (6.626 x 10^{-34} J·s), again reiterating the potential significance of the phenomena associated with electrons in this process. It is relevant that the energy equivalence of the mass of an electron multiplied by the square of the fine-structure velocity for a Bohr magneton

when multiplied by the time required to complete one orbit is effectively Planck's constant.

Movement in a circle is uniquely interesting because the process would always be accelerating ($m \cdot s^{-2}$) and a changing rate of this acceleration ($m \cdot s^{-3}$) often referenced as a "jerks", would be a second derivative containing the potential temporal non-continuities that could encourage the conditions we assume may be associated with the observed excess correlations. They could spread over the Minkowski four-dimensional field (Eardley & Moncrief, 1982) and appear to violate directional causality. In other words the "effects" of these "jerks" could occur before events and appear to violate causal principles but not necessarily the concept of entanglement. The presence of non-local and advanced correlations for geomagnetic effects had been reported by Korotaev and his colleagues (Korotaev, 2004; 2005). In the present experiments despite random determination for when a given condition would be initiated, the negative shift in magnetic field intensity in the Y component (east-west) only began to emerge about 40 to 60 s before the initiation of only the excess correlation protocol. The other two (the reversed and control protocol) did not show this "temporal anomaly".

We suspect that these "jerks" or "sputters" could be coupled to the rotation (angular momentum) of the Earth. Minute but measureable changes in angular momentum or the terrestrial spin have been detected over durations of days or months. Eubanks et al (1985) noted fluctuations with amplitudes in the order of 0.5 ms over periods of 40 to 60 days. They are sometimes coupled to alterations in solar wind velocity and geomagnetic activity. Although there are many potential models to describe the duration of a "unit sputter", parsimony suggests that it might be a ratio of g to

rotational velocity. Hence for the velocity of the earth in Sudbury, Ontario (N 46.69) would be ~420 m s^{-1} and when divided by 9.8 m s^{-2} would involve a more or less fixed interval of 43 s. This value is within the range of the "retro-occurrence" of the decrease in the east-west component of the static magnetic field inside of the toroid during the excess correlation protocol. The concept of specious present, if valid, would predict that the functional increment of time (Δt) associated with the observation of phenomenon within a relativistic framework could change such that the "future" of one framework could become the "present" of another. When the perceptual Δt is expanded significantly from that of the reference Δt events that appear serial and causal in the smaller temporal window may appear to be simultaneous and superimposed within the wider temporal frame.

We are pursuing the possibility that the excess correlation between two loci at non-traditional distances for photon emissions from chemical reactions, cells, and brain activity when the technology described in this paper has been employed involves a narrow range of energies where geomagnetic activity and gravitational processes interact. According to dimensional analysis the product of G ($m^3 \cdot kg^{-1} s^{-2}$), magnetic field intensity ($kg \cdot A^{-1} s^{-2}$) and unit charge ($A \cdot s$) would be a cubed velocity term. With actual values for ΔG, that is 3×10^{-3} of 6.67×10^{-11} $m^3 \cdot kg^{-1} s^{-2}$, 10^{-9} T, and 1.6×10^{-19} $A \cdot s$, the real value is 32×10^{-42} $m^3 \cdot s^{-3}$ or 3.16×10^{-14} $m \cdot s^{-1}$. The frequency associated with the radius of classic electron, 2.82×10^{-15} m, would be ~11 Hz. This is precisely within the range of the second harmonic of Schumann resonance (Schumann, 1952), the standing wave oscillations within the ionosphere-Earth surface cavity, that Minkakov et al (1992) predicted would interface with gravitational waves originating from anywhere in the

universe. This convergence does not prove the mathematical solutions of Minkakov's brilliant insights but supports the supposition that within a narrow range of inverse variations between ΔG and geomagnetic intensity where photons may be manifested (Persinger, 2012), excess correlations could be maximized but only for a limited duration. From a theoretical perspective we expect the duration of excess correlation to be limited. If it were not, then causal connections coupled to locality would ultimately be diluted over time.

Researchers in our laboratory have been designing experiments and testing various configurations of magnetic fields within circular arrays in order to discern potentially the parameters by which excess correlation might occur. We have been pursuing the potential validity of Mach's principle of "prominence of the universe" (Brans & Dicke, 1961) which indicates that an event that occurs in one small part of the universe influences the entire universe and vice versa. The presumption is based upon angular momentum. For this to occur within feasible temporal frames Persinger and Koren (2013) showed that a term for diffusivity based upon the four-dimensional product of basic circular geometries, particularly $2\pi r$, $4\pi r^2$, $4/3\pi r^3$ and $2\pi rf$, or $21.3\pi^4 r^7 s^{-1}$. By applying dimensional analysis to obtain a similar aggregate based upon universal values they found:

$$21.3\pi^4 r^7 s^{-1} = G^2 m^2 d s^3 \quad (5),$$

where G was the Gravitational Constant ($m^3 kg^{-1} s^{-2}$) mass was the estimated mass (Whitrow, 1946) of the universe (kg), d was the estimated width of the universe, and s was its age. A higher dimensional "diffusivity" term was obtained that produced the resulting velocity of 2.4×10^{23} $m \cdot s^{-1}$. This velocity, if it reflected "entanglement" latency,

should be reflected in the dragging of inertial frames such as those noted in satellite orbits. The predicted temporal value for this drag for the orbit of a satellite was within the same order of magnitude and coefficient (10^{-16} s) as that measured directly and derived from more complex mathematical models (Ciufolini, 2007).

The time required for such entanglement to occur around the circumference of the Earth ($4 \cdot 10^{7}$ m) would be that value divided by the entanglement velocity or 2×10^{-16} s. When applied to the diffusion velocity of a charge within the variations of G and 1 nT geomagnetic variation as noted previously, that is 1.7×10^{-14} m·s^{-1}, the distance would be 3.4×10^{-30} m. This value is about 2.1×10^{5} more than Planck's Length (1.6×10^{-35} m). The potential significance of this value becomes apparent when the expansion time for an electron is incorporated. Persinger and Koren (2007) had calculated that assuming an average (based upon Hubble and Planck telescope data) Hubble's parameter of 70 km per s per MParsec (3.1×10^{22} m) or 2.3×10^{-18} s^{-1}, the length (twice the radius, 4.86×10^{-15} m) of an electron would have a velocity of 11.66×10^{-33} m·s^{-1}. When divided into Planck's length (1.6×10^{-35} m), the time required would be 1.1 ms. There is now experimental evidence that the supports this solution for the electron and the proton (Rouleau et al., 2014).

With this assumption the time required to expand 2.1×10^{5} of that value would about 4 to 5 min. A range in this duration would be expected given the significant standard deviation for the actual Hubble parameter which is not a fixed value. The 4 to 5 min duration is within the range of the "entanglement time" noted in our excess correlations for shifts in pH of water when employing the equipment reported in this paper and the displacement of the Y-axis of 1 nT of the magnetic field within the toroid

but only during the excess correlation protocol. If this explanation is valid then the "time limited" excess correlations and the anomalous diminishment of intensity of the east-west magnetic component within the toroid during the specific sequence of changing angular velocities (interacting with the earth's angular momentum at the electron level) would reflect the dynamics of this "expansion time". We suggest there is a moderate probability that the consistency of quantification could relate Planck-level phenomena to the macrolevel we have measured in the laboratory.

Conclusions

The data indicated a temporally non-linear effect within the toroid space which was exclusive to the excess correlation field presentation sequence. Quantitative solutions converged upon the hydrogen line as a standing wave source which might be accessed for practical use in entanglement. Coriolis-like forces present a relativistic approach to excess correlation phenomena, where the local space is affected by planetary rotation. An approximate mechanism was presented which relates physical parameters of the electron to fundamental processes at quantum and universal scales of discourse.

References

Brans, C., & Dicke, R. H. (1961). Mach's principle and a relativistic theory of gravitation. *Physical Review*, *124*(3), 925.

http://dx.doi.org/10.1103/physrev.124.925

Burke, R. C., Gauthier, M. Y., Rouleau, N., & Persinger, M. A. (2013). Experimental demonstration of potential entanglement of brain activity over 300 Km for pairs of subjects sharing the same circular rotating, angular accelerating Magnetic fields: verification by s_LORETA, QEEG measurements. *Journal of Consciousness Exploration & Research*, *4*(1).

Calsamiglia, J., Hartmann, L., Dür, W., & Briegel, H. J. (2005). Spin gases: Quantum entanglement driven by classical kinematics. *Physical review letters*,*95*(18), 180502. http://dx.doi.org/10.1103/physrevlett.95.180502

Ciufolini, I. (2007). Dragging of inertial frames. *Nature*, 449(7158), 41-47. http://dx.doi.org/10.1038/nature06071

Dotta, B. T., Buckner, C. A., Lafrenie, R. M., & Persinger, M. A. (2011). Photon emissions from human brain and cell culture exposed to distally rotating magnetic fields shared by separate light-stimulated brains and cells. *Brain Research*, *1388*, 77-88. http://dx.doi.org/10.1016/j.brainres.2011.03.001

Dotta, B. T., Lafrenie, R. M., Karbowski, L. M., & Persinger, M. A. (2014). Photon emission from melanoma cells during brief stimulation by patterned magnetic fields: Is the source coupled to rotational diffusion within the membrane?. *General Physiology and Biophysics*, *33*(1), 63.

http://dx.doi.org/10.4149/gpb_2013066

Dotta, B. T., Mulligan, B. P., Hunter, M. D., & Persinger, M. A. (2009). Evidence of macroscopic quantum entanglement during double quantitative

electroencephalographic measurements of friends vs strangers. *NeuroQuantology*, *7*(4). http://dx.doi.org/10.14704/nq.2009.7.4.251

Dotta, B. T., Murugan, N. J., Karbowski, L. M., & Persinger, M. A. (2013). Excessive correlated shifts in pH within distal solutions sharing phase-uncoupled angular accelerating magnetic fields: Macro-entanglement and information transfer. *Int J Phys Sci*, *8*, 1783-1787. http://dx.doi.org/10.9734/irjpac/2015/13156

Dotta, B. T., & Persinger, M. A. (2012). "Doubling" of local photon emissions when two simultaneous, spatially-separated, chemiluminescent reactions share the same magnetic field configurations. *Journal of Biophysical Chemistry*,*3*(01), 72-80. http://dx.doi.org/10.4236/jbpc.2012.31009

Eardley, D. M., & Moncrief, V. (1982). The global existence of Yang-Mills-Higgs fields in 4-dimensional Minkowski space. *Communications in Mathematical Physics*, *83*(2), 171-191. http://dx.doi.org/10.1007/bf01976040

Eubanks, T. M., Steppe, J. A., Dickey, J. O., & Callahan, P. S. (1985). A spectral analysis of the Earth's angular momentum budget. *Journal of Geophysical Research: Solid Earth (1978–2012)*, *90*(B7), 5385-5404.

http://dx.doi.org/10.1029/jb090ib07p05385

Korotaev, S. M.; Morozov, A. N.; Serdyuk, V. O.; Gorohov, J. V.; Machinin, V. A. (2005). Experimental study of macroscopic nonlocality of large-scale natural dissipative processes. *NeuroQuantology*. 4, 275-94.

http://dx.doi.org/10.14704/nq.2005.3.4.79

Korotaev, S. M., Serdyuk, V. O., Gorohov, J. V., Pulinets, S. A., & Machinin, V. A. (2004). Forecasting effect of macroscopic nonlocality. *Frontier Perspectives*, *13*(1), 41-45. http://dx.doi.org/10.14704/nq.2005.3.4.79

Minakov, A. A., Nikolaenko, A. P., & Rabinovich, L. M. (1992). Gravitational-to-electromagnetic wave conversion in electrostatic field of earth-ionosphere resonator. *Radiophysics and Quantum Electronics*, 35(6-7), 318-323. http://dx.doi.org/10.1007/bf01041780

Persinger, M. A. (2012). Potential origins of a quantitative equivalence between gravity and light. *The Open Astronomy Journal*, 5, 41-43.

http://dx.doi.org/10.2174/1874381101205010041

Persinger, M. A., & Koren, S. A. (2007). A theory of neurophysics and quantum neuroscience: implications for brain function and the limits of consciousness.*International Journal of Neuroscience*, *117*(2), 157-175. http://dx.doi.org/10.1080/00207450500535784

Persinger, M. A., & Koren, S. A. (2013). Dimensional Analyses of Geometric Products and the Boundary Condi-tions of the Universe: Implications for a Quantitative Value for the La-tency to Display Entanglement. *Open Astronomy Journal*, *6*, 10-13. http://dx.doi.org/10.2174/1874381101306010010

Persinger, M. A., Dotta, B. T., Saroka, K. S., & Scott, M. A. (2013). Congruence of energies for cerebral photon emissions, quantitative EEG activities and~ 5 nT changes in the proximal geomagnetic field support spin-based hypothesis of consciousness. *Journal of Consciousness Exploration & Research*, *4*(1).

Persinger, M. A., & St-Pierre, L. S. (2014). Is There a Geomagnetic Component Involved with the Determination of G?. *International Journal of Geosciences*,*5*(04), 450. http://dx.doi.org/10.4236/ijg.2014.54042

Rouleau, N., Carniello, T. N., & Persinger, M. A. (2014). Non-Local pH Shifts and Shared Changing Angular Velocity Magnetic Fields: Discrete Energies and the Importance of Point Durations. *Journal of Biophysical Chemistry*, *2014*. http://dx.doi.org/10.4236/jbpc.2014.52006

Schumann, W.O., 1952: "Uber de strahlundslosen Eigenschwingungen einer leitenden Kugel, die von einer Luftschicht und einer Ionospharenhulle umgeben ist". *Z. Naturforsch* 7a 149.

Tu, L. C., Luo, J., & Gillies, G. T. (2005). The mass of the photon. *Reports on Progress in Physics*, *68*(1), 77-130. http://dx.doi.org/10.1088/0034-4885/68/1/r02

Vedral, V. (2003). Quantum physics: Entanglement hits the big time. *Nature*, *425*(6953), 28-29. http://dx.doi.org/10.1038/425028a

Vladimirsky, B.M. and Bruns, A.V. (1998) Influence of the Sector Structure of the Interplanetary Magnetic Field on the Results of Measurements of the Gravitational Constant. *Biophysics*, 43, 720-725.

Whitrow, G. J. (1946). The mass of the universe. *Nature*, 158, 165-166. http://dx.doi.org/10.1038/158165b0

Chapter 6: General Discussion

The concepts involved in the former half of this dissertation can be partially formalized as follows: The neuron is a macromolecular aggregate that has been characterized in the literature as a structure which necessitates functional properties of the brain such as network formation and consciousness as inferred by characteristic frequency spectra. The data presented here suggest that some functional properties of the brain can be expressed by the non-aggregated, chemical constituents of cells operating within energetic parameters characteristic of cellular function. If the premises hold true, it follows that some functional properties of the brain do not depend upon the neuron as a structural unit. If this principle can be generalized to other cell types, cells can be conceptualized as facilitators rather than generators of physical-chemical processes ascribed to biological organisms. This would be entirely compatible with what is known about neuronal structure and function.

Enzymes, for example, accelerate chemical reactions within the cell by lowering activation energy. Because thermal energy is available in any system whose temperature is greater than 0˚K, cells can harness the medium itself as a source of energy by selectively reducing the activation energy of reactions within discrete spaces and for brief periods of time. Chemical reactions, including those related to metabolism, can and do occur without the assistance of enzymes (Keller et al., 2014); however, the level of precision and control afforded to cells by enzymes illustrates the necessary-sufficiency distinction as it relates to cellular biology and maintaining the integrity of structure. Enzymes allow the cell to execute a controlled-burn, minimizing catastrophic dissolution of the cell itself. In other words, chemical reactions are not functions of cells; cells merely harness what occurs readily outside the cell under optimal conditions.

Cells are therefore not necessary conditions for biologically-relevant chemical reactions (Keller et al., 2014).

In Chapter 3, it was implied that at least one configuration of an inanimate object can learn. Given the aforementioned example, it is sensible to suggest that learning is not restricted to biological organisms, organs, or even cells. Necessary conditions for associative learning do not include these biological units or aggregates. Instead, the data would suggest that some property or combination of properties associated with the material examined is sufficient to produce associative learning. Among the constituents of the material, the prime candidate is water (H_2O). Water displays many properties which converge upon the operating principles of biology.

If the contents of cells, seriated by mass, are any indication of relative contribution to cellular function, water accounts for more function than all other units combined. The physical significance of water as it relates to abiogenesis has been thoroughly discussed by Persinger (2014), who has pointed out that the diffusion term of a proton applied to the average viscosity of water at 25˚C results in an energy of $\sim 1.5 \cdot 10^{-20}$J when applied over the distance of two O-H bonds, imbuing the water molecule with an intrinsic energy equivalent to that of the resting membrane potential and the energy associated with the net change in voltage from an action potential on a unit charge. Water at a boundary condition displays properties which are not observed in bulk water (Guo et al., 2014). In combination with previously outlined properties of the proton, it is apparent that when discussing biology, we are really discussing the interactions between semi-isolated units of water separated by matrices of water with protein inclusions (e.g. ground substance). The characteristic frequencies emergent given specified geometrical and chemical parameters in Chapter 2 illustrate the role of

proton dynamics in brain-like systems. Experimental modelling of this sort cannot be discounted as a valid method of testing the fundamental properties of the brain.

The concepts introduced in the latter half of this dissertation relate to the brain in two ways. First, it is inevitable that future technologies will be engineered which will allow brains separated in space (and perhaps time) to communicate wirelessly, sparking a revolution in communication unlike those of the 19th and 20th centuries. The electromagnetic field applications outlined in Chapters 4 and 5 demonstrate the fundamental principles by which a technology facilitating brain-to-brain communication might operate. These physical-chemical demonstrations are perhaps confirming the mechanism underlying results published by Burke at al. (2013), which suggest successful transfer of information between brains over 300km. What remains is to "tune" this technology in order to transfer large quantities of information over vast expanses of space. The calculations provided in Chapter 5 would indicate that this can be accomplished by widening the temporal "window" through which information transfer can occur. If the temporal bandwidth and the velocity of the signal are limited by some fundamental operator, perhaps parallel processing by use of many simultaneous toroids will be required.

The second way in which these concepts relate to the brain is that we have perhaps demonstrated an external application of what the brain can already do on its own and to a restricted degree given limited resources. A neuronal basis for non-locality and "excess correlation" is not fully established and requires a combination of scientific efforts on the part of physicists and neuroscientists among other interdisciplinary researchers. Theoretical works indicate that the brain is optimally suited to interact with fundamental signal-carriers that are omnipresent within the Universe (Persinger et al.,

2008). Energy densities within the human brain and the interstellar medium are convergent (Persinger, 2011) implying redundancy or perhaps interconnectedness. These are not mutually exclusive options. Even if we suppose that any reflection of the cosmos within the brain is merely a confirmation that the brain was generated within a Universe expressing definite physical parameters, this does not disconfirm any possibility that the brain is inextricably connected to the Universe. The degree to which this connection is practical in the sense of being of any functional purpose is now of consequence and demands inquiry. It is, after all, demonstrable that all matter in space exerts a gravitational force upon all other matter in space where the magnitude is contingent upon and proportional to the square of the distance between the units:

$$F = G \frac{m1\, m2}{r^2} \quad (1),$$

where F is the force, G is the gravitational constant ($6.67 \cdot 10^{-11}$ m^3 kg^{-1} s^{-2}) , m1 and m2 are the masses of the units, and r is the distance between the centers of the masses. Newton's equation demonstrates that the force between two masses does not exist in a binary state and can only be modulated – not negated – by separation in space. Coulomb's law is represented by what is essentially the same equation, replacing G with k for the electrostatic constant ($8.99 \cdot 10^9$ N m^2 C^{-2}) and each mass term with a point-charge in coulombs:

$$F = k \frac{q1\, q2}{r^2} \quad (2),$$

Forces of infinite range are present in our Universe. If we accept this as true and of practical significance beyond mathematical triviality, the implication is that many potential *ethers* exist which can link brains separated in space. If neurons within a single brain or across two brains separated in space display a similar non-local

relationship whereby the force is always present but is diminished or enhanced as a function of some definite set of parameters, the toroid technology outlined here could constitute a method by which the signals can be amplified. In other words, a bridge between brains already exists and all that is needed is to ensure the safe passage of information.

References

Guo, J., Meng, X., Chen, J., Peng, J., Sheng, J., Li, X. Z., ... & Jiang, Y. (2014). Real-space imaging of interfacial water with submolecular resolution. *Nature Materials*, 13(2), 184-189.

Keller, M. A., Turchyn, A. V., & Ralser, M. (2014). Non-enzymatic glycolysis and pentose phosphate pathway-like reactions in a plausible Archean ocean. *Molecular Systems Biology*, 10(4).

Persinger, M. A. (2011). Electromagnetic bases of the universality of the characteristics of consciousness: quantitative support. *Journal of Cosmology*, 14.

Persinger, M. A. (2014). Quantitative Convergence between Physical-Chemical Constants of the Proton and the Properties of Water: Implications for Sequestered Magnetic Fields and a Universal Quantity. *Physics and Astronomy*, 2, 1-10.

Persinger, M. A., Koren, S. A., & Lafreniere, G. F. (2008). A neuroquantologic approach to how human thought might affect the universe. *NeuroQuantology*, 6(3), 262-271.